NTNU
Norwegian University of
Science and Technology

Velocity and Reflectivity variations of Overpressured Jurassic Sandstones in the Norwegian Sea

Naphtali Chukwuka
Ochonogor

Petroleum Geosciences
Submission date: June 2016
Supervisor: Kenneth Duffaut, IPT

Norwegian University of Science and Technology
Department of Petroleum Engineering and Applied Geophysics

Abstract/Summary

The Garn Formation is one of the reservoir sands amongst the Jurassic Sandstones in the Norwegian-Sea. The pore-pressure and its influence on the rock properties within the Haltenbanken province in the Norwegian-Sea has been studied very well over the years. This work uses the Eberhart-Phillips model to study the stress sensitivity and its impact on the velocity and reflectivity variations within brine-saturated Sandstone within the Haltenbanken province in the Norwegian-Sea using Garn Formation as the target Formation. Dataset of six different wells at different in-situ differential stress conditions was selected for this work. The validity of the Eberhart-Phillips model in predicting the velocity variations as a factor of porosity, clay content and the differential (effective) stress was investigated. The results show that the standard Eberhart-Phillips is a good model for brine saturated Garn Formation within the selected Wells and can potentially predict the velocity variations within the brine saturated Garn Formation in this study. AVO modelling of the single interface 1D and the layered 1D model was used to look at the reflectivity variations with angles (offset) of the brine saturated Garn Formation in one of the Wells selected **(Well 6505/12-1)**. The essence was to investigate and differentiate between lithology and overpressure effects on AVO response. The single interface 1D AVO modelling predicts that the effects of lithology was more than the effect of overpressure on reflectivity at the near (0° to 30°) and far (30° to 40°) angles (offsets) while the effects of overpressure on reflectivity could be possibly detected at the ultra-far (above 40°) angles (offsets). In the layered 1D AVO modelling, the lithology effect on the AVO response (reflectivity with offset) was more than the overpressure effect on reflectivity too. Hence, it is difficult to detect the effects of overpressure within the brine-saturated Garn Formation.

Table of Content

Contents

List of Figures

List of Tables

CHAPTER 1

1.0. INTRODUCTION

Hydrocarbon explorations and productions in sedimentary basins are often associated with challenges and uncertainties, especially in drilling deep reservoirs. One of these challenges is the determination of pre-drill pore-pressures. The need to understand the changes within the reservoir and its drainage system during production has also become of the tasks in the field of Geoscience over the years. Knowing the pressure within the reservoir helps Geoscientists to understand the hydrocarbon reserve, and avoid drilling uncertainties and high risks. It also helps in an optimized oil and gas recovery. Techniques such as the seismic while drilling has been applied by the oil Industry to monitor and control seemingly dangerous abnormal pressures (Carcione and Helle, 2002). Seismic velocities and empirical models have also found major application in predicting pre-drill pore-pressures over the years. Rock-Physics and Seismic amplitude versus angle or offset **(AVO)** modelling are major tools that are commonly applied to map predrill pore-pressures. These tools have been very useful in the exploration of Hydrocarbon, production and Reservoir monitoring.

The Garn, Ile, Tofte and Tilje Formations represents the Jurassic sandstones within the Haltenbanken in the Norwegian-Sea. The geological properties of these Formations has been thoroughly studied and documented over the years by several researchers (Bolås and Hermanrud, 2003, Storvoll and Bjørlykke, 2004, Hermanrud et al., 1998, Teige et al., 1999, MESSINA et al., 2014). The Garn Formation consists of medium to coarse grained, moderately to well sorted sandstones that is Mica rich, deposited in a shallow-marine deltaic environment, the Ile formation consist of fine to medium and occasionally coarse grained sandstones with varying sorting interbedded with thinly laminated siltstones and shales deposited in a tidal influenced delta or coastline settings. The Tofte Formation is a coarse grained, poorly sorted, cross-stratified sandstone, deposited in a local deltaic fan environment. The Tilje Formation consists of interbedded sand and shale sequences deposited in a tide influenced environment (NPD, Storvoll et al., 2005). Koch and Heum (1995) in Storvoll et al. (2005), stated that the thicknesses of these Formations varies within the Haltenbanken. The lateral distribution, and reservoir quality within the individual sand-units also changes within the sedimentary basin. These Sandstones are the major reservoirs within the Haltenbanken province. Different pore-pressure regimes has been

encountered within the sandstones at different oil fields within the Haltenbanken. In the Lavrans Field, the pore pressures are higher than hydrostatic (≈ 50 MPa), while at the Kristin Field there has been measured pressures up to 90 MPa (NPD, Kvam, 2005). Fluid pressure measurement in the Smørbukk field has shown a pressure difference of 30 MPa between a watering bearing reservoir in well 6506/11-1 and hydrocarbon bearing reservoirs in wells 6506/12-1 (Aplin et al., 1999). The origin and magnitudes of the pressures and the seismic velocity trend within the Jurassic Sandstones at the Haltenbanken has been studied by different researchers (Skar et al., 1999, Nysæther, 2006, Aplin et al., 1999, Storvoll et al., 2005, Kvam, 2005). Kvam (2005) used rock-physics model (Hertz-Mindlin's theory) and amplitude analysis to predict the Pore-pressure, while Nysæther (2006) used fluid-flow modelling to determine the overpressures in sandstone within the Haltenbanken. Storvoll et al. (2005) investigated the velocity-depth trends in the Norwegian Shelf using sediment composition, porosity, pore-pressure, burial history, and compaction process.

In this work, I want to test the validity of the "Eberhart-Phillips empirical Rock Physics model" by applying it to establish a relationship between velocities and differential stress within brine saturated Garn Formation in six selected wells within the Haltenbanken province. I will also carry out seismic reflectivity modelling and analysis of the Top Garn reflector with one of the selected wells **(Well 6506/12-1),** to study the effects of lithology and overpressure on the AVO response at the Top Garn interface. The target interfaces for this work are: (i) the Lyr Formation on top of brine saturated Garn Formation and (ii) the overburden Lyr-Spekke-Melke Formations on top of the brine saturated Garn Formation.

1.1 RESEARCH AIMS AND OBJECTIVES

The aim of this research work is in two folds.

- Firstly, I want to test the validity of the Eberhart-Phillips empirical method by using it to establish a velocity versus differential stress (effective stress) model within the brine saturated Garn Formation from selected dry-wells that are under different differential stress conditions within Haltenbanken in the Norwegian Sea.
- The second task will be the amplitude versus offset (AVO) modelling of the single interface of the Lyr on top of the Garn Formations and AVO modelling of combined lithologies (Lyr-Spekke-Melke) on top of the Garn Formation. The **Well 6506/12-1** was used for this task. The aim is to investigate and differentiate between the effects of lithology and overpressure on the AVO signature at the Garn reflector. The possibility of applying this idea into mapping or detecting pore-pressure within sedimentary basins would be considered at the end of the research.

In order to meet the above aims, the following objectives were carried out:

- Analysis of well logs from the selected wells to extract parameters such as the Porosity, Density, Velocity (P-wave and S-wave) of the brine saturated Garn Formation within the selected wells.
- Computation of the stresses (Lithostatic stress, Hydrostatic Stress) and Pore-pressure within the Garn Formation.
- AVO modelling by changing the lithology on top of the brine saturated Garn Formation and under different differential stress conditions using Well 6506/12-1.

CHAPTER 2

2.0. BACKGROUND GEOLOGY OF THE AREA OF STUDY

This chapter gives a short overview of the Norwegian Sea, the geological setting of the Haltenbanken and brief descriptions of the Formation groups within the area of study (Haltenbanken province). Most of the information and discussions that has been given here were adapted from the NPD website, bulletin and fact page.

2.1 THE NORWEGIAN SEA:

The Norwegian Sea covers most of the continental margin between approximately 62° and 69°3° N (Figure 2.1). The lithostratigraphic chart of the Norwegian–Sea is shown in Figure 2.2.

Three major episodes marks the tectonic history of the Norwegian Sea.

These are;

- Final closure of the Iapetus Ocean during the Caledonian Orogeny (Late Silurian/Early Devonian).
- A series of mainly extensional deformation episodes (Late Devonian to Palaeocene), culminating with the continental separation between Greenland and Eurasia.
- Active seafloor spreading in the North Atlantic between Eurasia and Greenland (Earliest Eocene to present).

A detailed description of the Evolution of the Norwegian-Sea can be found in Nøttvedt (2000), Eldholm (1987).

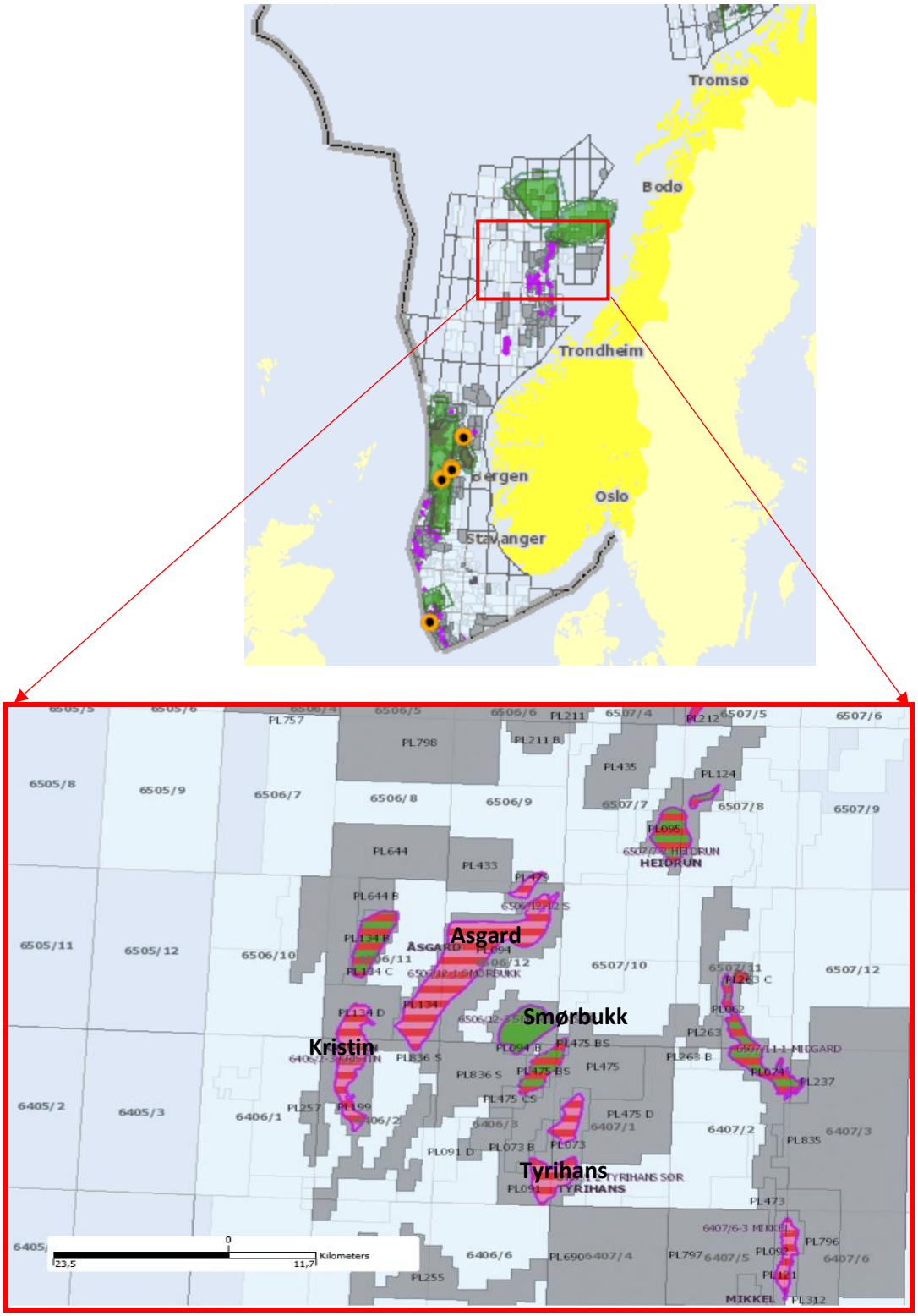

Figure 2.1:The location of the study area in the Haltenbanken, Norwegian Sea (source NPD).

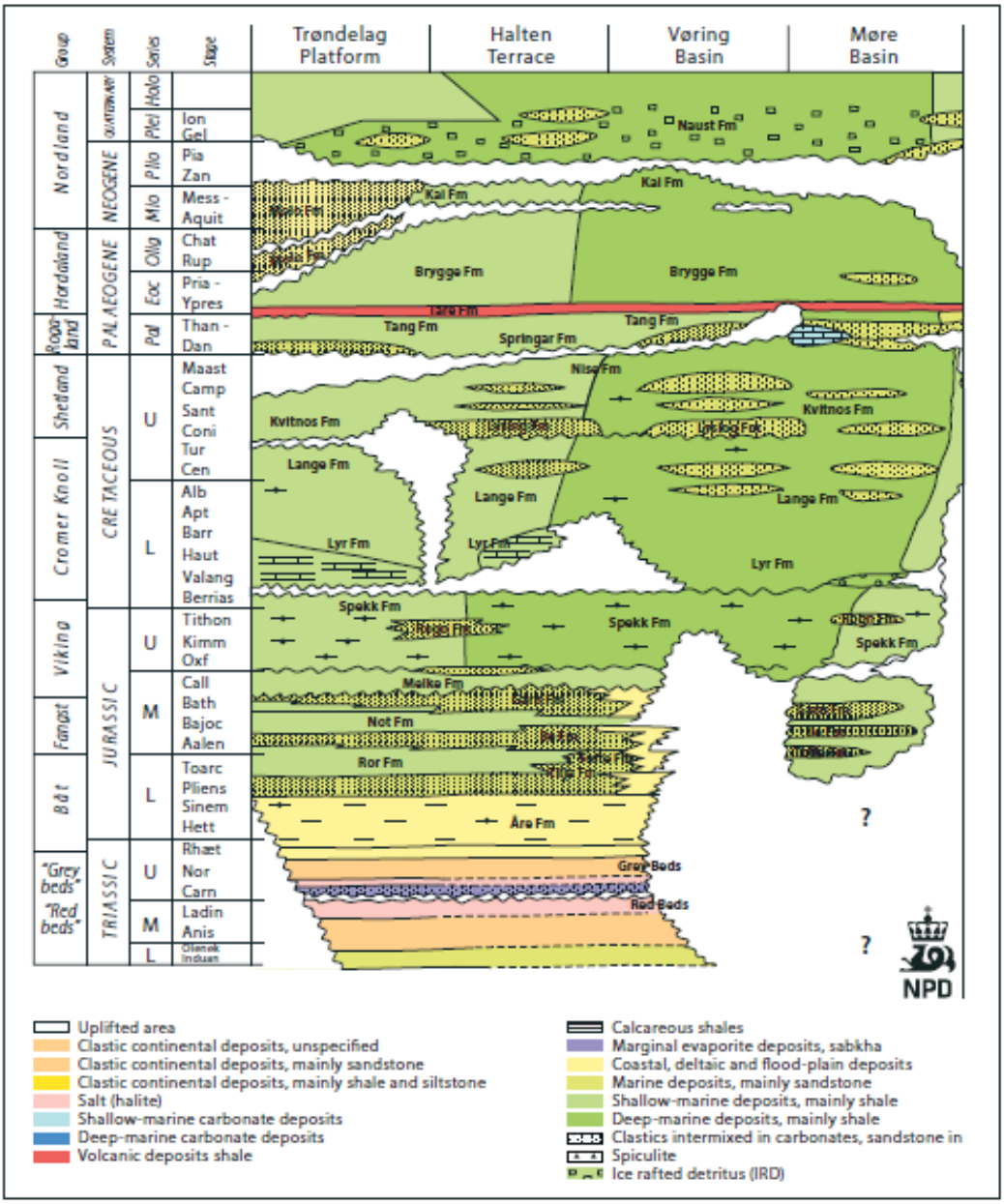

Figure 2.2: Lithostratigraphic Chart of the Norwegian-Sea (Copied from NPD).

Seven dry wells under different pressure (stress) conditions (both overpressure and normal hydrostatic pressure) at the Haltenbanken in the Norwegian Sea were selected assessed and investigated in this work.

2.2 THE HALTENBANKEN

The name 'Haltenbanken' was coined from the small Halten Island and light-house which is located on the outermost coast of the Sør-Trondelag (Blystad, 1995). It is located on the mid Norwegian Continental Margin between 64°N and 65°N and 6°E and 8°E bordered at the east by the Trøndelag Platform and to the west by the Vøring Basin. According to Martinius et al. (2014), Larsen and Heum (1988), the Halten terrace is one of the three major structural elements within the Haltenbanken Petroleum Province. The other two structural elements are the Trøndelag platform and the Deep Moere Basin. It was formed in response to the late Jurassic east-west rifting and early and middle Cretaceous north-south dextral wrenching (Larsen and Heum, 1988, Martinius et al., 2014) . It is a highly prospective geological province in the Norwegian Sea, different giant's fields such as the Asgard, Kristin, Victoria, Tyrihans, and Heidrun have been discovered within the Halten terrace. However, the dry wells will be used in this work. The evolutional history of the Halten terrace was marked by different Geological events such as the Pliocene uplift of the Fennoscandian Shield, and the rapid westward shelf progradation and deposition of sediments. This Pliocene event also led to the development of overpressure within the upper Jurassic to Palaeocene sequences within the Halten terrace. Martinius et al. (2014), Larsen and Heum (1988), Martinius et al. (2014) has documented a detailed lithostratigraphic and the tectonic history Halten terrace.

Detailed tectono-stratigraphic information about the Norwegian Sea the Halten terrace can be found in Blystad (1995), Ehrenberg et al. (1992), Faleide et al. (2015), Martinius et al. (2014), Dalland et al. (1988), Larsen and Heum (1988).

The main stratigraphic column of the Haltenbanken area is shown in Figure 2.3 below.

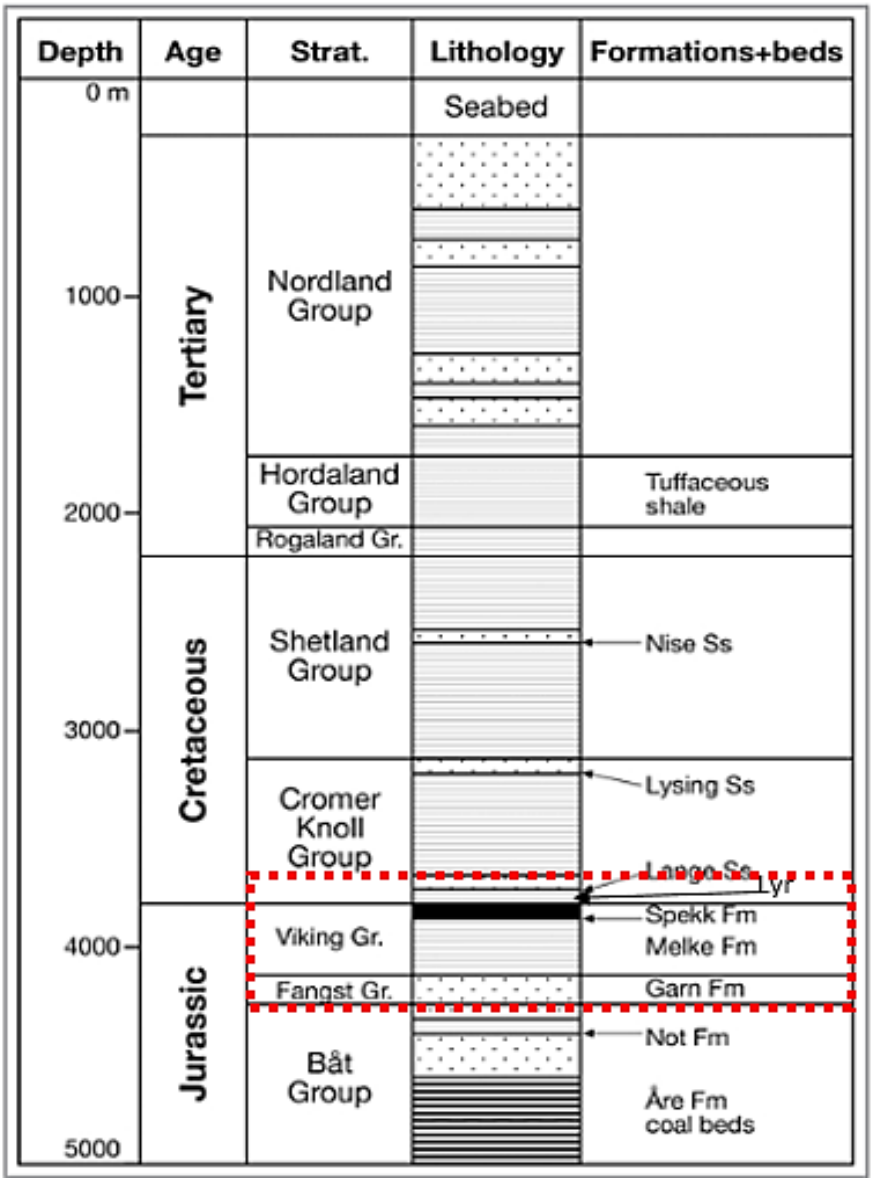

Figure 2.3: Stratigraphic Column of the HaltenBanken area. modified from (Dalland et al., 1988). The red dotted lines indicates the studied Formations.

The groups that typifies the formations found within study area (Haltenbanken) in the Norwegian-Sea includes:

2.2.1 The Nordland Group

Deegan & Scull (1977) named the group after the county of Nordland in Norway. The group consists of claystone, siltstone and sandstone of early Miocene to Recent in age. The sediments were deposited in a marine environment in a rapidly subsiding basin. Report in the NPD website shows that the upper part of the formation is of glacial to glacio-marine origin. The Nordland Group consists of the Kai, Molo, Naust and Utsira Formations (NPD).

2.2.2 The Hordaland Group

Deegan and Scull (1977) named this group after the county of Hordaland in Norway (NPD). The group is of Eocene to Early Miocene age. The typical lithology is marine claystone with minor sandstone. The claystones are normally light grey to brown, fissile and fossiliferous. Red and green claystones sometimes occur at the base. Thin limestones and streaks of dolomite are present. Sandstones are developed at various levels in the group. These are generally very fine to medium grained, and are often interbedded with claystones. The environment of deposition is the deep water. This group is characterised by the Brygge, Frigg, Grid, Skade and Vade Formations (NPD).

2.2.3 Rogaland Group

Deegan & Scull (1977) named this group after the county of Rogaland in southwest Norway (NPD). The typical lithology is claystone with minor local siltstone. Tuff is found in the upper part of the lithology within an outcrop. Dominant lithologies in the west are sandstones interbedded with shales, which are of Danian to Lats Palaeocene age deposited in the deep marine environment. The Tare and the Tang formations within the area of study typify this group (NPD).

2.2.4 Shetland Group

Deegan & Scull (1977) named the group from the Shetland Islands off the north coast of Scotland. In Haltenbanken, the lithology is claystone interbedded with minor amounts of carbonates and sandstones, which are of Turonian to Maastrichtian age deposited in an open marine environment. Although in some area, the group may consists of the chalk facies of chalky limestones, limestones, marls, and calcareous shales and mudstones. Chert (flint) occurs throughout the facies. The siliciclastic facies consists of mudstones and shales, partly interbedded with limestones. The Springar, Nise and Kvitnos Formations represents this group within the area of study (NPD).

2.2.5 Cromer Knoll Group

The Cromer Knoll Group consists mainly of fine-grained, argillaceous, marine sediments with a varying content of calcareous material. Calcareous claystones, siltstones and marlstones dominate, but subordinate layers of limestone and sandstone occur. The claystones are generally light to dark grey, olive-grey, greenish and brownish, often becoming light grey, light greenish-grey and light olive-grey marlstones. Mica, pyrite and glauconite are common. Generally, marlstones become the more dominant lithology in both the upper and lower parts of the group. The sediments were deposited in a shallow to deep marine environment within the Norwegian Sea. The age of this group is Ryazanian to Turonian. The Lysing, Lange and Lyr Formations represent this group. Lyr Formation is consists of light/medium grey to light green marls with interbedded carbonates. The environment of deposition is the open marine condition (Dalland et al., 1988) (NPD).

2.2.6 Viking Group

The Spekke, and Melke Formations, represents this group. The name of the group was taken from the Viking Graben where the group is well developed. The Viking Group consists of shales and mudstones on Haltenbanken and thin beds of carbonate and scattered sandstone stringers could be found within the lithology, which were deposited in the marine environment, mainly below wave base. The age of the Formation is from Bajocian to Ryazanian. The Spekke Formation is predominantly a dark brown to grey Shale. The Shale is non-calcareous. The formation is silty at

some areas. The Spekke has a very high content of organic material. Its environment of deposition is the marine anoxic bottom water condition. The Melke Formation is consist mostly Claystones with Siltstones and limestone interbeds and stringers of Sandstones. The Claystone is dark grey to brown. The environment of deposition is the open marine system. (NPD)(Dalland et al., 1988)

2.2.7 Fangst Group

The group's name was coined from the Norwegian name for Catch and comprises typically of three lithological units namely, a lower fine to medium-grained sandstone with numerous shaly interbeds, a middle mudstone, and an upper relatively massive fine to coarse-grained sandstone which are of Late Toarcian to Bathonian age. The environment of deposition of the sediments is shallow marine to coastal/deltaic facies dominate sequences on the Halten Terrace. The group is represented by the Garn, Not, and the Ile Formations within the study area (NPD). Garn Formation consists of medium to coarse-grained moderately to well-sorted Sandstones. There exists mica-rich zones. The Sandstones is occasionally carbonate-cemented. The Garn Formation may represent different environment of deposition. It may represent progradations of braided delta lobes, delta top and delta front facies with fluvial and wave influenced processes are recognised. (NPD)(Dalland et al., 1988)

2.2.8 Båt Group

The group's name corresponds to the Norwegian name for boat, and the Ror, Tofte, Tilje and the Åre Formations represent it. The lithology is typically an alternating sandstone and shale/siltstone units, with sandstone as the dominant lithology, which are of Rhaetian to Toarcian age. The environment of deposition of the sediments is shallow marine to deltaic environments dominated during deposition of the group (NPD).

2.3 DATASET

The selection of the wells used in this study was based on the Bolås and Hermanrud (2003) article on the Hydrocarbon leakage processes and trap retention capacities offshore Norway. The dataset set of the six different selected dry-wells was provided by the Norwegian Petroleum Directorate.

2.3.1 Well 6406/2-5

This well was drilled on the Kristin structure in the north-western part of block 6406/2, south-west of the Smørbukk Field and north-west of the Lavrans Field on Haltenbanken. The main objective was to test the hydrocarbon potential of the Garn and Ile Formations in a down flank position. In addition the well would test a secondary reservoir target of late Jurassic age, the Rogn sandstone, which was predicted based on seismic observations. The well penetrates the Lyr, Spekke, Melke and the Garn Formations (NPD).

2.3.2 Well 6406/3-1

This well is located in the southern end of the block, west of the Tyrihans Sør Field on the Mid Norway continental shelf. The primary objective was to test the reservoir potential of the Middle Jurassic sandstones. Secondary objectives were the Early Jurassic sandstones, penetration of the Triassic Grey Beds and Red Beds, and sampling of potential source rocks. The Spekke, Melke and Garn are found in this well. No Lyr Formation (NPD).

2.3.3 Well 6506/11-3

This well is located in the Haltenbanken region, North West of the Smørbukk area. The objectives of well 6506/11-3 were: to prove oil in the Lysing, Lange (Cretaceous) and the Rogn (Jurassic) Formation; to test the hydrocarbon potential of the Nise Formation and the Åre Formation; and to penetrate the Upper Triassic and test the reservoir potential in order to prepare for relinquishment. The well penetrates the Lyr, Spekke, Melke and the Garn Formations (NPD).

2.3.4 Well 6406/6-1

This well was drilled on the Eta structure in the northwest corner of a block located just south of the Trestakk and Smørbukk discoveries. The main objective was hydrocarbon accumulations in Middle Jurassic sandstones. The second objective was Early Jurassic sandstone. Total depth was to be in rocks of Triassic age in order to satisfy the licence commitment. The Spekke, Melke and Garn are found in this well. No Lyr Formation. (NPD)

2.3.5 Well 6506/11-1

This Well was designed to prove hydrocarbons in the G-structure in the easternmost part of block 6506/11 close to Smørbukk Field. The primary purpose of the well was to prove significant hydrocarbon accumulations in the Middle-Early Jurassic reservoirs. Secondary targets were sands of Cretaceous age, especially the Lysing Formation that has been proven to be oil-bearing in the area. The well should also test the hypothesis of a western ultra-high pore pressure area, verify the geophysical and structural interpretation and to improve the geological, paleontological, and geochemical understanding of the area. Total depth was planned 200 m into the coal-bearing Åre Formation. The well penetrates the Lyr, Spekke, Melke and the Garn Formations (NPD).

2.3.6 Well 6506/12-1

This was drilled on the Alpha structure in the northwest part of the block. The main objective was middle Jurassic sandstones in an anti-form structure. The secondary and tertiary objectives were Early Jurassic and Triassic sandstones on the same structure. Late and Early Cretaceous were also considered possible zones of hydrocarbon accumulations. Further objectives, of a more general exploratory nature, included the sampling of potential source rocks. Total depth was to be in rocks of Triassic age, or 4000 m in order to satisfy the licence commitment. It is a reference well for the Cromer Knoll Group and for the Springar, Nise, and Kvitnos Formations. The well penetrates the Lyr, Spekke, Melke and the Garn Formations (NPD).

The summary of the locations, RKBs, Water Depths (total depth, TD) of the different brine-saturated wells used in this work Table 2.1 below.

Table 2.1: The summary of the names, locations, RKBs, and water depth of the various wells investigated according to the information on the NPD website .

S/N	WELL NAME	LOCATION	RKB (m)	WATER DEPTH (TVD) (m)	PURPOSE	FINAL TVD mRKB	SPEKK, MELKE	LYR
1.	**6406/2-5**	Kristin	23	341	Appraisal	5438	✓	✓
2.	**6406/3-1**	Tyrihans Sør	22	256	Wildcat	4896	✓	-
3.	**6506/11-3**	North-West Smørbukk	24	328	Wildcat	4346	✓	✓
4.	**6406/6-1**	Between Trestakk and Smørbukk	25	243	Wildcat	4708	✓	-
5.	**6506/11-1**	Smørbukk	29	246	Wildcat	4672	✓	✓
6.	**6506/12-1**	Asgård	22	250	Wildcat	4924	✓	✓

✓ means the Formation is present, - means not present

CHAPTER 3

3.0. CONCEPTS OF PRESSURE AND STRESS CALCULATIONS

The idea here is to give a brief explanations of the different pressure (stress) concepts that are necessary to have a full grasp of the ideas behind this research work.

Different authors and researchers have worked on the various types and detailed concepts of pressures that are often encountered within the sedimentary basins. Various techniques and methods applied in the detection and measuring of pore-pressures within the sedimentary basins have been proposed by these researchers (Bowers, 1995, Dutta, 2002, Dvorkin et al., 1999, Fertl, 1981, Tingay et al., 2009) etc.

N.B: The term "Pressure" and "stress" are considered to be the same in this work. Although they are not exactly the same since stress is a tensor while fluid pressure is isotropic.

3.1 HYDROSTATIC-PRESSURE AND PORE-PRESSURE

Pore pressure is the pressure affecting the fluids within the pore spaces of a rock. In an open system where is an interconnected pore system to the surface, the pore pressure is known as hydrostatic pressure as shown in Figure 3.1. Hydrostatic pressure at any depth within the subsurface is the pressure exerted by the water column at rest at that particular depth. It is the normal fluid pressure encountered in subsurface rocks due to the weight of overlying waters (Hyne, 2014). This is expressed mathematically as;

$$P_h = g \int_0^z p_w \, dh \qquad (3.1)$$

Where P_h is the hydrostatic pressure (Pa), ρ_w is the water density (kg/ m^3), g is the gravitational constant (m/s^2) and dh is the vertical height of the water column (m).

Hydrostatic pressure trend within a sedimentary basin is referred to as normal pressure condition, and any deviation from this, is termed an overpressure or a geopressure (Dutta, 2002). Pore pressure concepts is applicable in exploration, production and development of Hydrocarbon fields. It helps to analyse the migration path for hydrocarbon, and the seal capacity at the exploration

stage. Again, Pressure data helps to know the reservoir drive and connectivity at the field development stage. Therefore, knowing pore pressure is necessary for the safe drilling project. It is also important in well design, borehole stability, rig selection, mud schedule and protection from blowout hazards (Bruce, 2002).

According to Borge (2002), the mechanisms that causes overpressures are:

- Porosity Reductions,
- Change in the volume of fluids.

Some of the mechanisms that causes overpressures within the sedimentary basins according to Dutta (2002) includes:

- Mechanical compaction disequilibrium,
- Clay dehydration and alteration due to burial diagenesis, dipping or lenticular permeable beds embedded in shale,
- Buoyancy,
- Tectonism/ uplift and erosion,
- Aquathermal pressuring,
- Hydrocarbon generation from Kerogen.

A summary of the wells selected and the Pore-pressures at the various Garn formations depths within the selected wells according to the Bolås and Hermanrud (2003) is shown in Table 3.1 below.

Table 3.1: Showing the Depth and measured Pore-Pressure within the Garn Formation in the six wells. These datas are according to the Bolås and Hermanrud (2003) article on 'the Hydrocarbon leakage processes and trap retention capacities offshore Norway'.

S/N	Wells	Depth of Garn Formation (m)	Pore- Pressure (MPa)
1.	6406/3_1	3780	67.5
2.	6406/2_5	4792	90
3.	6506/11_3	4180	75.9
4.	6406/6_1	4210	72.3
5.	6506/11_1	4140	75.5
6.	6506/12_1	3952	67.5

3.2 LITHOSTATIC STRESS

Lithostatic stress is caused all overlying material both solid and fluid (Figure 3.1). This is mathematically expressed as;

$$\sigma_L = g \int_0^z p_b \, dh, \tag{3.2}$$

Where p_b is the depth dependent bulk density given by:

$$p_b = \varphi p_f + (1 - \varphi) p_m \tag{3.3}$$

p_f is the pore fluid density,φ is the total porosity, p_m is the density of the matrix (grain density) respectively.

3.3 DIFFERENTIAL STRESS

The differential stress (σ_D) is the amount of the overburden stress carried by the rock grains. According to Terzaghi's principle (Terzaghi, 1943), it is the difference between the lithostatic stress (σ_L) and the hydrostatic pressure (P_h). This is expressed mathematically as;

$$\sigma_D = \sigma_L - nP_h (\, P_h = P_{pore}) \tag{3.4}$$

n= Biot-coefficient, which is usually given as equal to 1 for soft materials (Fjar et al., 2008).

$$\text{Thus}, \sigma_D = g \int_0^z p_b \, dh - \int_0^z p_w \, g dh \tag{3.5}$$

$$\sigma_D = g \int_0^z (p_b - p_w) \, dh \tag{3.6}$$

Differential stress controls the compaction of sediments with depth. The geophysical properties such as the sonic velocity, density, and resistivity of a normally pressured formation will increase with depth of burial (Bruce and Bowers, 2002). Therefore, any deviation from this velocity trend suggests an anomaly which could be calibrated with overpressure.

Plate 1 to Plate 9 in appendix B shows the plots of the various stress and pore-pressure values against depth within the selected brine-filled wells.

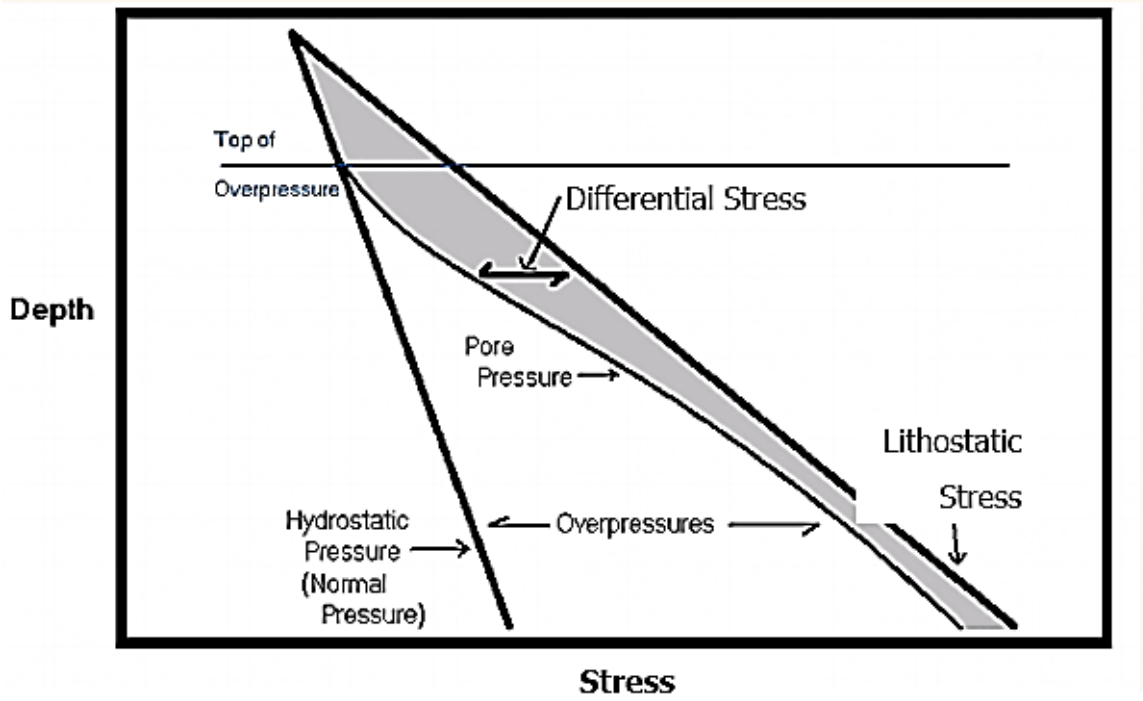

Figure 3.1: Stress plotted against depth showing Pore-pressure, Differential stress, Lithostatic stress modified from Bruce and Bowers (2002).

3.4 RELATIONSHIP BETWEEN PRESSURE (STRESS) AND ROCK VELOCITY

Rock velocity is the velocity of sound waves (P-wave, seismic) travelling through a piece of rock. Factors such as porosity, fluid saturation, state of stress, pore and confining stress, pore structure, temperature, pore fluid type and its thermodynamic state, lithology, clay content, cementation, and frequency of the propagating wave controls the rock velocity. These parameters are interdependent on each other (Dutta, 2002). Analysis of the relations between the rock velocities and differential stress (difference between the lithostatic stress and Pore-pressure) of the Berea sandstone in Dutta (2002) shows that:

- Velocity increases with differential stress such that it was rapid at first, and becomes gradual until an approximately constant terminal velocity is reached.
- The velocity increases rapidly by a small amount and then becomes almost constant for the effective stress.
- The behaviour for small effective stresses is almost the same for that of a zero effective stress.

Schön (2011) also stated that there is a characteristic nonlinear relationship of velocity on depth or pressure. In most cases, wave velocities increase strongly with increasing stress or pressure at low levels and less at high pressure or stress. The increase of the velocity with increasing pressure or stress in sedimentary rocks is associated with:

- Decrease of porosity;
- Improvement of grain-grain contact conditions;
- Closure of fractures, cracks, and other "defects."

Seismic methods uses either explicitly or implicitly a relation between the rock velocity and differential stress to for pressure prediction (Dutta, 2002). Empirical relations such as the Eaton approach and the Bower's relationship have been applied in pressure prediction while drilling. Eaton's method relies on establishment of a local "normal" compaction trend which is often complicated by the geologic history of the local section. Bowers' relationship is more general but still requires an understanding of burial history and structural configuration to be properly applied for prediction of pore pressures in sands (Bruce and Bowers, 2002).

Rock physics models have also found major applications in the relationship between rock velocities and stress. The models also provide links between the changes in the static and dynamic properties of a reservoir such as the fluid saturation, clay content porosity, and temperature lithology pressure (stress) etc. and the elastic properties of the reservoir as P-wave Velocity (Vp), Shear wave Velocity (Vs), and Density (ρ) (Johnston, 2013).

However, rock physics models have their respective applications and limitations. The essence of this work is not to give an in-depth analysis of the various rock physics models but to talk briefly about the ones that are relevant to this work. Detailed work in rock physics models can be found in (Mavko et al., 2009, Avseth et al., 2010a, Wang, 2001, Avseth et al., 2010b, Bjorlykke, 2010).

Examples of the commonly used rock physics models includes:

- Theoretical Bounds,
- Empirical Models,
- Gassmann's Equation,
- Contact Models,

- Inclusion Models.

3.5 EMPIRICAL MODELS

Empirical models are derived from fits made to experimental results. It involves a simple regressions relationship between two or three parameters such as compressional velocity, density, porosity, clay content, shear velocity and resistivity (Simm et al., 2014). Detailed knowledge of empirical models can be found in Mavko et al. (2009) .

The most commonly used models are the Gardner's relation or equation, Wyllie's time average equation, the Han's relations (see Appendix B) and the Eberhart-Phillips model or relation which is used in this work.

3.5.1 Eberhart-Phillips Model

Eberhart-Phillips et al. (1989) used a multivariate analysis to study the combined influence of effective pressure, porosity, and clay content on the compressional velocity and shear velocity of water-saturated sandstones. They combined laboratory measurements to form empirical relationships that could be applied in the field to estimate the in-situ properties of rocks.

The experiment was based on Han's laboratory measurement from compressional velocity and shear velocity over a range of effective pressure of 0.02 to 0.49 k bar on samples taken from quarries, borehole, tight gas sandstones and unconsolidated samples from well in the gulf of Mexico. The samples were water saturated such that the effect of gas and oil was not considered. The porosity of the samples ranged from 0.02 to 0.30 and the clay content is 0.00 to 0.50 (Eberhart-Phillips et al., 1989). 64 sandstone samples with porosities ranging between 4.6% and 29.4% and a clay content ranging between 0% and 40% were used for this experiment (Schön, 2011). The best fitting formulations are:

$$Vp = 5.77 - 6.94\varphi - 1.73\sqrt{C} + 0.446(P_e - e^{-16.7Pe}) \quad (3.7)$$

$$Vs = 3.70 - 4.94\varphi - 1.57\sqrt{C} + 0.361(P_e - e^{-16.7Pe}) \quad (3.8)$$

where; Pe= Effective Pressure (differential stress in this work) in kilobar or MPa, C= Clay content, φ = Porosity

The coefficients in the equations 3.7 and 3.8 was determined by simple regression approach. The stress terms in equations 3.7 and 3.8 are referred to as effective stress but in this work the terms are referred to as differential stress. However, Hofmann et al. (2005) explains the misunderstanding between the concepts of differential pressure (difference between confining of lithostatic pressure and pore-pressure) and effective pressure. The deformation of soils and unconsolidated rocks are controlled by differential pressures while the effective pressure controls the rock deformation of consolidated rocks. The effective pressure (stress) is expressed as:

$$P_e = P_{lith} - \alpha P_{pore} \tag{3.9}$$

P_e= Effective Pressure,

P_{lith}=Lithostatic Pressure,

P_{pore}=Pore Pressure,

α= $\left(1 - \frac{K_{skeleton}}{K_{solid}}\right)$ is a coefficient which depends on the compressibility of the material.

$K_{skeleton}$=Dry Bulk modulus,

K_{solid}=Modulus of the solid matrix material.

If α is taken as 1, then:

$$P_e = P_{lith} - P_{pore} \tag{3.10}$$

$$P_{effective}=P_{differential} \tag{3.11}$$

Therefore, for clarity in this work, I have assumed the differential and effective stress to be the same.

Just like other rock-physics empirical models, some of the limitations and assumptions that are commonly associated with the Eberhart-Phillips models are (Mavko et al., 2009):

- That the model is just an empirical relation and it is strictly applicable to only the sets of rocks studied.
- The model does not fit to the values of porosity or clay contents outside the range of that used in the experiments.

3.6 METHODOLOGY

The selection of the six dry-wells used in this work was guided by the Bolås and Hermanrud (2003) paper on the 'Hydrocarbon leakage processes and trap retention capacities offshore Norway'. The criteria are as follows:

- The wells must penetrate the Garn Formation, which is our main target in this work,
- The wells must be under different stress conditions,
- The wells must be water saturated or at least the Garn Formation should be water saturated.

The first task was to create the well-logs signatures for the selected six wells using the wireline log data from the Norwegian Petroleum Directorate website (NPD). This was done by importing the data into MATLAB (Mathworks) software. A MATLAB script was then coded to create the well log signatures of the various well data (Plate 8-24 in Appendix B). The well-log signature in some of the selected wells (wells 6406/2-5, Well 6406/3-1 and well 6506/12-1) did not extend to the surface, therefore, an exponential function was coded into MATLAB to extrapolate the well-logs to the surface using the sonic log. The log signatures from the selected brine-filled wells are displayed in Plate 8-24 in Appendix B.

The lithostatic stress, differential stress and the hydrostatic pore-pressure gradients of the brine saturated Garn Formation were estimated, and plotted against the total vertical depth (TVD) for each of the wells. This was done in MATLAB by simple coding of equations 3.1 to 3.6 into a MATLAB script. See plate 2 to plate 7 in Appendix B for the plots of the various stresses and the hydrostatic pore-pressure values against depth (TVD) of the selected brine-filled wells.

The well log suite did not come with the S-wave velocity. The S-wave velocity is important to fulfil the rock-physics modelling task (testing the validity of the Eberhart-Phillips Empirical model) in the Garn Formation (brine-filled) within the selected wells. To solve this problem, the Greenberg-Castagna's equation (equation 4.10) was used to compute the S-wave log by simple coding in MATLAB.

The gamma-ray log was used to calculate the volume of clay within the Garn Formation interval for the selected well simply by inputting equation 3.12 into MATLAB:

$$V_{Clay} = \frac{GR_{log} - GR_{sand}}{GR_{shale} - GR_{sand}} \quad (3.12)$$

where Vclay is the volume of clay content,

GRlog = Gamma-Ray log value in GAPI units,

GRsand= Gamma-Ray log value at the interpreted sand baseline,

GRshale= Gamma-Ray log value at the interpreted Shale baseline.

The porosities and bulk density of the brine-filled Garn Formation within the selected wells was computed using the neutron-porosity and bulk density logs. The Backus averaging technique was used to compute average porosity and bulk density values within the Garn Formation interval using simple arithmetic mean. The average values of the porosities and bulk densities of the Garn Formation within the selected wells are shown in Table 3.2.

The target Formation is the brine saturated Garn. The average values elastic properties (density, P-wave, S-wave) within the Garn Interval was computed using the Backus averaging technique.

3.6.1 Backus Averaging technique:

The Backus average describes the average compressional (Vp) and shear (Vs) velocities through a layered medium. The technique averages moduli rather than velocity. It is applicable in anisotropic and isotropic cases. The Isotropic condition was considered in this work. The Backus averaging determines the compressional (Vp) and shear (Vs) velocities using the Harmonic averages of the P-wave modulus (M) and the shear wave modulus (μ) (Simm et al., 2014, Backus, 1962).

The steps employed in using the Backus average technique are as follows:

i. Determine the P-wave modulus (M) and the shear wave (μ) modulus from the P-wave and S-wave velocity and density (Vp, Vs and p), using ;

$$\mu = V_s{}^2\rho \tag{3.13}$$

$$M = V_p{}^2\rho \tag{3.14}$$

ii. Calculate the average density (ρ) and the Harmonic average of the P-wave modulus and the S-wave modulus over the targeted brine-filled Garn Formation Interval,;

i.e.

Average Density:

$$\rho_{avg} = \frac{1}{n}\sum_{n=1}^{i=n}\rho \tag{3.15}$$

Average P-wave Modulus:

$$M_{avg}^{-1} = n^{-1}\sum M^{-1} \tag{3.16}$$

Average S-wave Modulus:

$$\mu_{avg}^{-1} = n^{-1}\sum \mu^{-1} \tag{3.17}$$

iii. Use the averaged parameters from step number (ii) to calculate the Backus average Velocities (P-wave and S-wave) Using:

$$V_{P\_Bavg} = \sqrt{\frac{M_{avg}}{\rho_{avg}}} \tag{3.18}$$

$$V_{S\_Bavg} = \sqrt{\frac{\mu_{avg}}{\rho_{avg}}} \tag{3.19}$$

The average P-wave and S-wave velocities within the brine saturated Garn formation of the selected wells was computed using the sonic log. The Backus averaging technique was used to calculate the average velocity values within the Garn Formation following the steps explained before, and using the equations 3.13 to 3.19.

The average parameters (Porosity, P-wave velocity, S-wave velocity, Density and Stress) that was computed using the MATLAB Software within the brine-filled Garn Formation Interval present in the six wells are given in Table 3.2.

The average velocity (P-wave and S-wave) values of the brine saturated Garn Formation computed using the Backus technique are plotted against the differential stresses (effective stress). The Eberhart-Phillips empirical model was then fitted into the plots in order to investigate the velocity variations. The validity of the model was also tested within the various brine-filled Garn Formation from the various selected wells as shown in Figure 3.2.

The Gassmann equation (Appendix B) was used to substitute the fluids inside the selected wells for pure brine. The reason is that we want to be sure that the Garn Formation we are interested in is only brine saturated since the presence of gas may interfere with the velocity.

Table 3.2: Showing the average parameters (Porosity, P-wave velocity and S-wave velocity predicted with the Greenberg-Castagna's equation, Density and Diferential stress) of the Garn Formation interval within the six selected wells using the Backus averaging technique.

S/N	Wells	Average Porosity (%)	Average Vp (m/s)	Average Vs (m/s)	Average Density (g/cm^2)	Differential Stress (MPa)
1.	6406/3_1	16	3793	2618	2.39	14.1
2.	6406/2_5	10	4362	2781	2.49	16
3.	6506/11_3	15	4385	2691	2.40	17.9
4.	6406/6_1	9	4387	2669	2.50	19.1
5.	6506/11_1	11	4253	2843	2.43	25
6.	6506/12_1	14	4538	2792	2.42	36

3.7 RESULTS

The Figure 3.2 below shows the plots of the computed average values of the P-wave velocity and the S-wave velocity of the brine-filled Garn Formation within the selected wells against the differential stress. The average velocities (P-wave and S-wave) were computed using the Backus averaging technique as discussed in section 3.6.1, while the differential stresses at the Garn Interval within the selected wells was calculated using equations 3.1 to 3.6 as explained in section 3.1 to 3.3. The Eberhart-Phillips model was fitted into these plots. The default parameters of the model by the authors were in the model as it was stated in equations 3.7 for P-wave velocity and equation 3.8 for S-wave velocity.

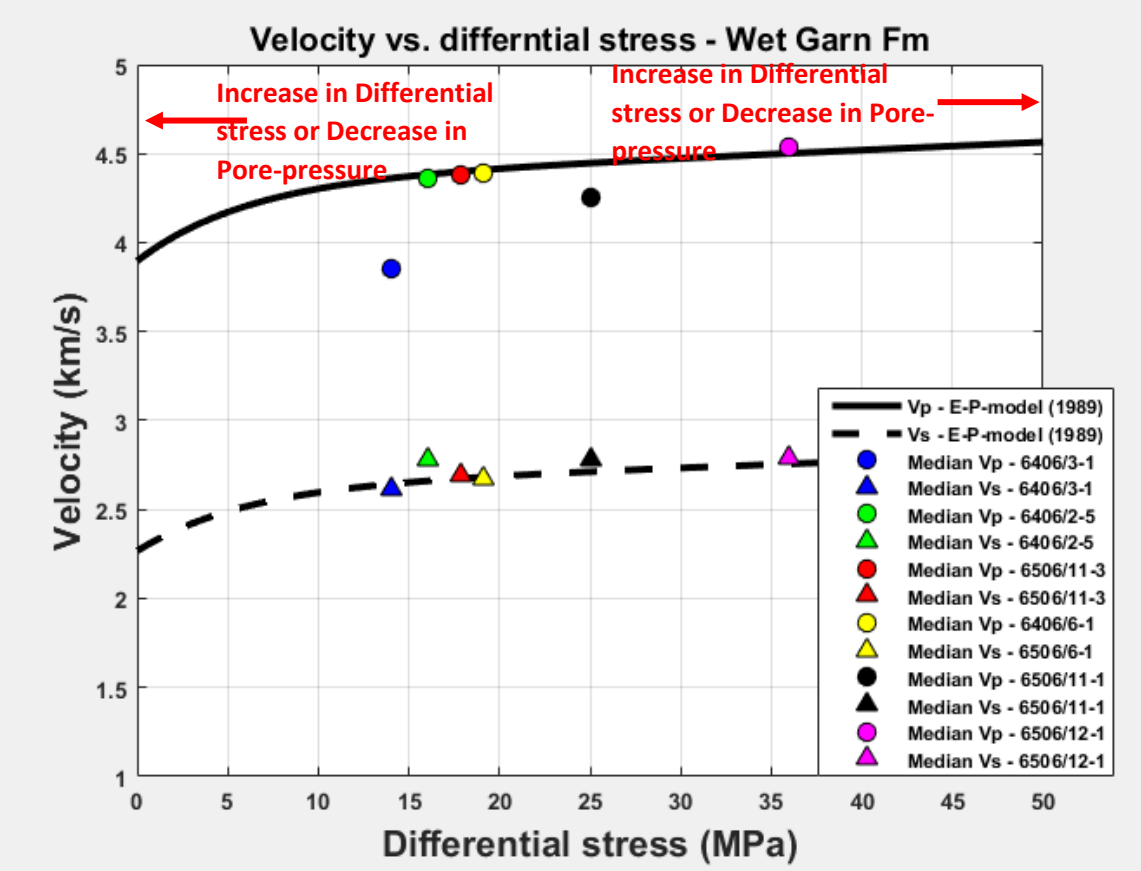

Figure 3.2: The plot of the computed average velocity (P-wave and S-wave) values against the differential stress of the brine-filled Garn Formations within the selected wells. The Eberhart-Phillips model was fitted into the plots to predict how the velocity varies within the Garn Formation of the selected wells using the default parameters by the authors (● represents the average P-wave velocities within the Garn Formation, while ▲ are the average S-wave velocities computed of the Garn Formation computed using the Greenberg-Castagna's equation).

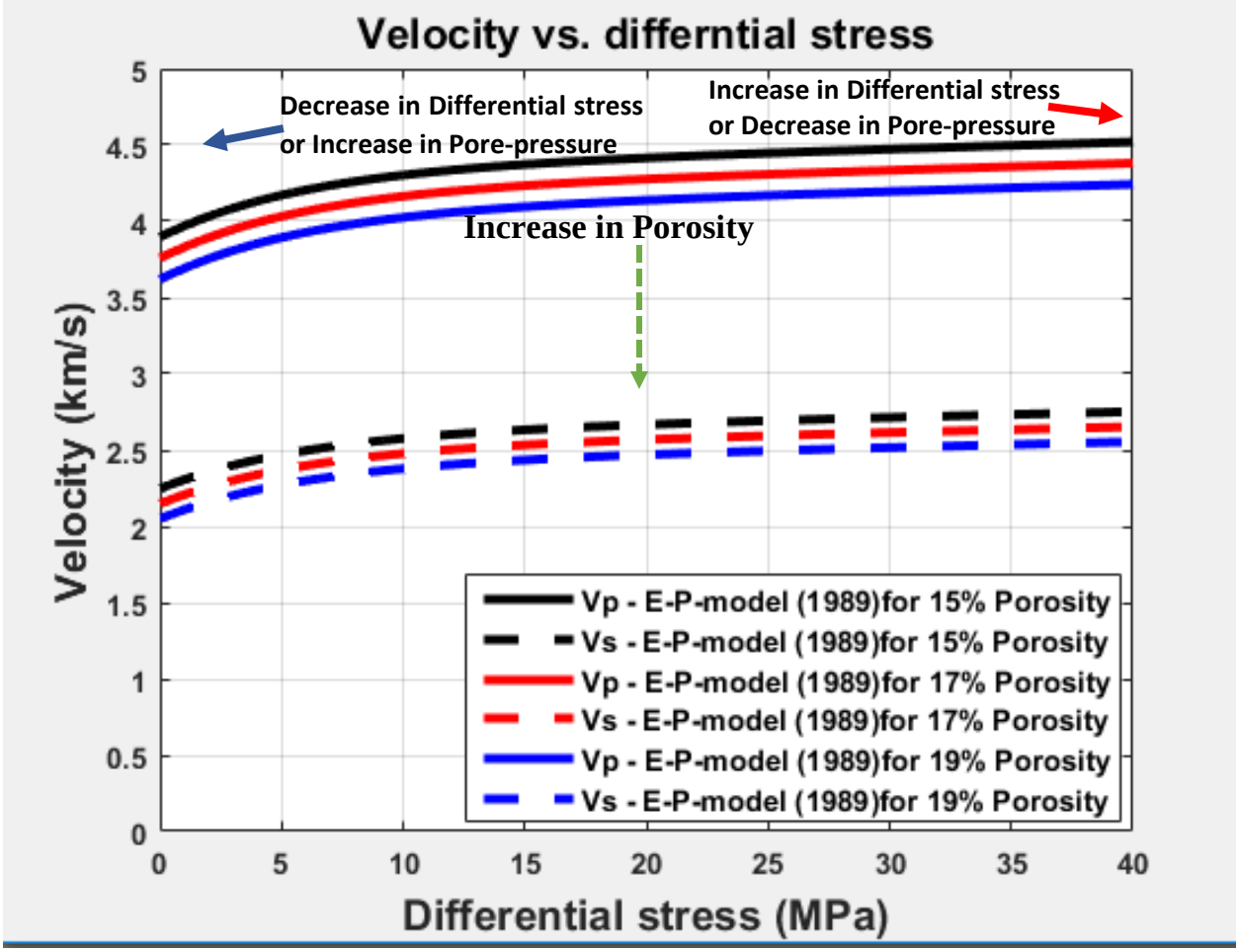

Figure 3.3: A Standard Eberhart-Phillips model showing the velocity and differential stress relationship. The model was plotted using 5% clay content, while varying the amount of porosity.The red arrow shows the directions of increase in differential stress or decrease in pore-pressure, while the blue arrow shows a decrease in dfferential stress or increase in pore-pressure. The green arrow shows the direction of an increase in porosity. These parameters explains what controls the velocity as it is related to the model.

CHAPTER 4

4.0. AVO MODELLING

Seismic amplitude variation with offset technique commonly referred to as AVO is based on the variation of seismic reflection coefficient and transmission coefficients with offset (the shot point and the receiver) or angle of incidence. Ostrander (1984) introduced the concept of AVO. It is a seismic analysis technique that uses the amplitude of the pre-stack seismic data for Hydrocarbon exploration. AVO can also be used to map lithologies (Aminzadeh and Dasgupta, 2013).

AVO modelling links the petrophysical parameters of the rocks to the seismic elastic properties. Seismic wave propagation and signatures directly depends on the seismic rock properties. These properties can be grouped into basic rock properties (P-wave velocity, S-wave velocity, Density, Vp/Vs ratio, Poisson's ratio), Impedance, modulus rock properties (Bulk modulus, Shear modulus, lamé's constant) and anisotropic rock properties (Li et al., 2007). The common task in the AVO modelling is to generate a synthetic seismogram from a given earth model. The generated seismogram is then compared with a real dataset in other to draw conclusion based on the comparison between the two (Hampson, 1991).The Forward modelling approach is commonly adopted in AVO modelling. Other approaches that are applied in AVO modelling includes: single interface modelling, single-gather modelling , 2D and 3D stratigraphic modelling, 2D and 3D elastic wave equation modelling (Li et al., 2007). Forward modelling of seismic reflections at an interface between two half-space involves setting an expectation for the character of the seismic traces or amplitudes between the overburden shale and sand reservoir at different fluid contacts as well as different unconformities. Computing the AVO modelling between two half space requires the elastic properties of both half-spaces (Dvorkin et al., 2014). The Forward modelling approach involves a trade-off between the complexity of the modelling system and the computer time required to compute the synthetic (Hampson-Russell, 2013).

In this work, the MATLAB software by Mathworks and the Hampson Russell Geoview were used to carry out the AVO modelling.

4.1 THEORY:

When a Seismic energy hits an interface, it partitions into a reflected and a transmitted energy (Castagna and Backus, 1993). For a non-zero angle of incidence, the P-wave energy is converted into an S-wave which is both reflected, and transmitted. Thus, the reflectivity is not only a function of the acoustic impedance difference but also a function of the S-wave as shown in Figure 4.1 (Aminzadeh and Dasgupta, 2013). According to Rutherford and Williams (1989), the Poisson's ratio at the interface between two layers of rocks also influences AVO in addition to the reflection coefficient. Ostrander (1984) collaborated Rutherford and Williams (1989) statement by saying that the P-wave reflection coefficient is dependent on the incident angle, and the Poisson's ratio between an interface such that a small change on the angle of incidence will result in a large difference in the reflection coefficient.

Considering a normal incident seismic wave on an interface, Zoeppritz and VIIIB (1919) suggested a simple equation to derive the reflectivity of the waves as:

$$R_{pp}(0) = \frac{Z_2 - Z_1}{Z_2 + Z_1} \qquad (4.1)$$

Here:

$R_{pp}(0)$= the normal-incidence P-P reflectivity at zero angle of incidence,

Z_2= Acoustic Impedance (Density*Velocity) of layer 2,

Z_1= Acoustic Impedance (Density*Velocity) of layer 1.

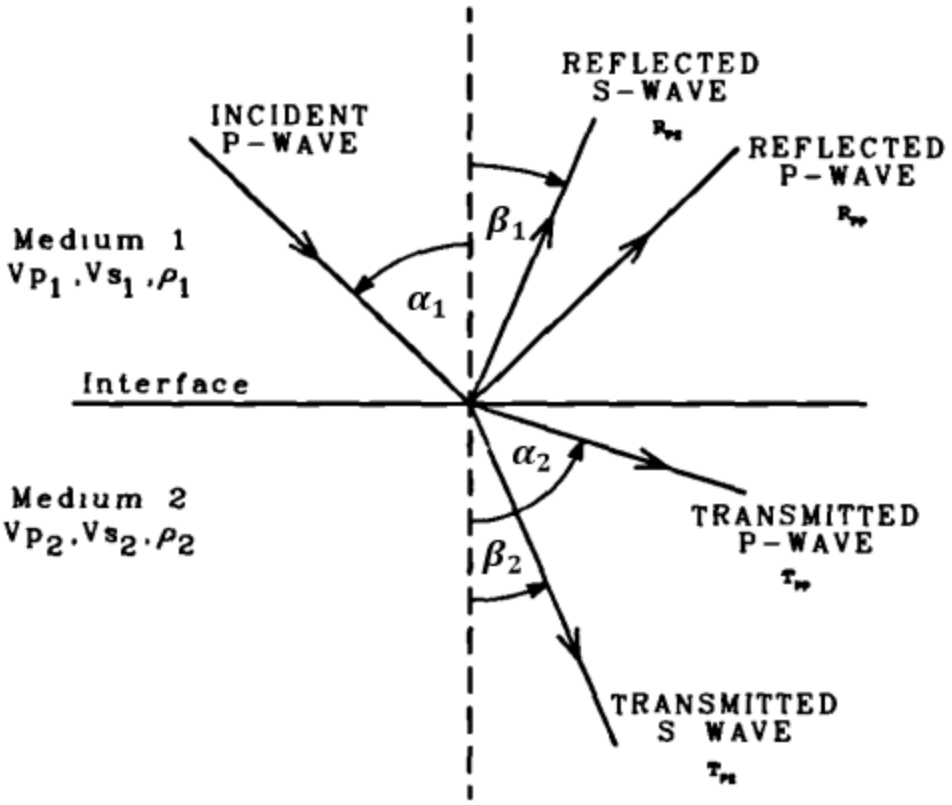

Figure 4.1:Reflection and transmission at an interface for an incident P-wave (modified from Castagna and Backus, 1993).

Using the Snell's law, the angle of incidence, reflected and transmitted rays at a boundary can be related according to (Figure 4.1);

$$p = \frac{\sin \alpha_1}{V_{p1}} = \frac{\sin \alpha_2}{V_{p2}} = \frac{\sin \beta_1}{V_{s1}} = \frac{\sin \beta_2}{V_{s2}} \qquad (4.2)$$

where V_{p1} is the P-wave velocity in medium 1; V_{p2} is the P-wave velocity in mdeium 2; V_{s1} is the S-wave velocity in medium 1; V_{s2} is the S-wave velocity is medium 2; θ_1 is the incident P-wave angle; θ_2 is the transmitted P-wave angle; φ_1 is the reflected S-wave angle; φ_2 is the transmitted S-wave angle, and p is the ray parameter.

For a case when the angle of incidence of becomes non-zero, the equation becomes complicated (Dvorkin et al., 2014). Several approximations (termed AVO approximations) for the Zoeppritz equation has been derived over the years (Aki and Richards, 1980, Smith and Gidlow, 1987, Shuey, 1985, Richards and Frasier, 1976).

The Zoeppritz matrix is expressed as (Aki and Richards, 1980):

$$\boldsymbol{A} = (\boldsymbol{R})^{-1}\boldsymbol{B} \tag{4.3}$$

$$\mathrm{R}=\begin{bmatrix} -\boldsymbol{sin\alpha_1} & \boldsymbol{cos\beta_1} & \boldsymbol{sin\alpha_2} & \boldsymbol{cos\beta_2} \\ \boldsymbol{cos\alpha_1} & -\boldsymbol{sin\beta_1} & \boldsymbol{cos\beta_2} & \boldsymbol{sin\alpha_2} \\ \boldsymbol{2\rho_1 V_{s1} sin\beta_1 cos\alpha_1} & \boldsymbol{\rho_1 V_{s1}(1-2(sin\alpha_1)^2)} & \boldsymbol{2\rho_2 V_{s2} sin\beta_2 cos\alpha_2} & \boldsymbol{\rho_2 V_{s2}(1-2(sin\alpha_2)^2)} \\ \boldsymbol{\rho_1 V_{s1}(1-2(sin\alpha_1)^2)} & \boldsymbol{\rho_1 V_{s1} sin2\beta_1} & \boldsymbol{\rho_2 V_{s2}(1-2(sin\alpha_2)^2)} & \boldsymbol{\rho_2 V_{s2} sin2\beta_2} \end{bmatrix} \tag{4.4}$$

$$\mathrm{B}=\begin{bmatrix} \boldsymbol{sin\alpha_1} & \boldsymbol{cos\beta_1} & \boldsymbol{-sin\alpha_2} & \boldsymbol{-cos\beta_2} \\ \boldsymbol{cos\alpha_1} & \boldsymbol{-sin\beta_1} & \boldsymbol{cos\beta_2} & \boldsymbol{-sin\alpha_2} \\ \boldsymbol{2\rho_1 V_{s1} sin\beta_1 cos\alpha_1} & \boldsymbol{\rho_1 V_{s1}(1-2(sin\alpha_1)^2)} & \boldsymbol{2\rho_2 V_{s2} sin\beta_2 cos\alpha_2} & \boldsymbol{\rho_2 V_{s2}(1-2(sin\alpha_2)^2)} \\ \boldsymbol{\rho_1 V_{s1}(1-2(sin\alpha_1)^2)} & \boldsymbol{-\rho_1 V_{s1} sin2\beta_1} & \boldsymbol{-\rho_2 V_{s2}(1-2(sin\alpha_2)^2)} & \boldsymbol{\rho_2 V_{s2} sin2\beta_2} \end{bmatrix} \tag{4.5}$$

One of the simplest of the AVO approximations is derived by Hilterman (1989). (Dvorkin et al., 2014)

$$\mathrm{R_{pp}}(\theta) \approx \mathrm{R_{pp}}(0)\cos\alpha^2 + 2.25\Delta v \sin^2\boldsymbol{\alpha} \tag{4.6}$$

The above equation is further equated to;

$$\mathrm{R_{pp}}(0) + 2.25\left[\Delta v - \mathrm{R_{pp}}(0)\right]\sin^2\alpha; \tag{4.7}$$

Where:

$\mathrm{R_{pp}}(0) = \frac{\mathrm{Z_2}-\mathrm{Z_1}}{\mathrm{Z_2}+\mathrm{Z_1}}$;

$\Delta v = v_2 - v_1$; The difference in Poisson ratios;

v_2= Poisson ratio of the lower half space;

v_1= Poisson ratio of the upper half space.

Intercept and Gradient is commonly used to characterise AVO curves.

Thus the two term parameter for, Hilterman (1989);

$$R_{pp} = I + G\sin^2\boldsymbol{\alpha} \quad (4.8)$$

Where:

I=$R_{pp}(0)$ called the Intercept,

G=$2.25\left[\Delta v - R_{pp}(0)\right]$ termed Gradient.

The above equations are applicable for small variations in layer parameters and angle of incidence commonly encountered in seismic reflections applications which is less or equal to 30° (Dvorkin et al., 2014).

4.1.1 Shear Wave Prediction

AVO modelling requires a log suite containing P-wave velocity, S-wave velocity, and Bulk density logs. However, the S-wave velocity log is either not available or questionable when present within log suites. In view of this, empirical relations such as the "mudrock line" by Castagna (Castagna et al., 1985), the relation by Krief and the Greenberg-Castagna equation are used to predict or derive the S-wave from the measured P-wave logs within the well based on simple regression. The assumptions here is that there is a linear relationship between the S-wave and the P-wave within a sequence of brine saturated rocks of the same lithology. The 'mudrock line' suggested by Castagna et al. (1985) to explain the trend between brine saturated sandstones and shales. It is proposed that variance on this order is about 5%. The Castagna's mudrock equation was used in the AVO modelling in Hampson Russell Geoview software to predict the S-wave velocity within the non-reservoir formation in this work. The linear relationship between the S-wave and P-wave can be expressed mathematically as:

$$Vp = 1.16Vs + 1.36 \quad (4.9)$$

Vp and Vs are the P-wave velocity and the S-wave velocity respectively in km/s. (Dvorkin et al., 2014).

The Greenberg-Castagna's method combines the empirical relations between the P-wave and S-wave velocities with the Gassmann's equations and accounts for mix lithologies and fluids. Multiple regressions are carried out to predict the S-wave velocity. The average of the harmonic and arithmetic averages is the S-wave velocity (Mavko et al., 2009).

The Greenberg-Castagna's relation is expressed as:

$$\mathrm{Vs} = aVp^2 + \mathrm{bVp} + c \qquad (4.10)$$

where a, b, c are coefficient which depends on type of lithologies,

Vp and Vs are the P-wave and S-wave velocities in km/s.

For sandstones and shale, the coefficients are presented in table…

Table 4.1:Regression Coefficients for Sandstone and Shale Lithologies used in the Greenberg-Castagna's equation (Mavko et al., 2009)

Lithology	a	b	c
Sandstone	0	0.804 16	-0.855 88
Shale	0	0.769 69	-0.867 35

In this work, the Greenberg-Castagna's equation was used to estimate the S-wave velocity in the reservoir (Garn-Formation) during the AVO modelling of the Garn reflector.

For a detailed discussion on the Shear wave velocity estimation please see (Greenberg and Castagna, 1992). Other empirical relations (Dvorkin, 2008, Han et al., 1986) have been proposed by different authors over the years in regards to estimating the shear wave velocity .

4.2 AVO CLASSES

AVO is classified into four types in Geophysics. Rutherford and Williams (1989) classified AVO responses of a gas sand based on the characteristic Impedance, gradient and the reflection coefficients.

4.2.1 AVO Class 1:

A strong positive impedance, negative gradient and a positive reflection coefficient, which decreases with the angle of incidence or offset, typify this class of AVO .

4.2.2 AVO Class 2:

This class of AVO response is characterised by a small normal incident or impedance, the gradient is negative. The reflectivity is minimal, and it decreases with offset.

4.2.3 AVO Class 3:

This class of AVO response have a large negative reflection coefficient at normal incidence and the magnitude increases with offset. Thus, impedance decreases and anomaly starts with a high amplitude and increases further with offset.

4.2.4 AVO Class 4:

Castagna and Swan (1997) named this class of AVO characterised by a decrease in Impedance. The amplitude starts high and decreases with offset .

Figure 4.2 below shows the plots of the various AVO classes described above (Simm et al., 2014, Bacon et al., 2007).

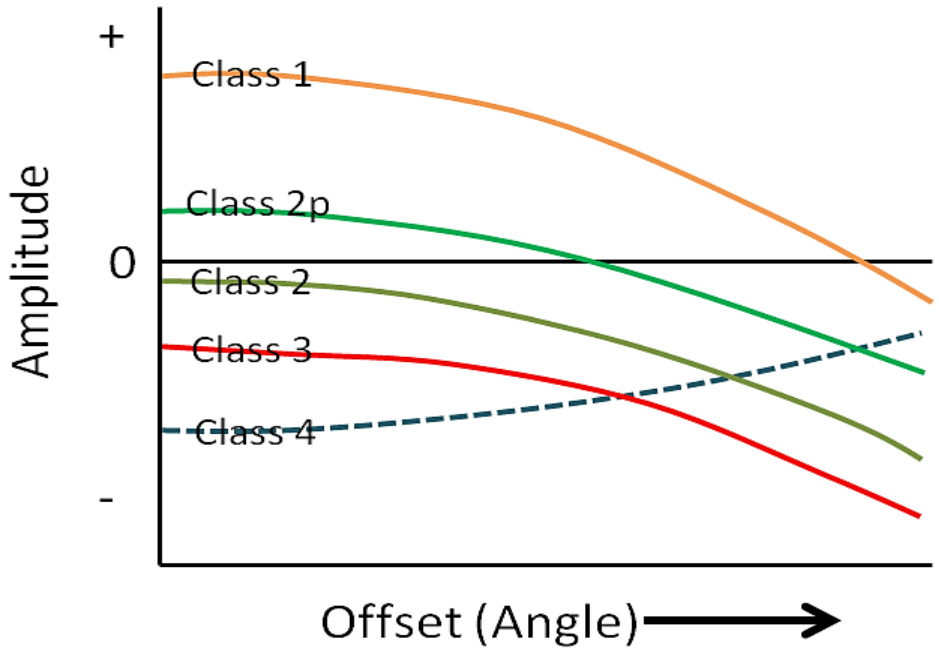

Figure 4.2: Classification of AVO responses class 1, class 2, class 3 and class 4 (Rutherford and Williams, 1989).

AVO signatures can be analysed or interpreted using the seismic extracted intercept and gradient as shown in Figure 4.3. This is commonly associated with the non-hydrocarbon reservoirs, which in the absence of hydrocarbon-bearing strata shows a well-defined 'background trend' when cross-plotted (Castagna et al., 1998).

Castagna et al. (1998) described simple formulas and 'rules of thumb' that aid AVO cross-plot interpretation. One of the approach used involves keeping the intercept term on one axis of the cross-plot, then recombine the intercept and gradient to provide a second axis more directly related to rock properties. The Wiggins et al. (1983) approximation is adopted here which assumes the ratio of the P-wave velocity to S-Wave velocity (Vp/Vs) as 2 (Dvorkin et al., 1999).

Another approach is to use the 'fluid angle' and the 'fluid line' of (Foster et al., 1993) as a reference point then cross-plot the Intercept and Gradient terms directly. Although in this work, we are only looking at the lithology and Pore-pressure effects.

To derive the background trend, the P-Wave velocity, S-Wave velocity and density are correlated by using different methodologies in order to establish a relationship between the angular coefficients of the Intercept and Gradient (Dvorkin et al., 2014).

Other relations regarding the relationships between the AVO Intercept and Gradient can be found in (Castagna et al., 1998).

The AVO classifications based on the cross-plot between the Gradient and the Intercept is shown in Figure 4.3 below.

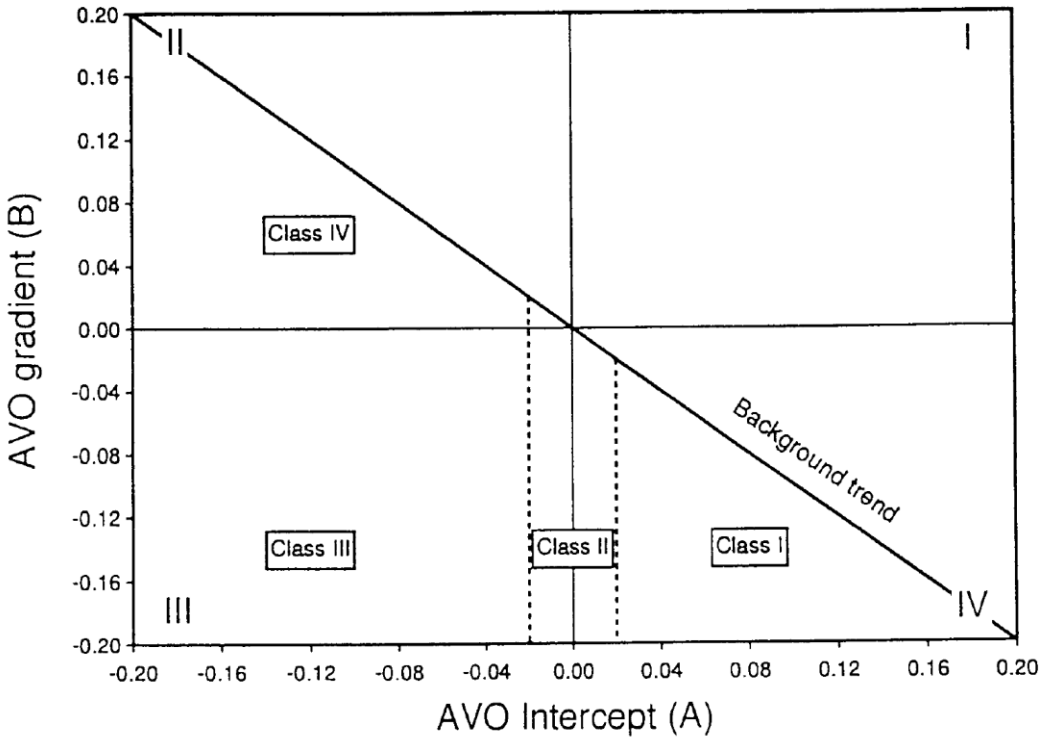

Figure 4.3: Crossplot of AVO intercept versus AVO gradient, showing the possible quadrants I-IV (Castagna et al., 1998).

4.3 TYPES OF SEISMIC MODELS

The Zoeppritz equations and its approximations are used as algorithms to model reflectivity response with offsets. The common types of seismic models are (Rock-Physics-Associates, 2007):

- The single interface model,
- The wedge model,
- The layered model.

The single interface model is a simple model that inputting the parameters (P-wave velocity, S-wave velocity, and density) for the upper and lower layers into the modelling algorithm (Zoeppritz, Shuey, Smith and Gidlow, Hilterman etc.) Figure 4.4 (Rock-Physics-Associates, 2007).

The wedge model explains interactions between reflections of two converging interfaces, while the layered model address the interface effects of fine layering and the mode of propagation of seismic waves Figure 4.4. The single interface and the layered models are considered specifically in this work (Rock-Physics-Associates, 2007).

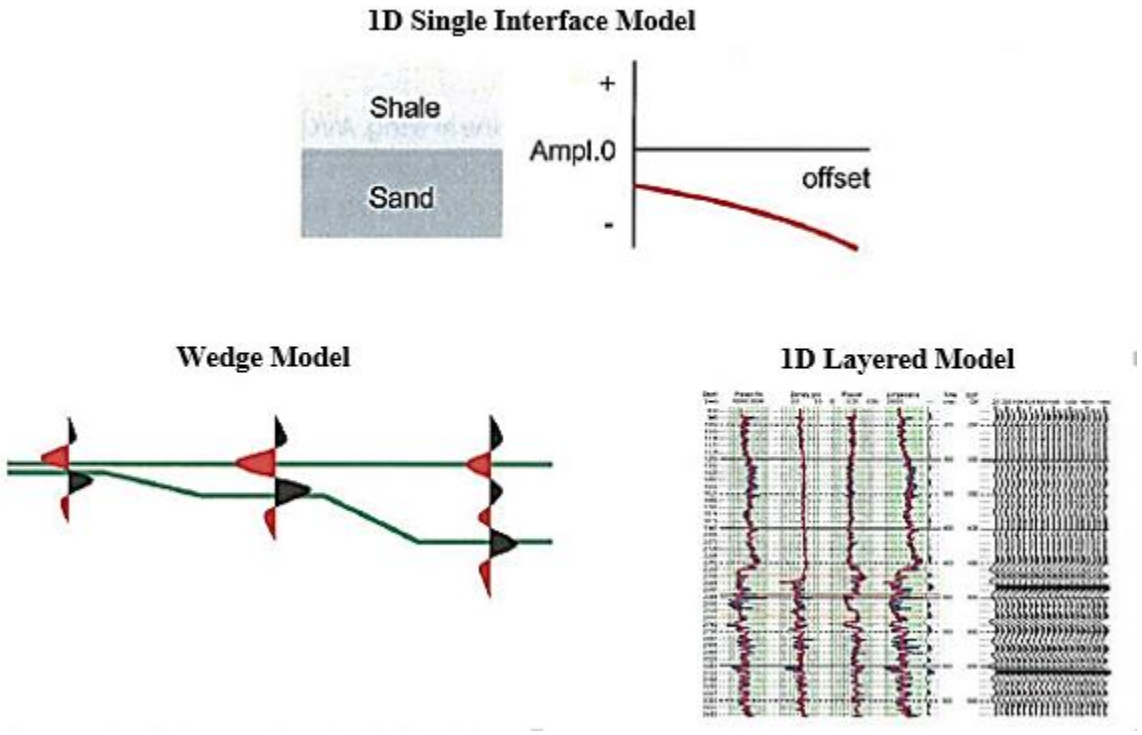

Figure 4.4: Types of Seismic Models modified from (Rock-Physics-Associates, 2007)

4.4 METHODOLOGY

Having established the velocity versus differential stress relationship within the brine saturated Garn Formation for the selected wells as seen in section 3.7, one of the wells (**Well 6506/12-1**) was used for an AVO modelling in order to investigate the effects of lithology and overpressure on the AVO response of the brine saturated Garn Interface against the Lyr Formation and the overdurden Lyr-Spekke-Melke within the well. The differential stress conditions considered are as follows:

- At In-situ stress condition (36MPa),
- At 20 MPa (Pore-pressure Increase),
- At 50 MPa (Pore-pressure Decrease).

The criteria for choosing the brine-filled well is that the well must have the Spekke, Melke and Lyr Formations on top of Garn.

In essesnce, the differential stress within the **Well 6506/12-1** is 36 MPa. This is the in-situ differential stress condition. We want to investigate the AVO response of the interface between the Lyr on top brine saturated Garn reflector and that of the interface between the overburden Lyr-Spekke-Melke on top of the brine saturated Garn reflector within this **Well 6506/12-1** at other differential stress conditions of 20 MPa and 50 MPa respectively.

The average elastic properties (Vp, Vs and density) at 20MPa and 50MPa conditions for the Lyr Formation and the overburden Lyr-Spekke-Melke Formation are assumed to be constant, while the average properties within the brine saturated Garn Formation is assumed to vary at the different differential stress conditions. The average velocities (Vp, and Vs) within the brine saturated Garn Formation at 20MPa and 50MPa are estimated by reading-off the average values at the points that corresponds to 20MPa and 50MPa on the Vp and Vs curve as illustrated in Figure 4.5 below.

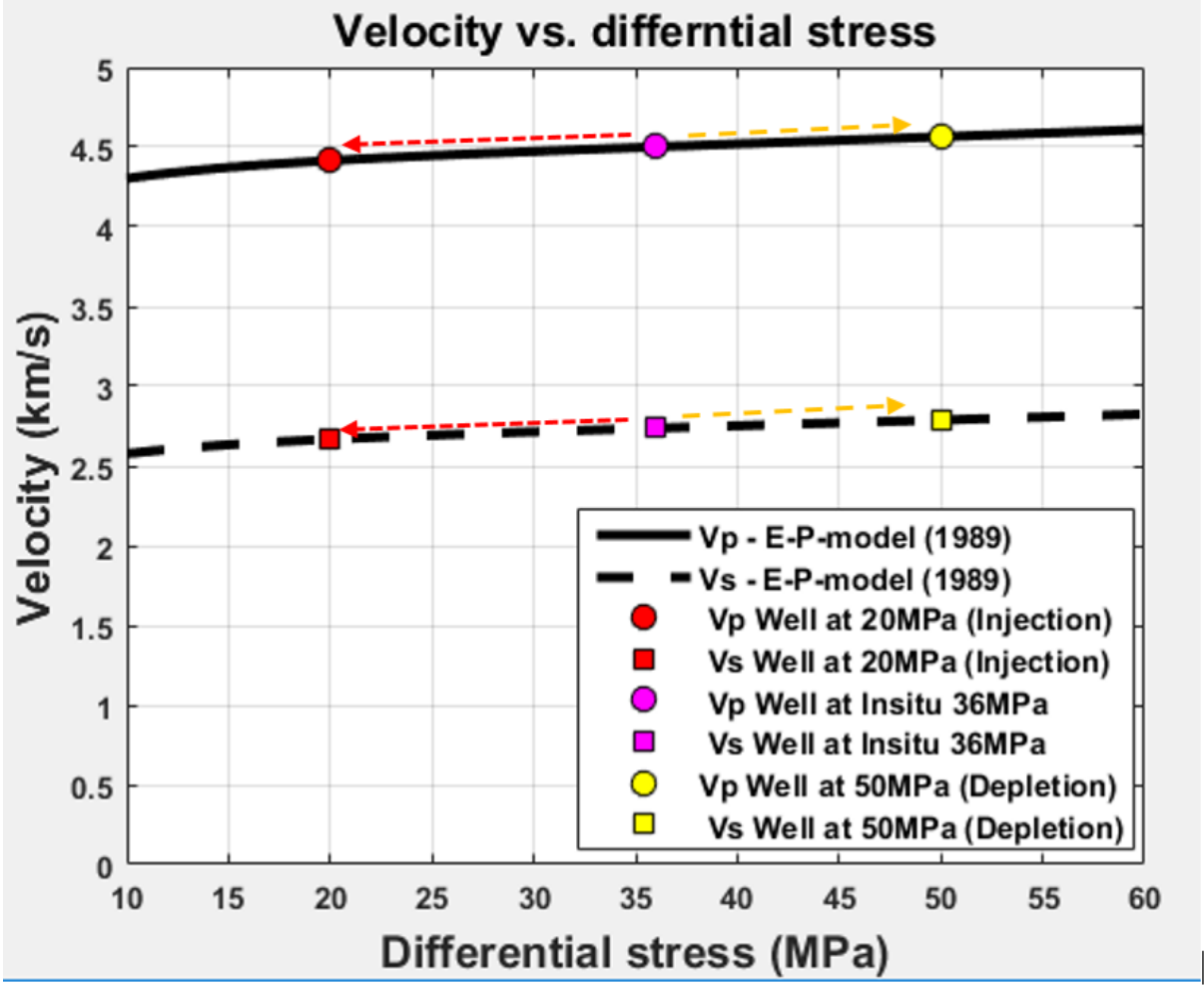

Figure 4.5: This figure shows the Well 6506/12-1 at the 36MPa Insitu differential stress condition, at 20 MPa (assumed Injection well) and 50 MPa (assumed depletion well) conditions. To estimate the Vp and Vs of the brine filled Garn Formation at the 50MPa, trace the yellow arrow and read-off the average values at the points indicated. Use the red arrow to read off the Vp, Vs estimated average values in the case of the 20MPa (assumed injection well) condition.

The single interface 1D AVO modelling was carried out using the MATLAB (Mathworks) software while the layered AVO 1D modelling method was carried out in the Hampson Russell Geoview Software. The procedures are detailed in the following sections.

4.4.1 AVO Modelling in MATLAB

The single interface 1D AVO modelling for the Lyr on top of the brine saturated Garn, and the overburden Lyr-Spekke-Melke on top of the Garn Formation requires the average properties of the different layers sharing the interface. The average elastic properties (Vp, Vs and density) are computed in MATLAB by blocking the Lyr interval (depth) and using a simple arithmetic averaging method to calculate the average velocities (Vp and Vs) and density within the interval. This method is also applied to estimate the average elastic parameters for the overburden Lyr-Spekke-Melke interval also.

Now we have the average elastic parameters for the different layers (Lyr Formation, the overburden Lyr-Spekke-Melke and the brine saturated Garn Formation). The next step involves the programming of the Zoeppritz matrix equation (equations 4.3 to 4.5) into MATLAB. The estimated average elastic parameters (Vp, Vs, and density) of the Lyr, the Lyr-Spekke-Melke and the Garn Formations computed using the Backus averaging technique as described in section 3.7 are then inputted into MATLAB to create the reflectivity variations with offset and the gradient versus intercept AVO crossplots using the Zoeppritz function in MATLAB.

The Lyr Formation does not sit directly on the brine saturated Garn Formation, therefore a MATLAB code was inputted to remove the Spekke-Melke Formations from the well log signature. So that the AVO modelling condition where the Lyr sits on top Garn is achieved or fulfilled.

The curves and crossplots are made with regards to the different differential stress conditions within the brine saturated Garn Formation. i.e. “at the In-situ stress condition of the well at 36 MPa, a reflectivity curve and a gradient versus intercept AVO crossplot was made for interface between the ‘Lyr on top of the Garn reflector’ and the interface between the ‘Lyr-Spekke-Melke on top of the Garn reflector (Figure 4.6 and 4.7), at 50 MPa Figure 4.8 and 4.9 (For a decrease in the pore-pressure) and at 20MPa Figure 4.10 and 4.11 (For an increase in the pore-pressure)” respectively. A total of six models was created as shown in Figures 4.4 to Figure 4.10.

At the In-situ differential stress condition (36 MPa), the default average elastic properties (Vp, Vs, and density) for the Garn, the Lyr, and the Lyr-Spekke-Melke Formations were used. When the differential stress was changed to 20 MPa and 50 MPa, the average elastic properties (Vp, Vs, and

density) within the Lyr, and Lyr-Spekke-Melke Formations were kept constant as stated earlier while the average elastic properties of the brine saturated Garn Formation are changed by reading of the average values at the 20MPa and 50MPa on the curve as shown in Figure 4.5. An 'ASC' file that will be used for the layered 1D AVO modelling in Hampson Russell Geoview was generated using by a code in MATLAB.

The summary of the average parameters used in the AVO modelling in MATLAB for the different differential stress conditions are given in Table 4.2, 4.3 and 4.4 for the In-situ 36MPa , 50MPa and 20MPa differential stress conditions.

4.4.2 Results

The results of the single interface 1D AVO modelling for the Lyr on top of the Garn Formation, and the Lyr-Spekke-Melke Formations on top the Garn Formation using MATLAB for the different differential stress conditions are displayed in Figure 4.6 to Figure 4.11. The offset dependent reflectivity curve for the three different stress conditions (36MPa, 50MPa, and 20MPa) are shown in Figure 4.6, Figure 4.8, and Figure 4.10, while the gradient versus intercept cross-plots are displayed in Figure 4.7, Figure 4.9, and Figure 4.11 respectively.

4.4.2.1 AT IN-SITU CONDITION (36 MPa)

Table 4.2: Showing the average properties of the rocks at In-situ differential stress condition (36MPa) computed using the Backus averaging technique for the reference **Well 6506/12-1** used for the single interface 1D AVO modelling in MATLAB.

Interfaces	Vp	Vs (Greenberg-Castagna)	Density
	Well at 36Mpa		
Lyr-Spekke-Melke	3396.2	1778.1	2463.6
Garn	4538.3	2792.4	2416.4
Lyr	3261.1	1707.6	2558.8
Garn	4538.3	2792.4	2416.4

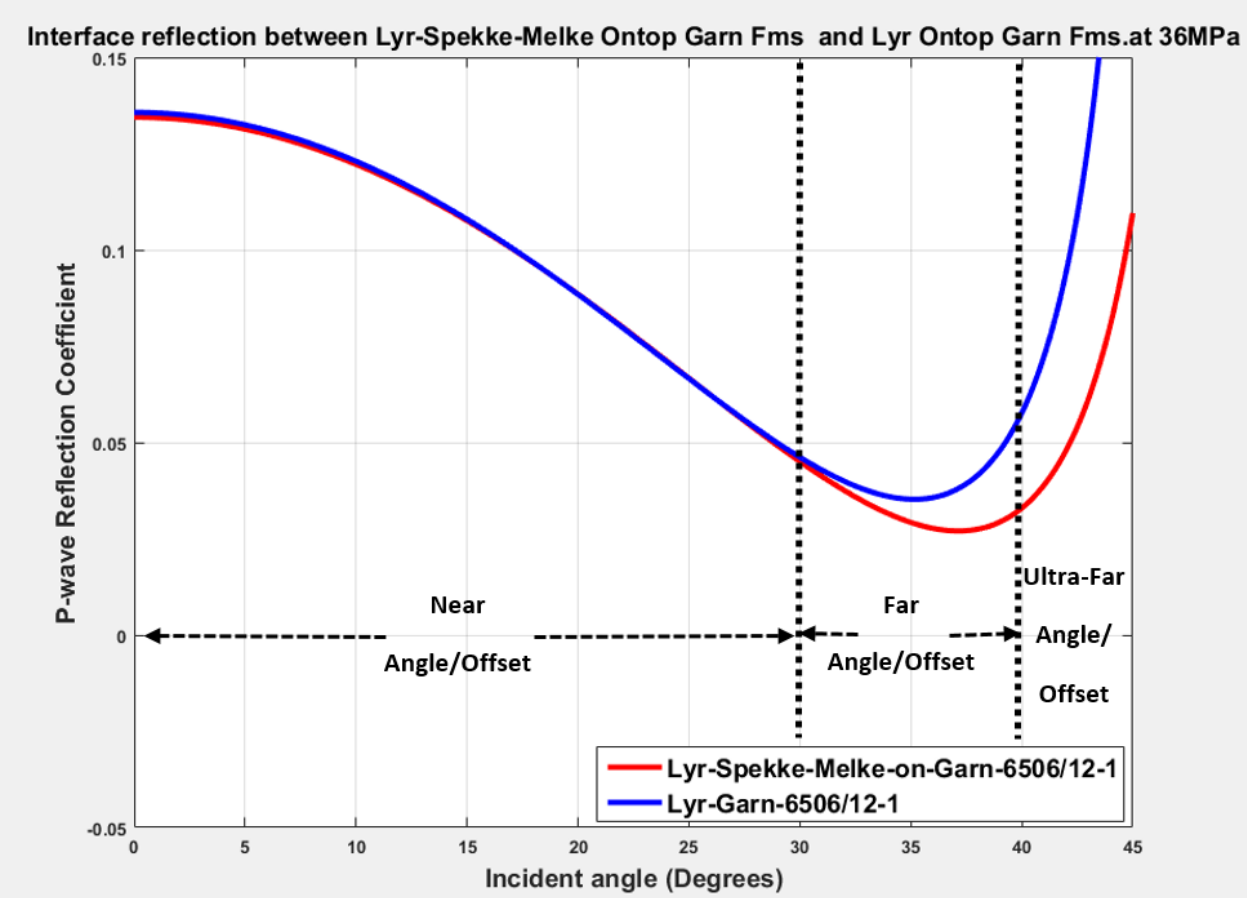

Figure 4.6: Comparison of the reflectivity signatures with angle for the single interface modelling between the Lyr on top of the Garn reflector (Blue Curve) and the Lyr-Spekke-Melke overburden on top of the Garn reflector (Red Curve) for the **Well 6506/12-1** at 36 MPa computed with the Zoeprritz equation. The figure shows the Near Angle/Offset (0° to 30 °), Far Offset/Angle (30° to 40°) and the Ultra-Far Offset/Angle above 40°.

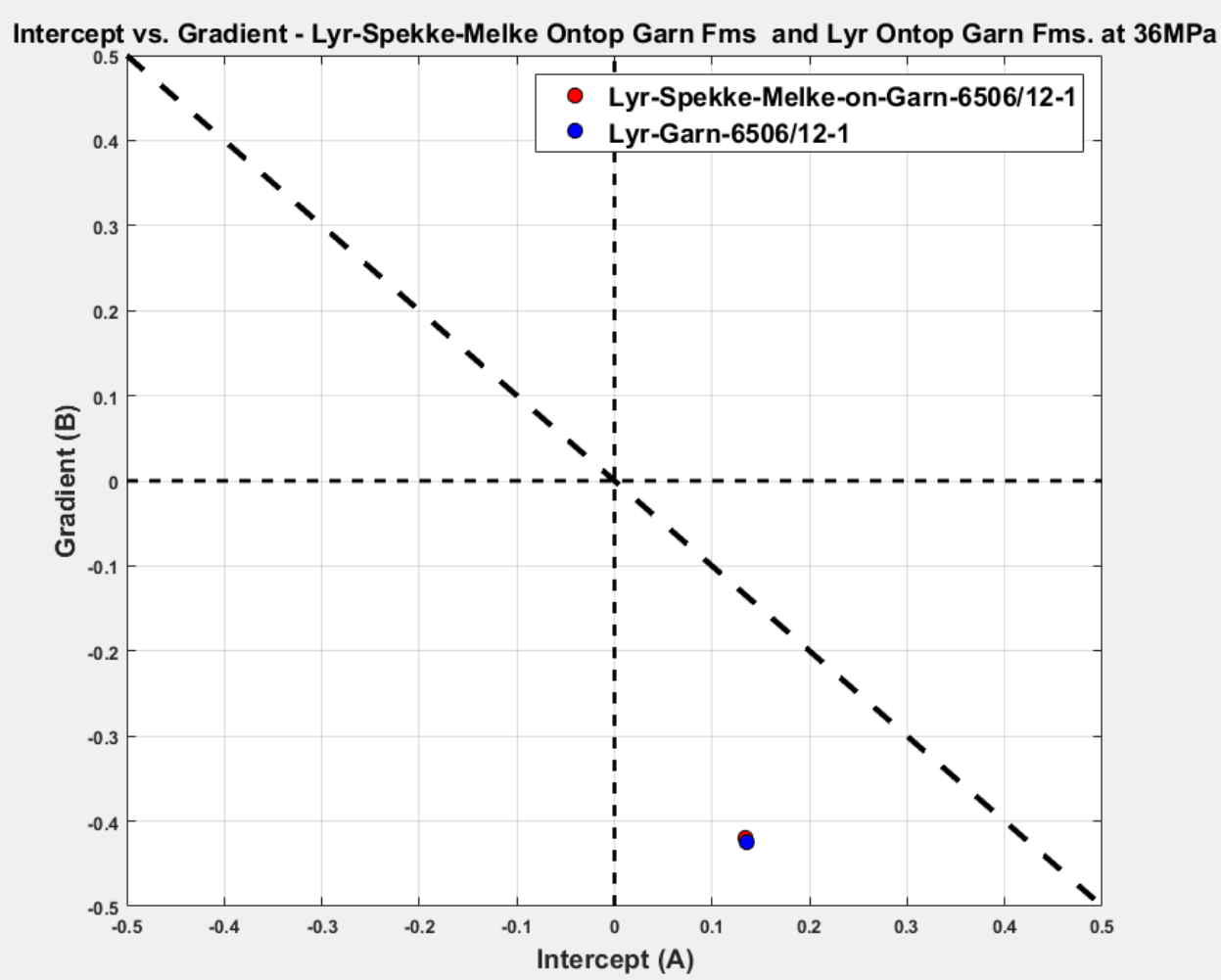

Figure 4.7: The Gradient-Intercept crossplots of the single interface Lyr-Garn reflector and the Lyr-Spekke-Melke on the Garn reflector at (Insitu) 36 MPa stress condition for Well 6506/12-1. The Crossplot shows a negative gradient values and a positive Intercept values for both case scenarios where we have the Lyr on top of the Garn Formation, and the Lyr-Spekke-Melke Formations on top of the Garn Formation respectively. They both seems to plot at almost the same point.

4.4.2.2 AT 50 MPa CONDITION (PORE-PRESSURE REDUCTION) USING MATLAB.

Table 4.3: Showing the average properties of the rocks at 50 MPa differential stress condition computed using the Backus averaging technique for the reference Well 6506/12-1 used for the single interface AVO modelling in MATLAB.

Interface	Vp	Vs (Greenberg-Castagna)	Density
	Well at 50 MPa		
Lyr-Spekke/Melke	3396.2	1778.1	2463.6
Garn	4565	2808.4	2416.4
Lyr	3261.6	1707.6	2558.8
Garn	4565	2808.4	2416.4

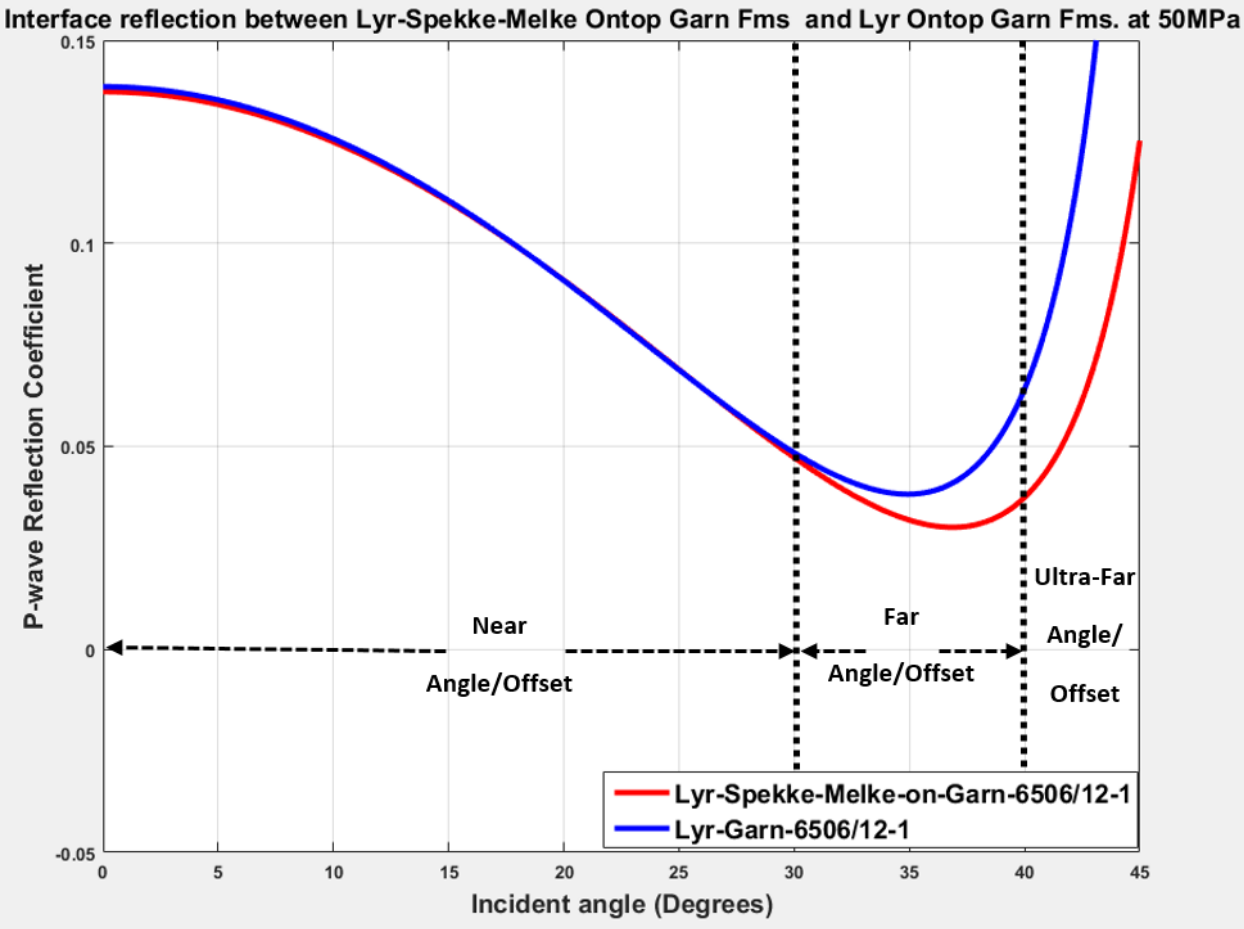

Figure 4.8: Comparison of the reflectivity signatures with angle for the single interface modelling between the Lyr on top of the Garn reflector (Blue curve) and the Lyr-Spekke-Melke on top of the Garn reflector (Red Curve) for Well 6506/12-1 at 50 MPa computed with the Zoeprritz equation. The figure shows the Near Angle/Offset (0° to 30 °), Far Offset/Angle (30° to 40°) and the Ultra-Far Offset/Angle above 40°.

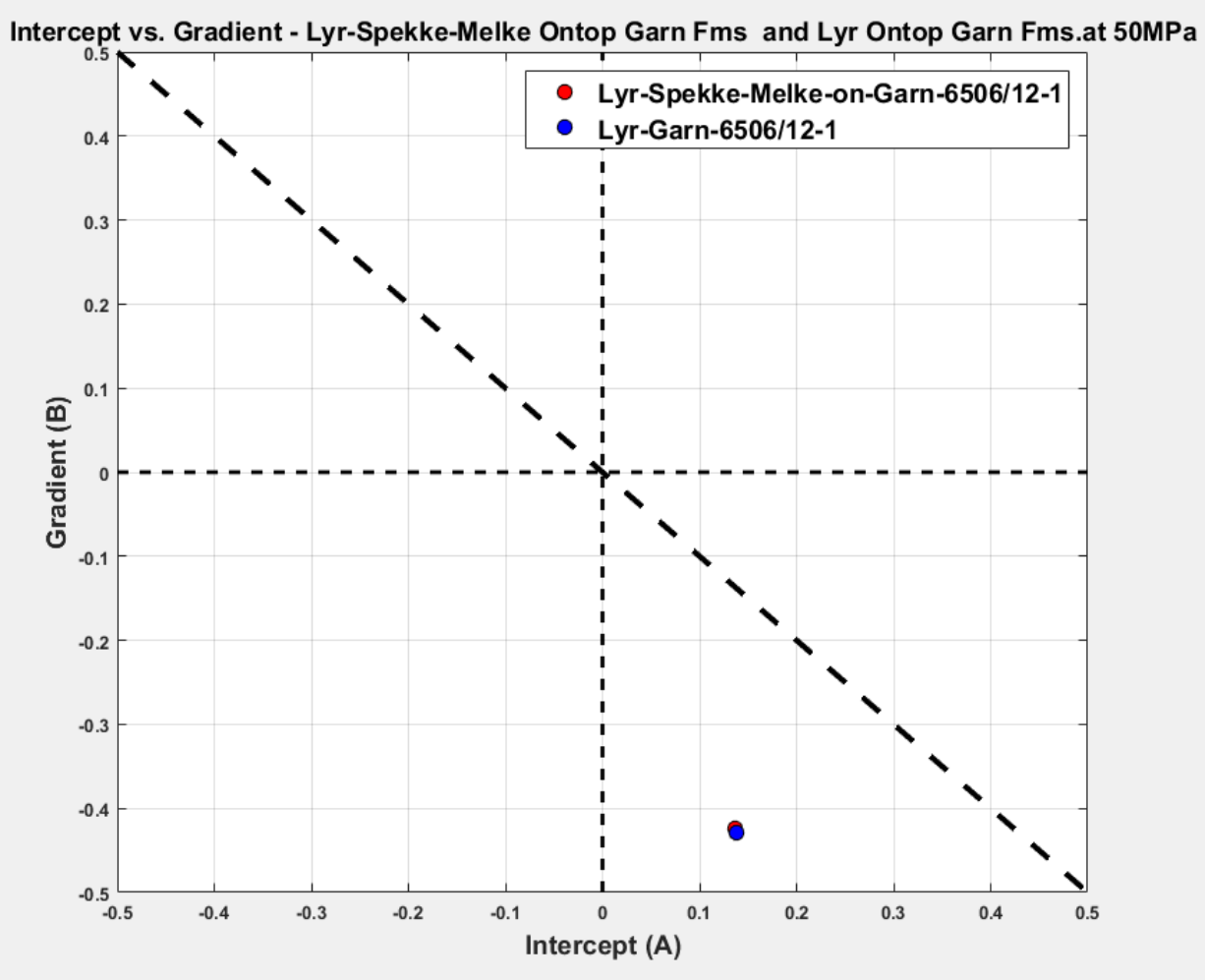

Figure 4.9: The Gradient-Intercept crossplots of the single interface Lyr-Garn reflector and the Lyr-Spekke-Melke on the Garn reflector at (Insitu) 36 MPa stress condition for the Well 6506/12-1. The Crossplot shows a negative gradient values and a positive Intercept values for both case scenarios where we have the Lyr on top of the Garn Formation, and the Lyr-Spekke-Melke Formations on top of the Garn Formation respectively. They both seems to plot at almost the same point.

4.4.2.3 AT 20 MPa CONDITION (PORE-PRESSURE INCREASE) USING MATLAB.

Table 4.4: Showing the average properties of the rocks at 20 MPa differential stress condition computed using the Backus averaging technique for the reference Well 6506/12-1 used for the single interface AVO modelling in MATLAB

Interface	Vp	Vs (Greenberg-Castagna)	Density
	Well at 20 MPa		
Lyr-Spekke-Melke	3396.2	1778.1	2463.6
Garn	4416	2688	2416.4
Lyr	3216.6	1707.6	2558.8
Garn	4416	2688	2416.4

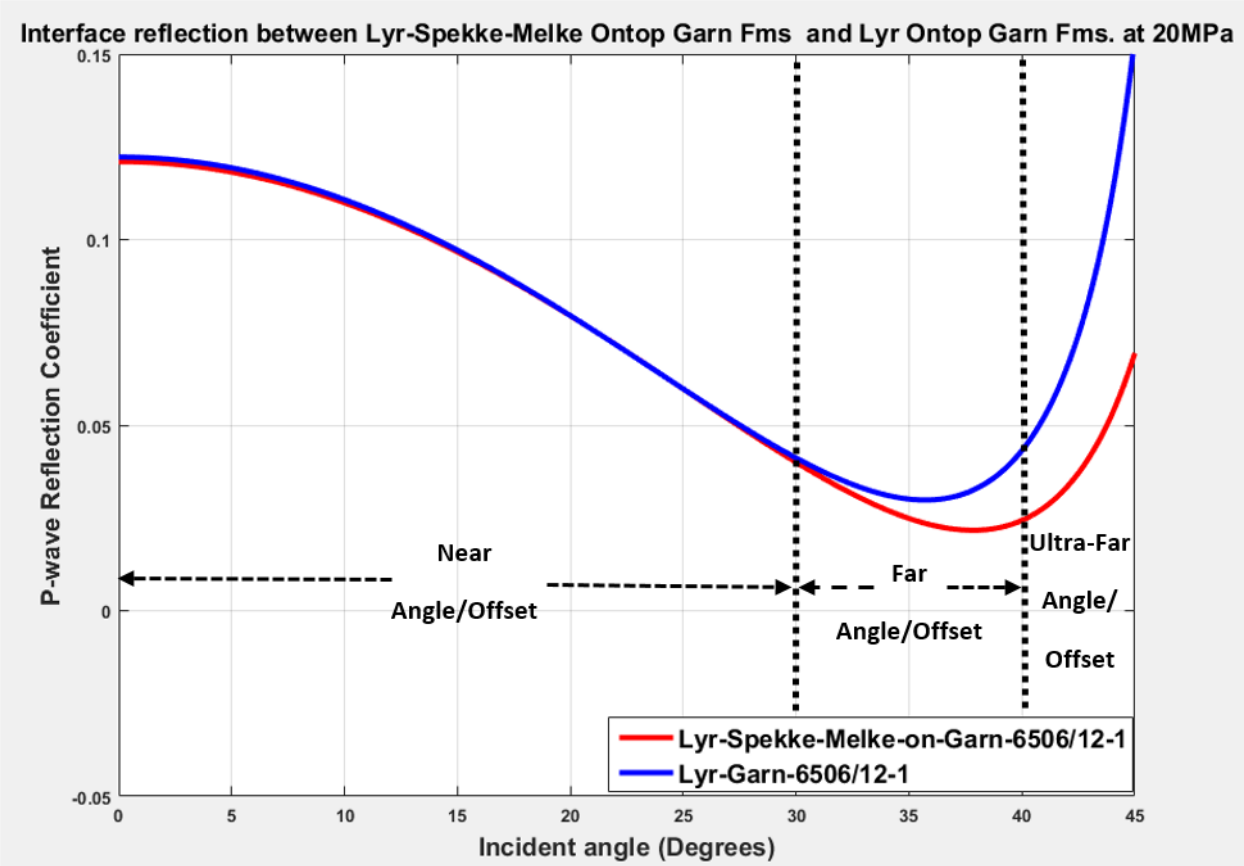

Figure 4.10: Comparison of the reflectivity signatures with angle for the single interface modelling between the Lyr on top of the Garn reflector (Blue curve) and the Lyr-Spekke-Melke on top of the Garn reflector (Red Curve) for the Well 6506/12-1 at 20 MPa computed with the Zoeprritz equation. The figure shows the Near Angle/Offset (0° to 30 °), Far Offset/Angle (30° to 40°) and the Ultra-Far Offset/Angle above 40°.

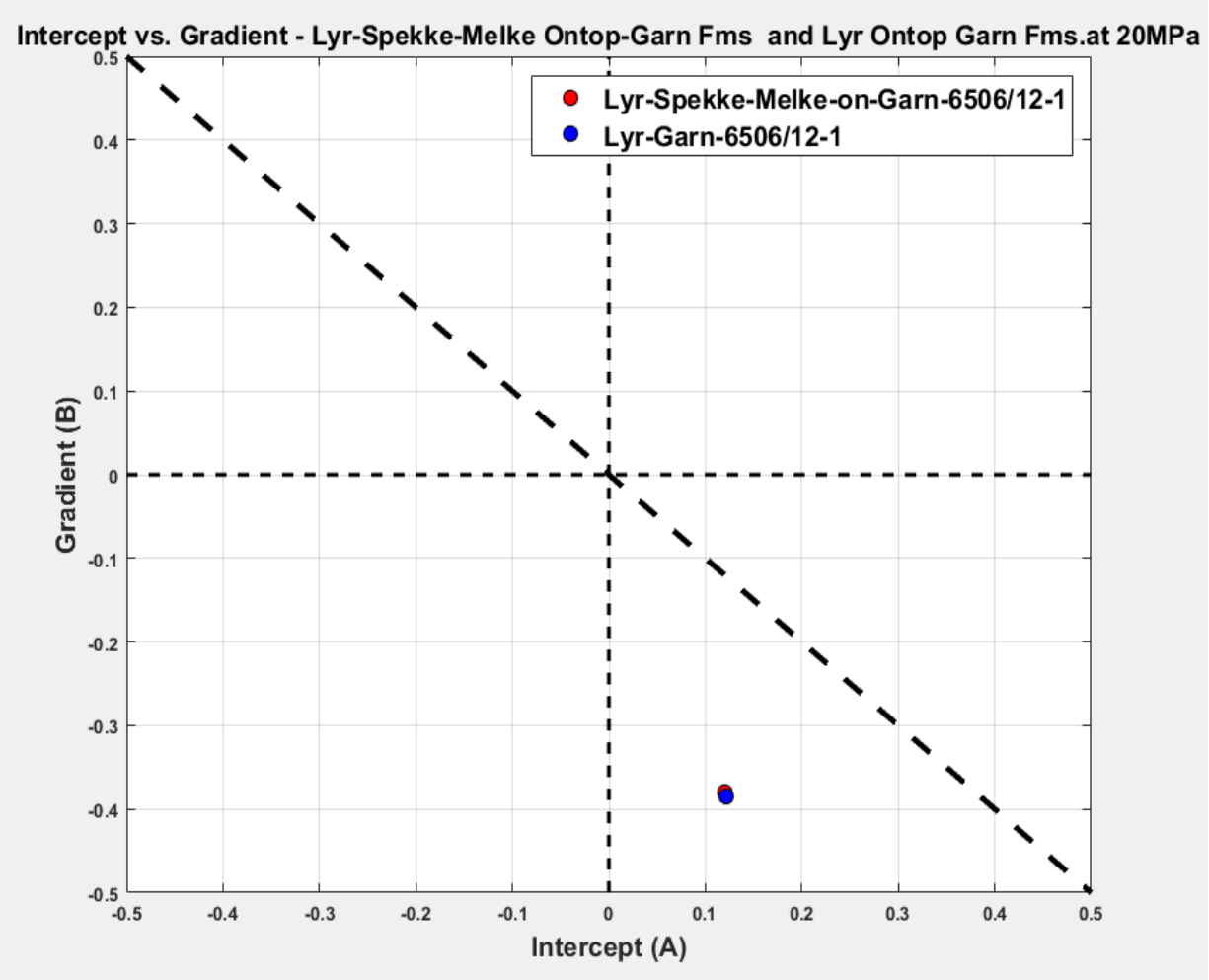

Figure 4.11: Comparison of the Gradient-Intercept crossplots of the single interface Lyr-Garn reflector and the Lyr-Spekke-Melke on the Garn reflector at (Insitu) 20 MPa stress condition for Well 6506/12-1. The Crossplot shows a negative gradient values and a positive Intercept values for both case scenarios where we have the Lyr on top of the Garn Formation, and the Lyr-Spekke-Melke Formations on top of the Garn Formation respectively. They both seems to plot at almost the same point.

Table 4.5: A summary of the AVO Modelling in MATLAB showing the Interfaces, the Stress Conditions, and the Reflectivities at Near Angle/Offset, Far Angle/Offset and Ultra-Far Angle/Offset.

Stress Conditions (MPa)	**Interfaces**	**Near Angle/Offset (0-30°)**	**Far Angle/Offset (30°-40°)**	**Ultra-Far Angle/Offset (40°-45°)**
20 MPa	**Lyr-Spekke-Melkeon Top Garn**	0.1210	0.0248	0.0391
	Lyr on top Garn	0.1223	0.0301	0.0782
36MPa	**Lyr-Spekke-Melkeon Top Garn**	0.1345	0.0292	0.0604
	Lyr on top Garn	0.1357	0.0353	0.1146
50MPa	**Lyr-Spekke-Melkeon Top Garn**	0.1373	0.0318	0.0664
	Lyr on top Garn	0.1386	0.0382	0.1152

4.4.3 AVO Modelling in Hampson Russell

This section explains the procedures and workflows used for the AVO modelling in Hampson Russell software. The well log data for **Well 6506/12-1** was also used for the AVO modelling in Hampson Russell.

The Hampson Russell allows carrying out AVO modelling and analysis in several ways. These are AVO reconnaissance analysis, forward modelling and AVO inversion. The forward modelling approach was used in this work. This approach is fast and involves a trade-off between the complexity of the modeling system and the computer time required to calculate the synthetic. AVO modelling is carried out using the Hampson Russell Geoview Software for 'In-situ' and 'what if' case scenarios (Hampson-Russell, 2013).

AVO modelling was carried under the following conditions:

- The Lyr Formation on top of Garn at **36 MPa, 50 MPa and 20 MPa** stress conditions,
- The Lyr-Spekke-Melke Formation on top of the Garn Formation at **36 MPa, 50 MPa and 20 MPa** stress conditions.

The ASC file format that was generated using MATLAB was imported into Hampson-Russell Geoview. The wireline log signatures were created using the imported data at a uniform sampling rate of 0.152.

The S-wave log was created in Hampson Russell software, using the Greenberg-Castagna's method for pure lithologies for reservoir sections while the Castagna's (mudrock) equation was applied for outside the reservoir using the P-wave as input in the log transform function of the software.

The ricker wavelet was used to generate the needed syntheic seismograms needed for AVO analysis. Acoustic impedance corresponds to a peak within the synthetic traces. A wavelet is the signature of a seismic source which defines the amplitude spectrum and the phase spectrum of the seismic source. the parameters used in the wavelet used in this project is as follows:

Peak= Increase in Acoustic Impedance (Normal),

Wavelet phase Type= Linear Phase,

Domain Frequency= 10,

Phase Rotation= 0,

Sample Rate (ms)= 2,

Wavelet Length=200

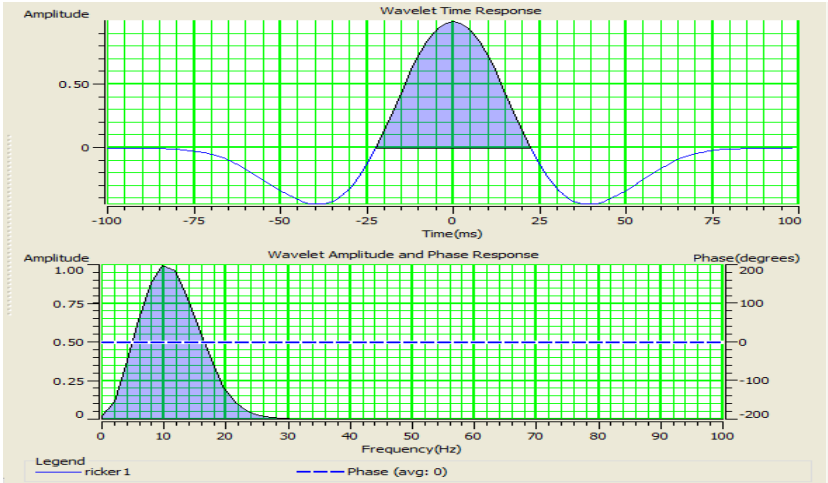

Figure 4.12: Ricker wavelet used in synthetic modelling in time and frequency domains

To create a synthetic seismogram for AVO modelling in Hampson Russell, different algorithms such as the Zeoprittz equation, Aki-Richards and the elastic wave equation are used. The ray tracing can be used to calculate angles as well as arrival times. The Aki-Richards equation (Aki and Richards, 1980) combined with ray tracing is usually used to generate a primaries-only synthetic gather. It is a fast and robust way of looking at modeled gathers. The full Zoeppritz equations can also be used.

The elastic wave equation can be used (direct waves, primary and multiple reflection waves, converted waves, head waves, and diffractions). The elastic wave method is usually done in 1D sense and does not require migration of data used (Chopra and Castagna, 2014). The Ray-tracing and Zoeprritz algorithm was used to create the synthetic seismogram used in this work. The automated ray tracing was used to calculate the angle of incidence which was used to generate an offset or angle dependent synthetic seismogram. The Zoeppritz equation was used to compute the amplitudes, while the Aki-Richard equation was used to analyse the amplitudes. An offset range of 0 to 4000m was used in this work.

Horizon processing was carried out through the picking of the top Garn formation with the rubber-band mode. The essence is to easily identify the AVO signature of the Lyr on top Garn and Lyr-Spekke-Melke on top Garn interfaces.

In summary, the following steps were taken to achieve the AVO modelling. This applies to the different stress conditions for 36 MPa, 50 MPa and 20 MPa and the case of changing the lithologies from Lyr Formation to the Lyr-Spekke-Melke Formations sitting on top Garn.

- A database was created in Hampson Russell,
- Import the different well log data and top Formations (the ASC files generated using MATLAB),
- A sampling rate of 0.152 was used in this work,
- The imported log values are in TVD measured from the surface,
- Compute the S-wave within the Reservoir interval using the Greenberg-Castagna's method within the reservoir, and the Castagna's mudrock equation for the non-reservoir section,
- Create wavelet (Ricker wavelet) using dominant frequency of 10Hz, Phase rotation =0, Sample rate = 2, and wavelength of 200m.
- Create the synthetic AVO seismogram using the Zoeppritz algorithm. The offset used was 60, setting the Near-offset to be 0 while the Far-offset was 4000m.
- Pick the horizon (Garn reflector) to analyse using the two term Aki-Richards algorithm.
- Perform the AVO analysis.

4.4.4 Results

The results of the layered 1D AVO modelling of the interface between the Lyr Formation on top of the brine-saturated Garn reflector and the overburden Lyr-Spekke-Melke Formations on top of the brine saturated Garn Formation at various differential stress conditions are presented here. Figures 4.13, 4.16, 4.19, 4.22, 4.25, and 4.28 shows the synthetic seismogram of the well at different stress conditions. Figures 4.14, 4.17, 4.20, 4.23, 4.26, and 4.29 shows the offset dependent reflectivity curves, while Figure 4.15, 4.18, 4.21, 4.24, 4.27 and 4.30 shows the Gradients versus Intercepts cross-plots of the interfaces at different stress conditions.

4.4.4.1 AT 36 MPa 'IN-SITU' CONDITION) WITH LYR-SPEKKE-MELKE ON TOP OF THE GARN REFLECTOR.

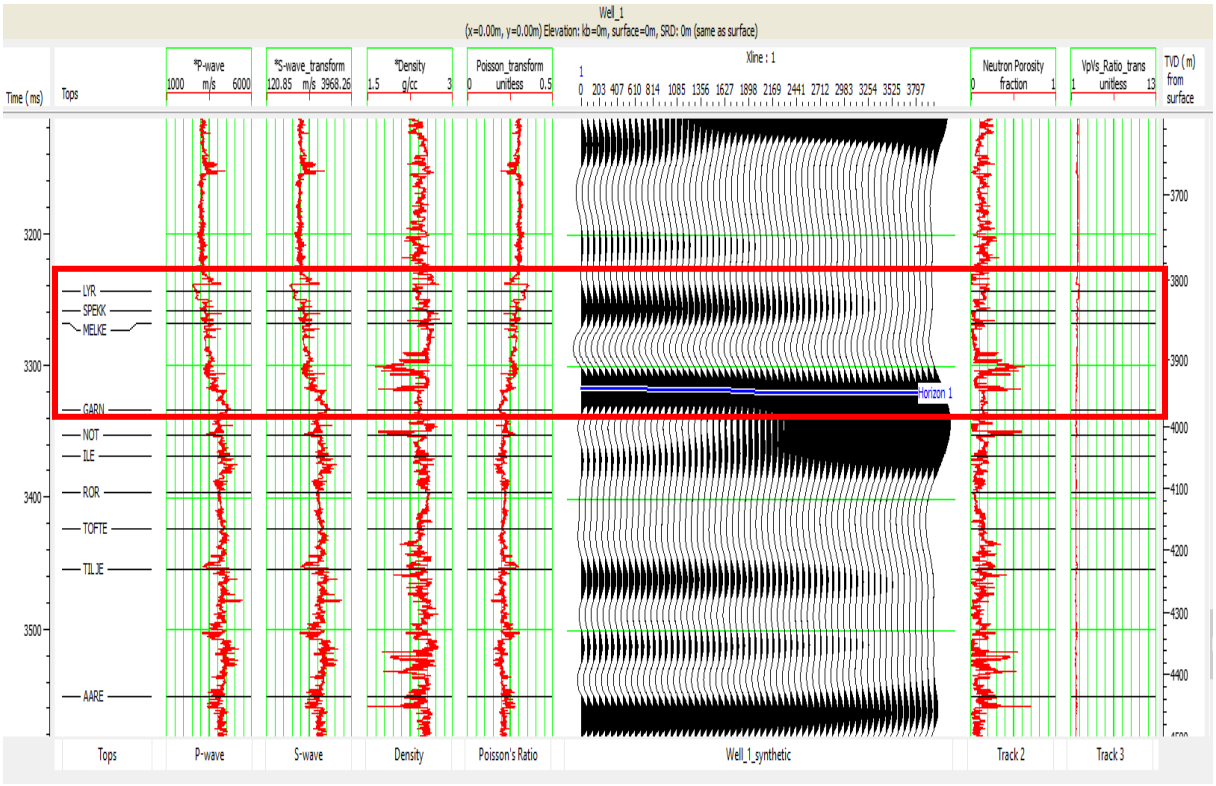

Figure 4.13: Synthetic Seismogram showing the AVO modelling for Lyr-Spekke-Melke Formation on the Garn at 36MPa for the Well 6506/12-1 using the Zoeppritz algorithm. The red rectangle highlights the analysed amplitude of the Garn reflector.

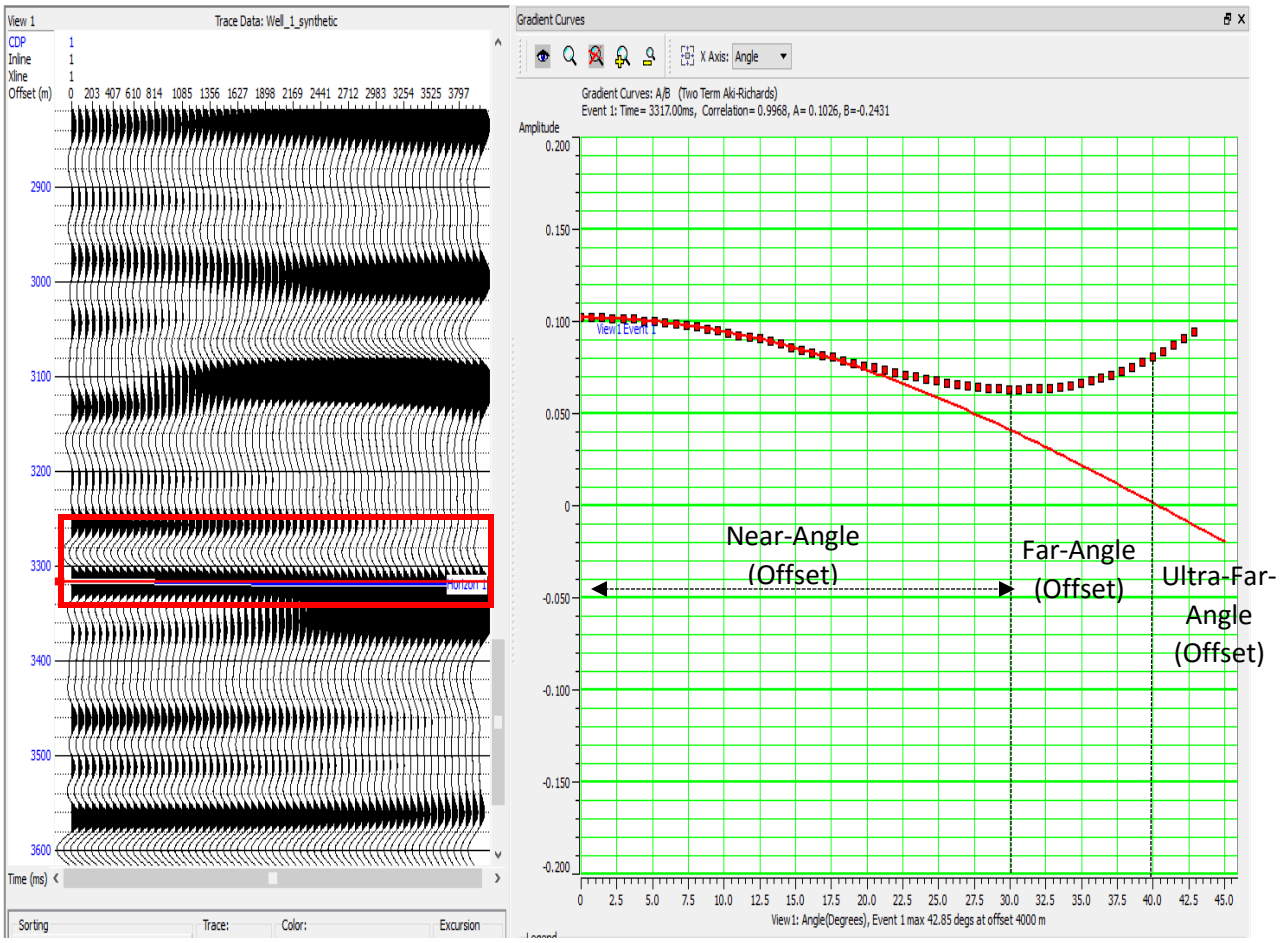

Figure 4.14: Reflectivity versus Angle (offset) of the interface between the overburden Lyr-Spekke-Melke on top Garn Formation at 36 MPa using Well 6506/12-1, showing a decrease in amplitude with increasing angles (offsets). The Near angles (offsets) is between 0° to 30° , the Far angles (offsets) is 30° to 40°, while the ultra-far angle (offsets) is above 40°

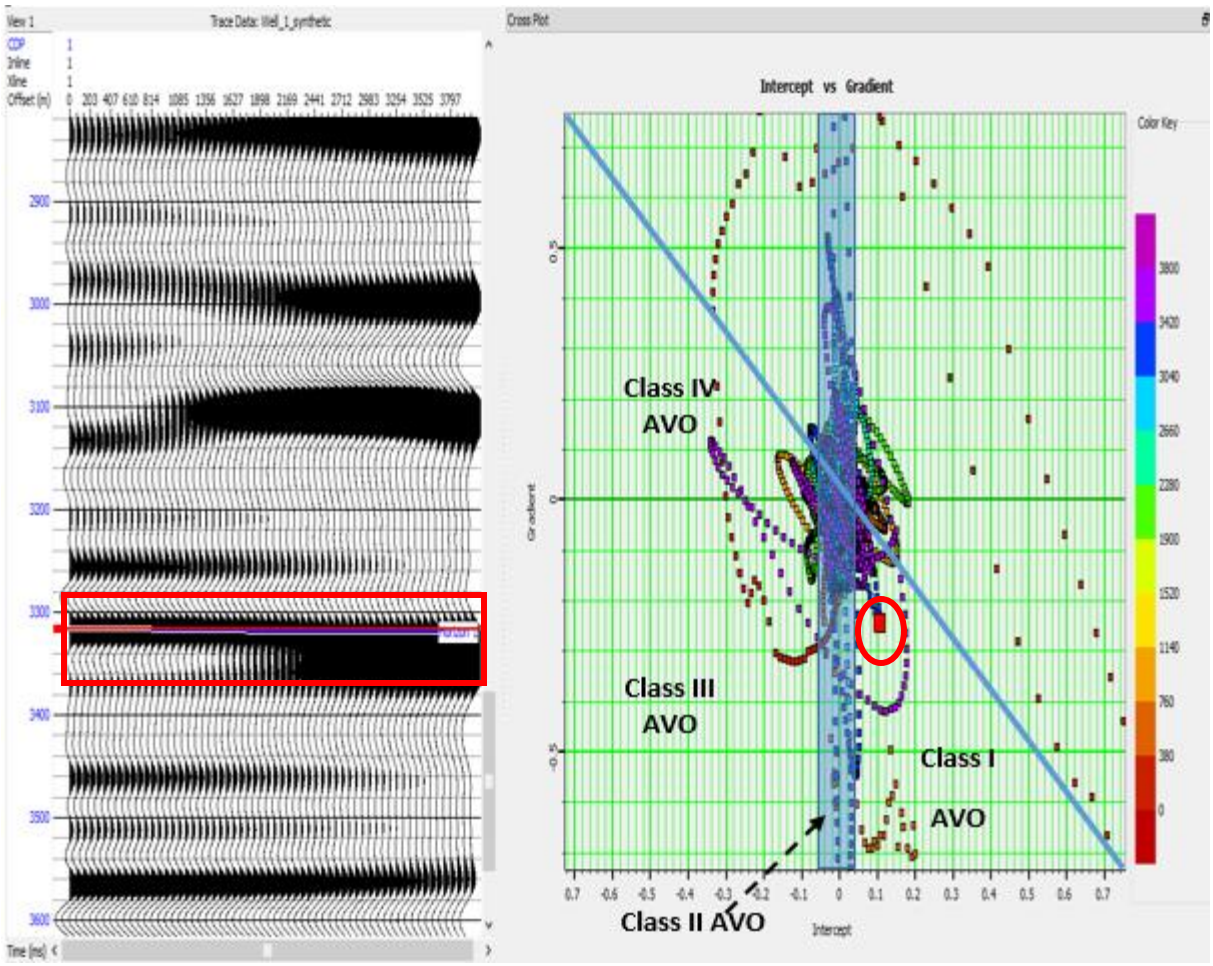

Figure 4.15: Gradient versus Intercept crossplot of Lyr-Spekke-Melke on top of the Garn Formation in Hampson Russell at 36 Mpa using Well 6506/12-1. The figure shows the horizon on the synthetic seismogram marked with the red rectangle while the red circle represent the class of the AVO response. It clearly shows a class 1 AVO according to Rutherford and Williams (1989).

4.4.4.2 AT 36 MPA ('IN-SITU' CONDITION) WITH ONLY THE LYR FORMATION ON TOP OF THE GARN REFLECTOR.

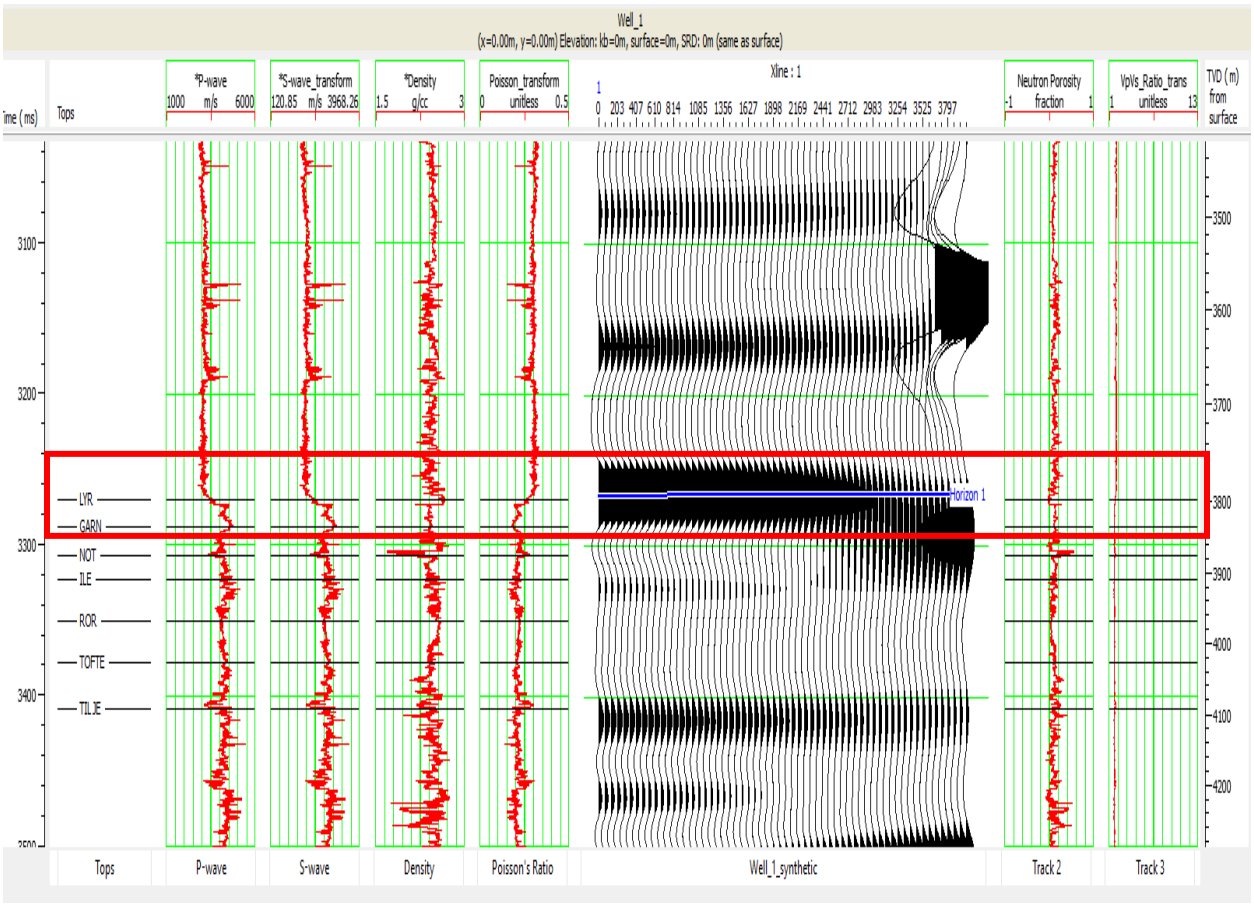

Figure 4.16: Synthetic Seismogram showing the AVO modelling for Lyr Formation on the Garn at 36MPa for the Well 6506/12-1 using the Zoeprritz algorithm. The red rectangle highlights the analysed amplitude of the Garn reflector.

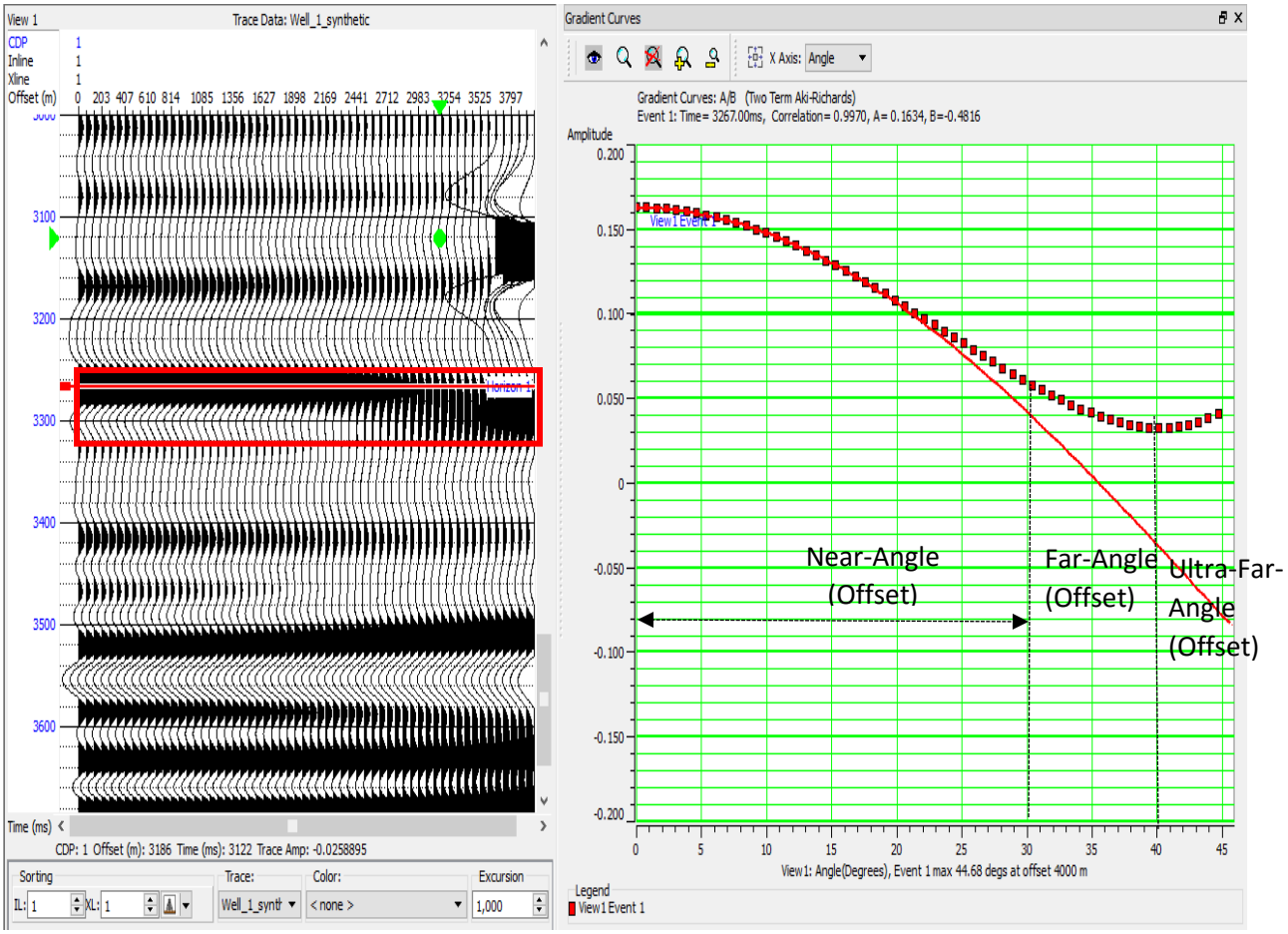

Figure 4.17: The Reflectivity versus angles (offset) of Lyr Formation on top Garn Formation at 36MPa using Well 6506/12-1, showing a decrease in amplitude with increasing angles (offsets). The Near angles (offsets) is between 0° to 30° , the Far angles (offsets) is 30° to 40°, while the ultra-far angle (offsets) is above 40 .

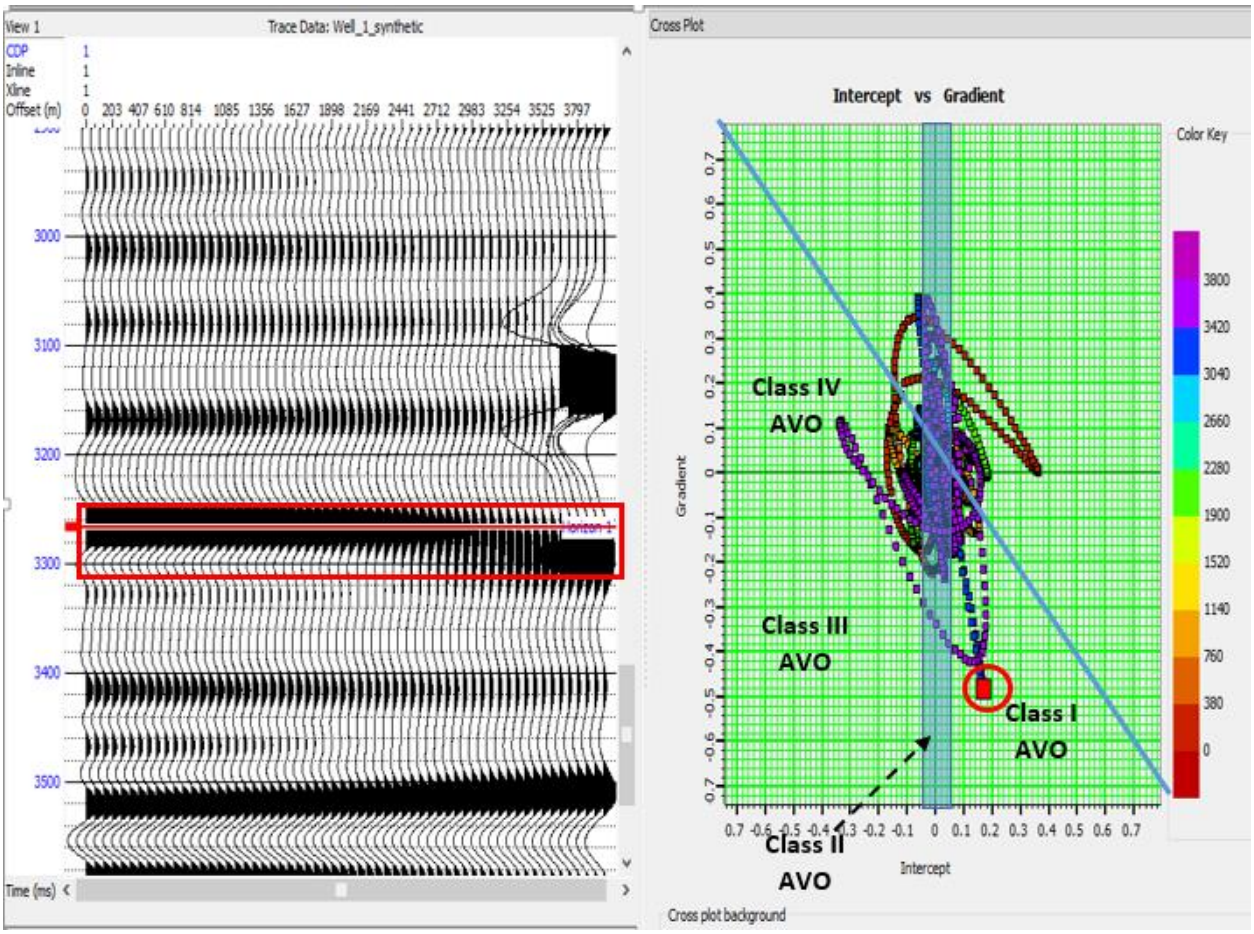

Figure 4.18 Gradient versus Intercept crossplot of Lyr on top of the Garn Formation in Hampson Russell at 36 MPa using Well 6506/12-1. The figure shows the horizon on the synthetic seismogram marked with the red rectangle while the red circle represent the class of the AVO response. It clearly shows a Class I AVO according to Rutherford and Williams (1989).

4.4.4.3 AT 50 MPa (PORE-PRESSURE DECREASE) WITH LYR-SPEKKE-MELKE ON TOP OF GARN.

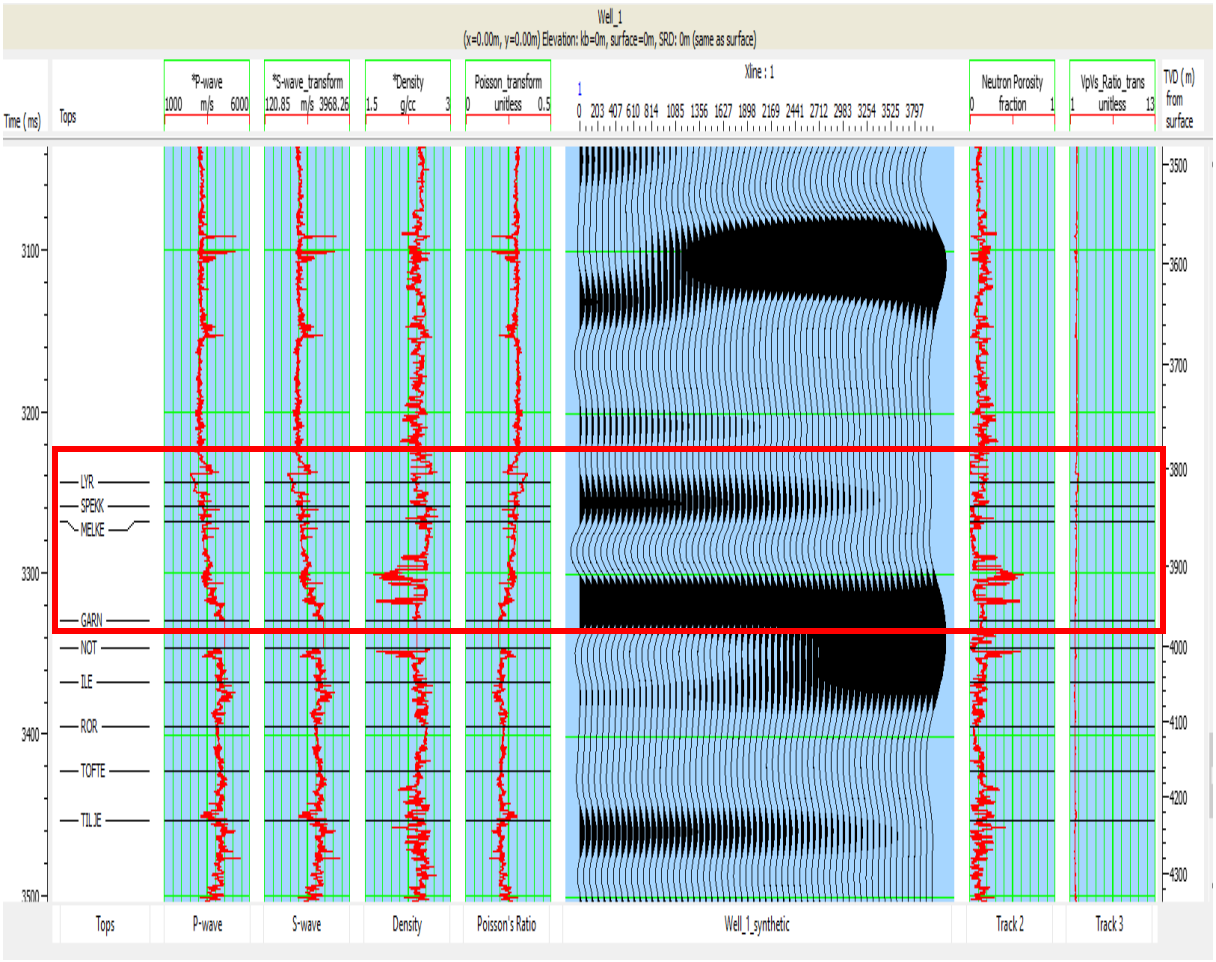

Figure 4.19: Synthetic Seismogram showing the AVO modelling for overburden Lyr-Spekke-Melke Formation on top of the brine saturated Garn Formation at 50 MPa for the Well 6506/12-1 using the Zoeppritz algorithm. The red box highlights the analysed amplitude of the Garn reflector.

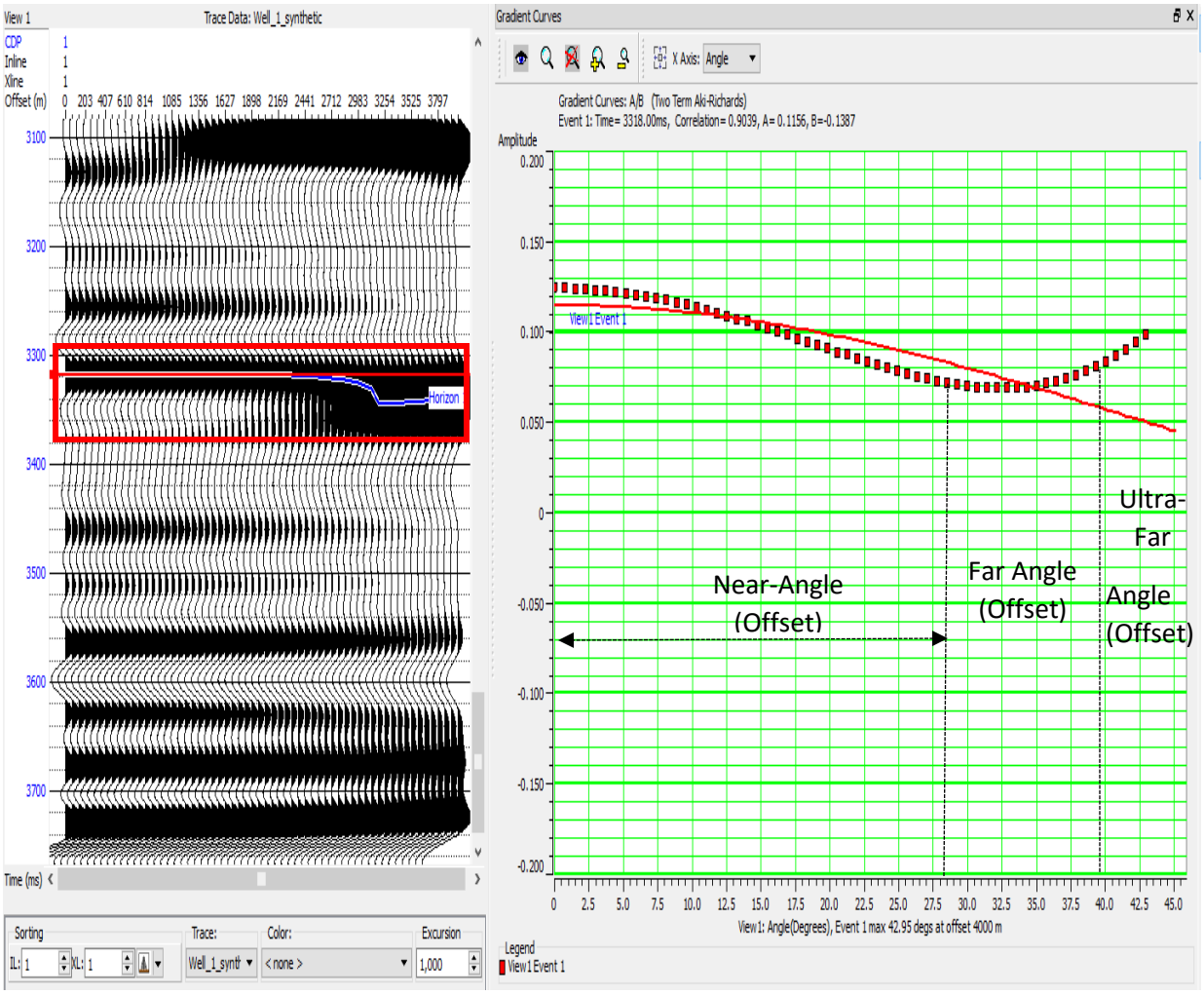

Figure 4.20: Reflectivity versus angles (offsets) of the overburden Lyr-Spekke-Melke on top of the brine saturated Garn Formation at 50MPa using Well 6506/12-1, showing a decrease in amplitude with increasing angles (offsets). The Near angles (offsets) is between 0° to 30° , the Far angles (offsets) is 30° to 40°, while the ultra-far angle (offsets) is above 40 .

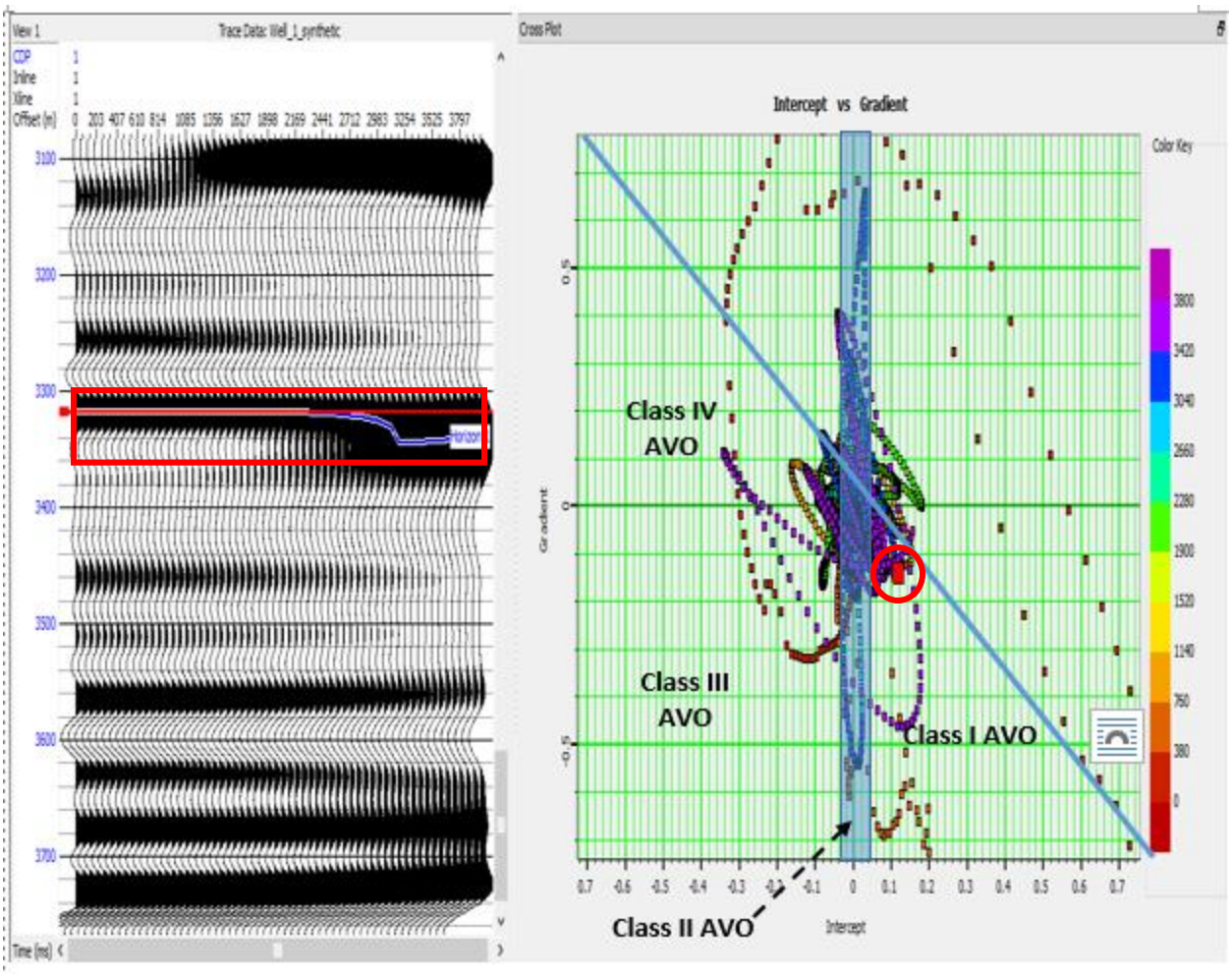

Figure 4.21: Gradient versus Intercept crossplot of Lyr-Spekke-Melke on top of the Garn Formation in Hampson Russell at 50MPa using Well 6506/12-1. The figure shows the horizon on the synthetic seismogram marked with the red rectangle while the red circle represent the class of the AVO response. It clearly shows a Class I AVO according to Rutherford and Williams (1989).

4.4.4.3.1 At 50 MPa (Pore-Pressure Decrease) With Only Lyr On Garn Formation

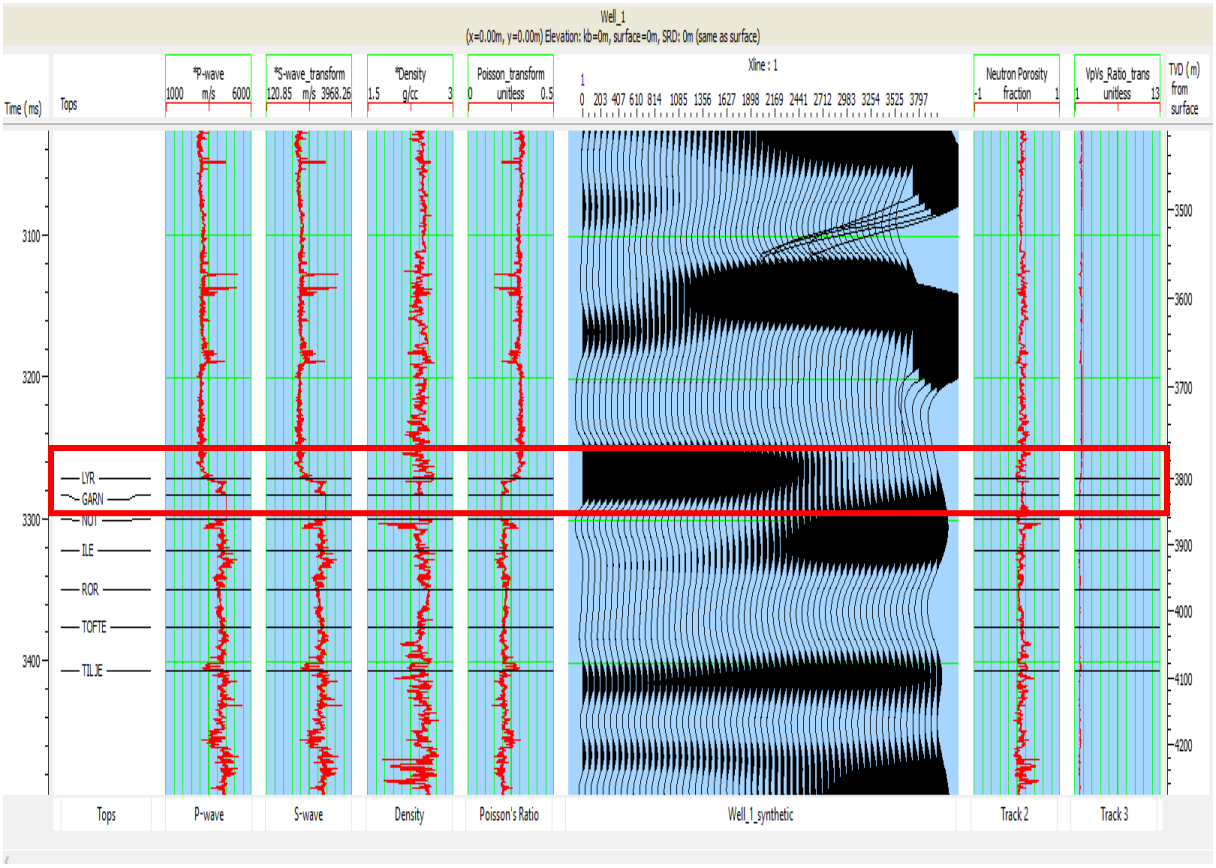

Figure 4.22: Synthetic Seismogram showing the AVO modelling for Lyr Formation on the Garn at 50MPa for the Well 6506/12-1 using the Zoeppritz algorithm. The red rectangle highlights the analysed amplitude of the Garn reflector.

.

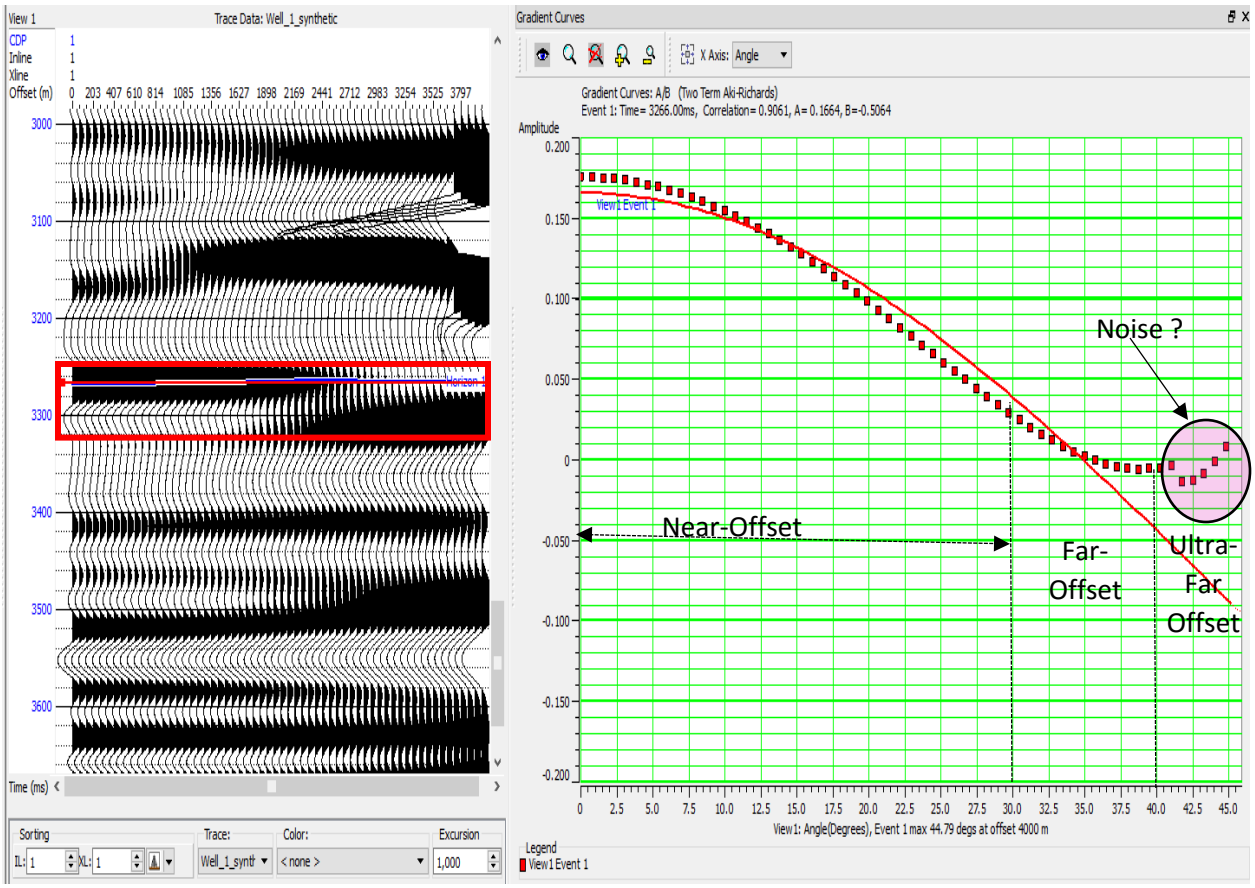

Figure 4.23: The reflectivity versus angle (offsets) of the Lyr Formation on top of the Garn Formation at 50 MPa, showing a decrease in amplitude with increasing angles (offsets). The Near angles (offsets) is between 0° to 30° , the Far angles (offsets) is 30° to 40°, while the ultra-far angle (offsets) is above 40 .The circle data points are probably noise.

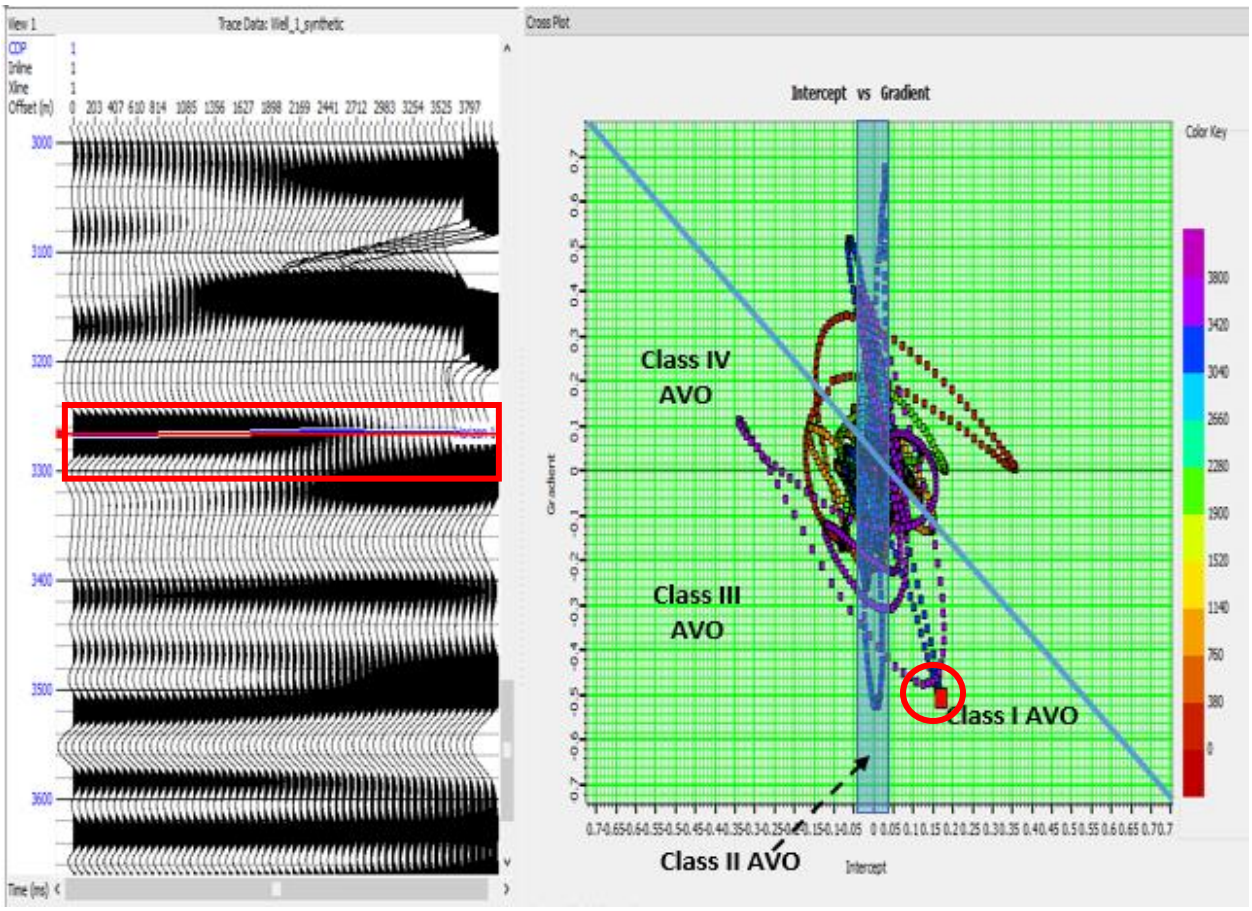

Figure 4.24: Gradient versus Intercept crossplot of Lyr on top of the Garn Formation in Hampson Russell at 50MPa. The figure shows the horizon on the synthetic seismogram marked with the red rectangle while the red circle represent the class of the AVO response. It clearly shows a Class I AVO according to Rutherford and Williams (1989).

4.4.4.3.2 At 20 MPa with Lyr-Spekke-Melke Formations on Garn Reflector

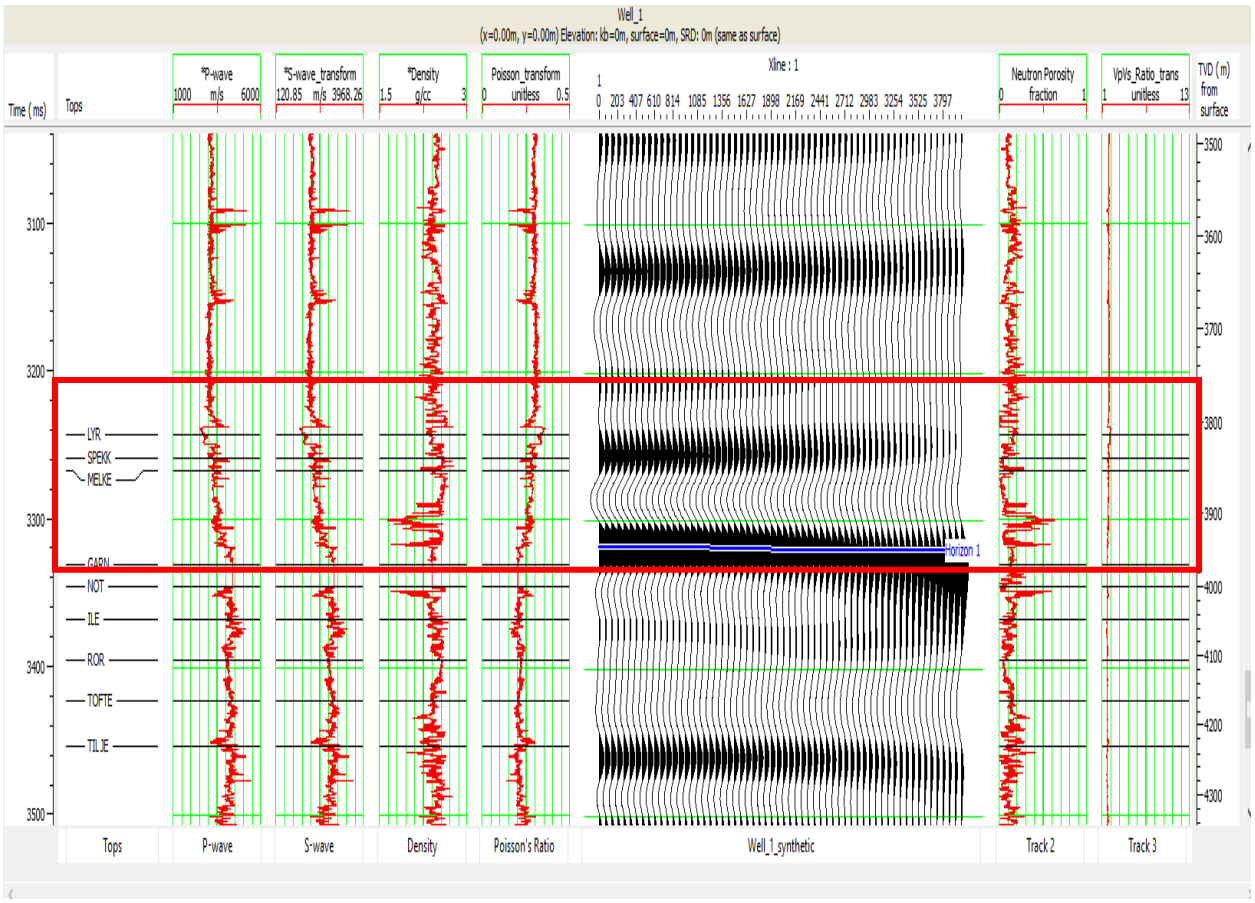

Figure 4.25: Synthetic Seismogram showing the AVO modelling for the overburden Lyr-Spekke-Melke Formation on top of the brine saturated Garn Formation at 20Mpa using the Zoeppritz algorithm . The red rectangle highlights the analysed amplitude of the Garn reflector.

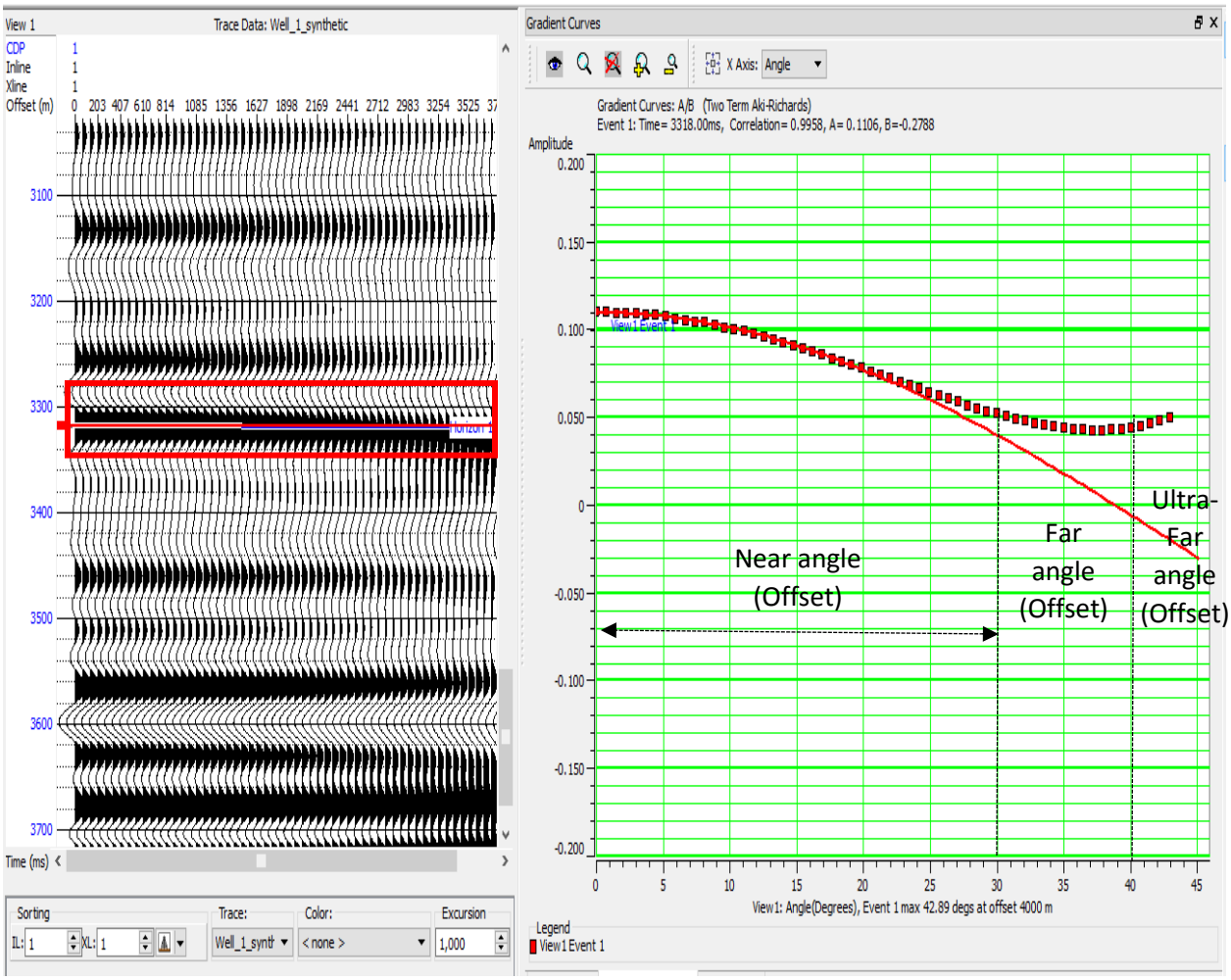

Figure 4.26: The feflectivity versus angles (offsets) plot of the overburden Lyr-Spekke-Melke on top of the brine saturated Garn Formation at 20 MPa showing a decrease in amplitude with increasing angles (offsets). The Near angles (offsets) is between 0° to 30° , the Far angles (offsets) is 30° to 40°, while the ultra-far angle (offsets) is above 40 .

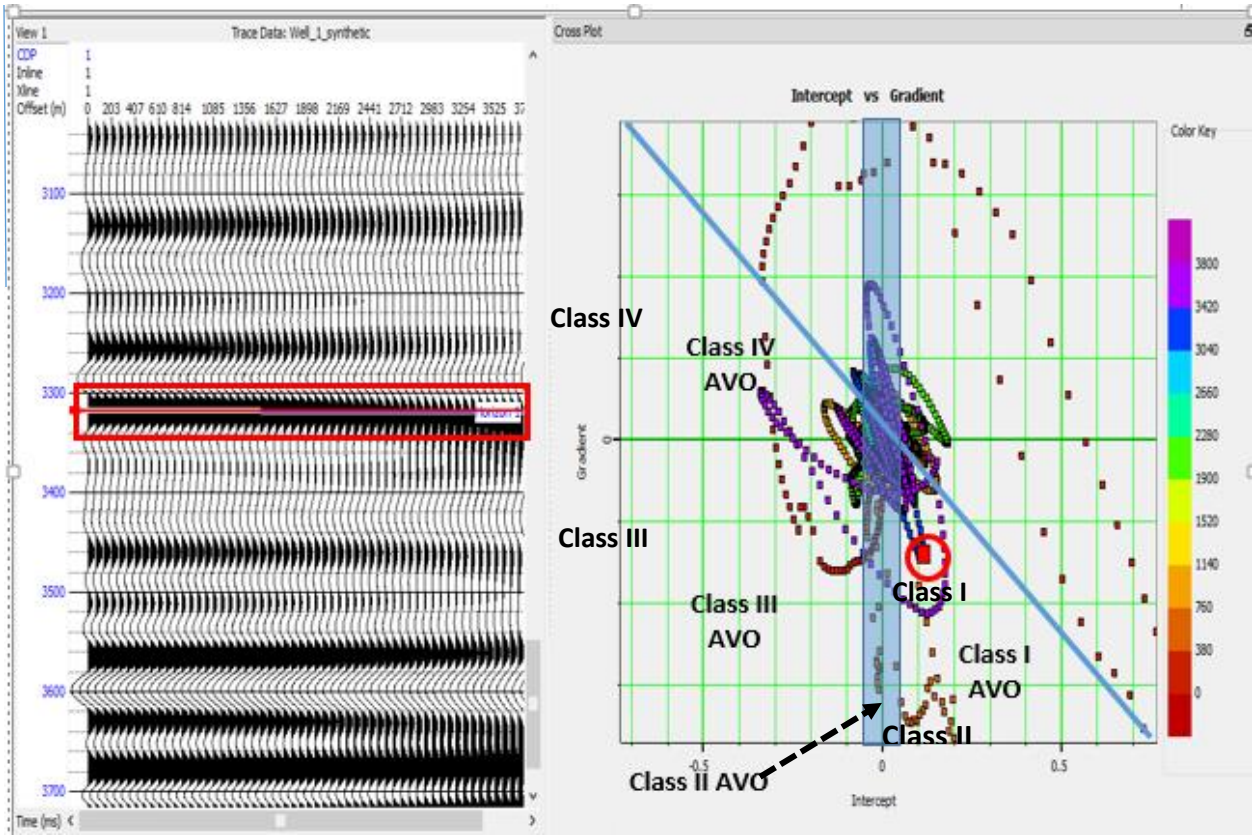

Figure 4.27: Gradient versus Intercept crossplot of the overburden Lyr-Spekke-Melke on top of the Garn Formation in Hampson Russell at 20MPa. The figure shows the horizon on the synthetic seismogram marked with the red rectangle while the red circle represent the class of the AVO response. It clearly shows a Class I AVO according to Rutherford and Williams (1989).

4.4.4.3.3 At 20 MPa with only Lyr on Top of the Garn Reflector

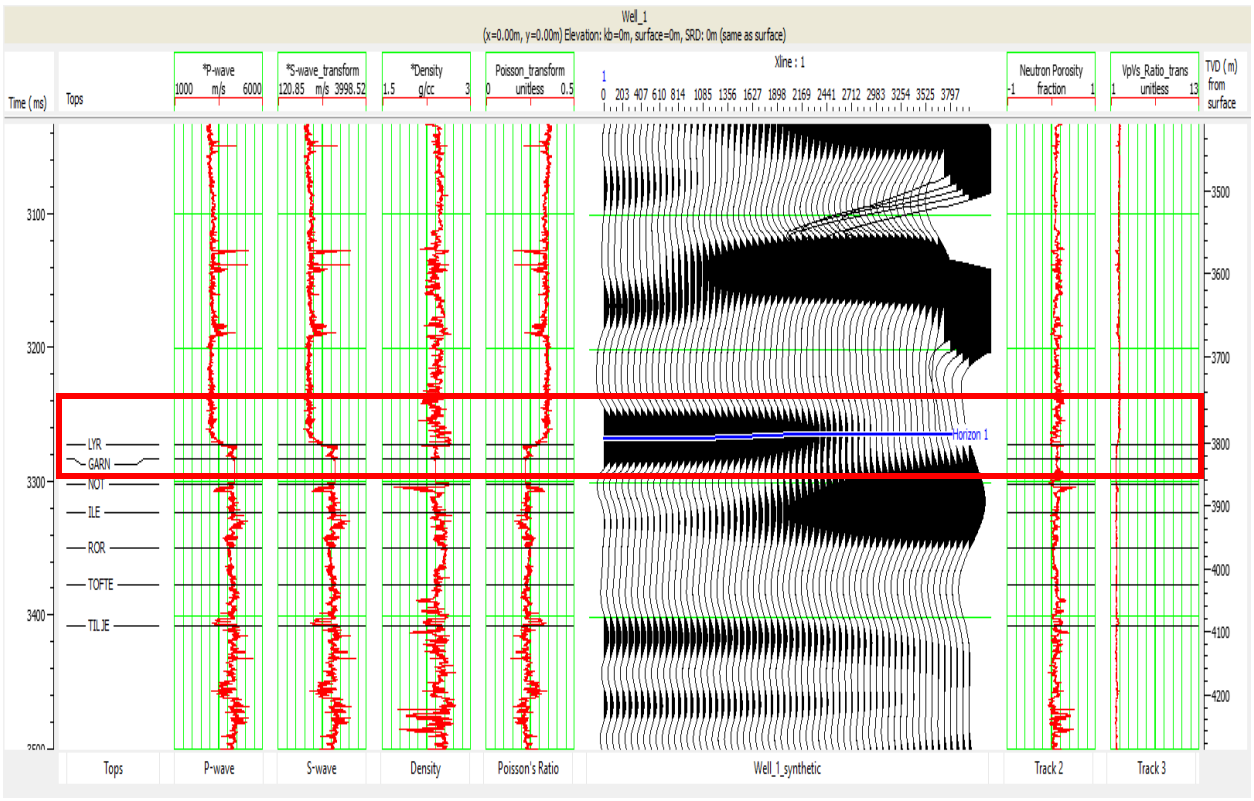

Figure 4.28: Synthetic Seismogram showing the AVO modelling for the Lyr Formation on the brine saturated Garn Formation at 20MPa for the Well 6506/12-1 using the Zoeppritz algorithm. The red box rectangle is the reflector/ interface bwteen the Lyr and Garn reflector.

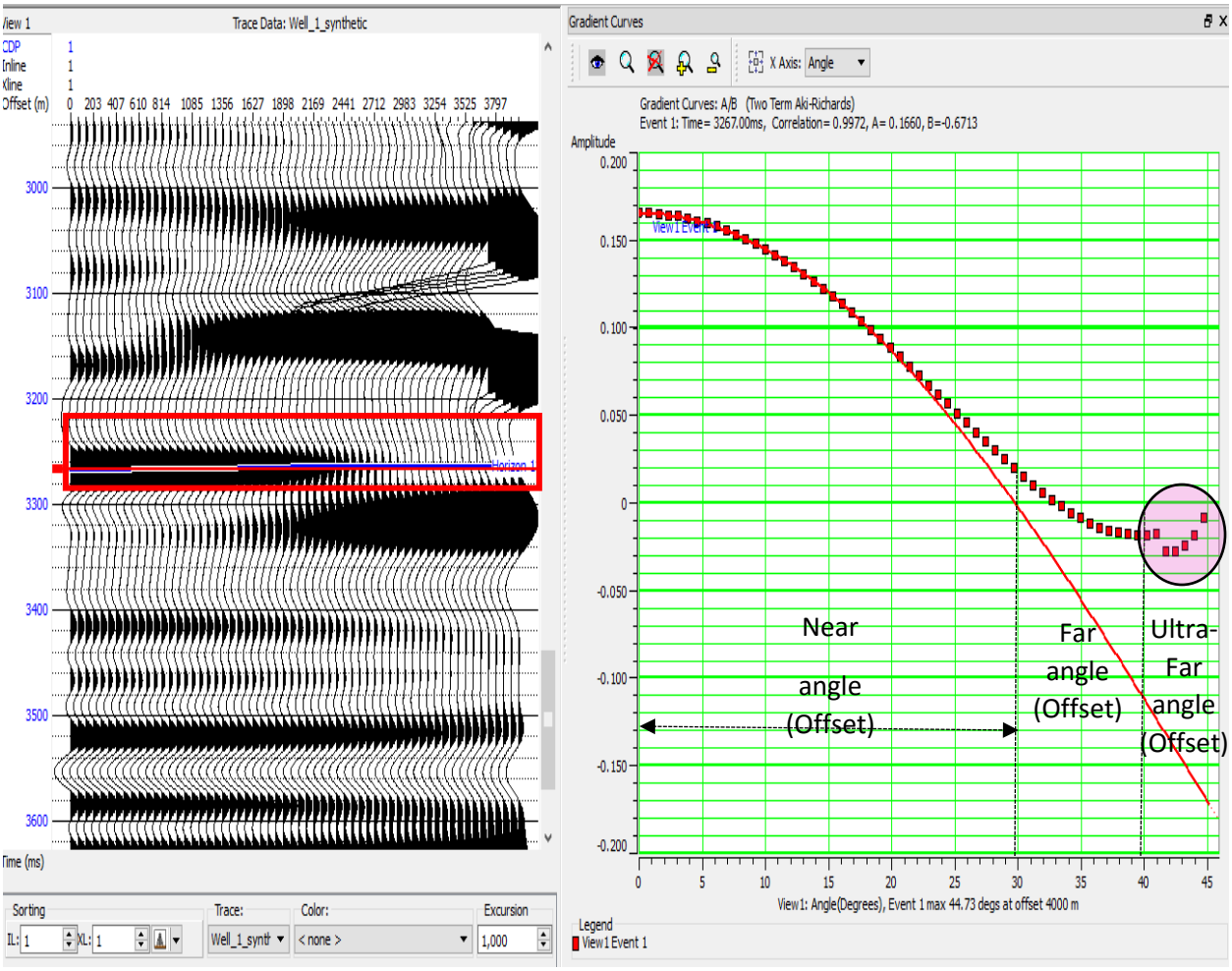

Figure 4.29: Showing Reflectivity versus Offset of Lyr on top Garn Formation at 20MPa.The picked horizon is marked with the red box. on the left of the diagram is the reflectivity variation with offset curve, showing a decrease in amplitude with increasing angles (offsets). The Near angles (offsets) is between 0° to 30° , the Far angles (offsets) is 30° to 40°, while the ultra-far angle (offsets) is above 40 . the circled data points are suspected to be noise associated with the data.

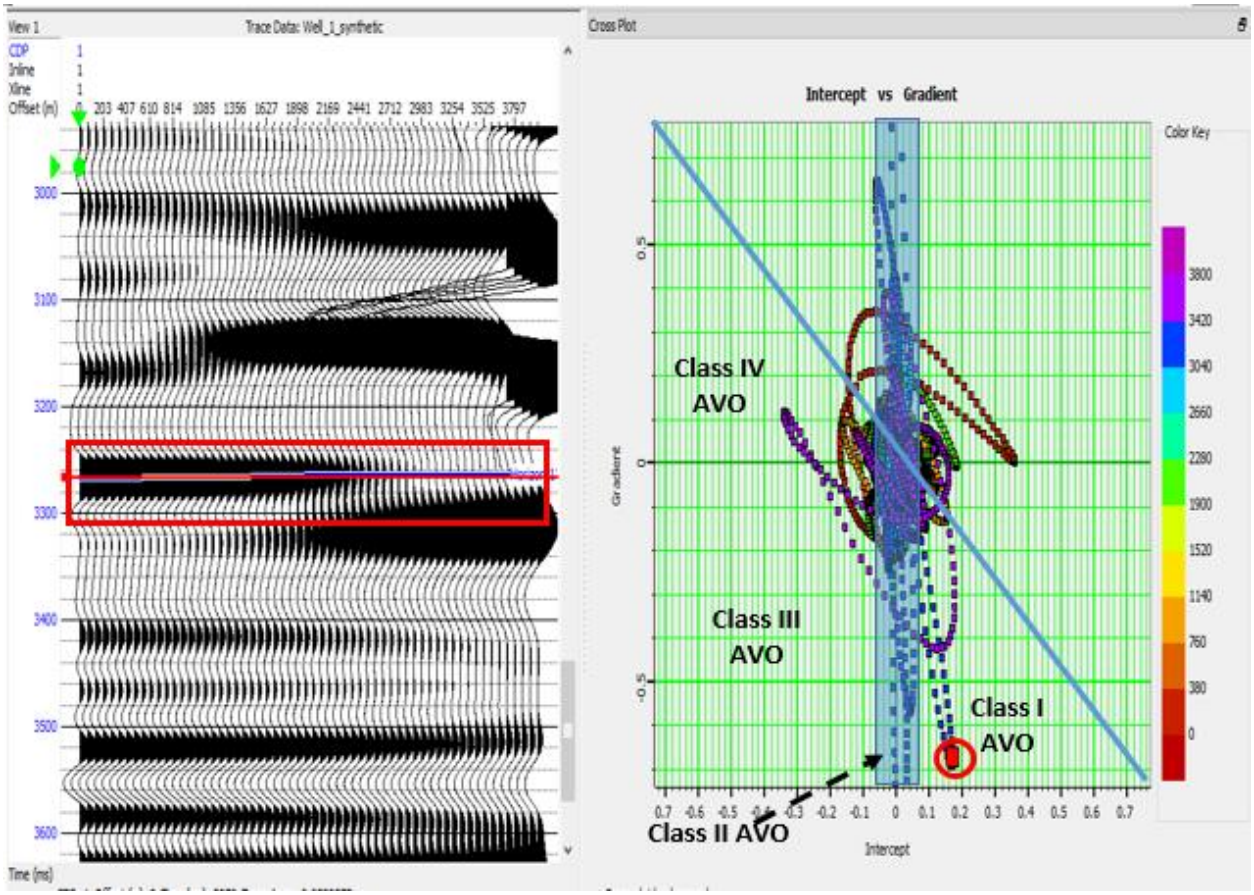

Figure 4.30: Gradient versus Intercept crossplot of Lyr on top of the Garn Formation in Hampson Russell at 20MPa. The figure shows the horizon on the synthetic seismogram marked with the red rectangle while the red circle represent the class of the AVO response. It clearly shows a Class I AVO according to Rutherford and Williams (1989).

Table 4.6:A summary of the AVO Modelling in HAMPSON RUSSELL showing the Interfaces, the Stress Conditions, and the Reflectivities at zero offsets.

S/N	**AVO MODELLING USING HAMPSON RUSSELL (GEOVIEW)**	
	INTERFACES	**REFLECTIVITY At Zero Offset**
1)	**LYR-SPEKKE-MELKE ON TOP GARN** AT **36MPa** (In-situ stress)	**0.103204**
2)	LYR ON TOP OF GARN FORMATION AT **36 MPa** (In-situ stress).	**0.163699**
3)	**LYR-SPEKKE-MELKE ON TOP GARN** AT **50MPa (PORE-PRESSURE DECREASE)**	**0.125281**
4)	LYR ON TOP OF GARN FORMATION AT **50 MPa. (PORE-PRESSURE DECREASE)**	**0.178294**
5)	**LYR-SPEKKE-MELKE ON TOP GARN** AT **20MPa (PORE-PRESSURE INCREASE)**	**0.111172**
6)	LYR ON TOP OF GARN FORMATION AT **20 MPa. (PORE-PRESSURE INCREASE)**	**0.166584**

CHAPTER 5

5.0. DISCUSSIONS

5.1 PART 1.

Velocity variations of the brine-filled Garn Formation within the selected wells.

The results in Figure 3.2 are used to show how velocity is varying within the brine-saturated Garn Formation from the selected wells and to analyse and confirm the potential of the Eberhart-Phillips model to predict the velocity variations within the brine saturated Garn Formation in the selected wells.

Well 6406/3-1 is a wildcat well drilled in the Tyrihans field within the Norwegian-Sea, whose objective was to test the reservoir potential of the Jurassic Sandstones. The brine saturated Garn formation is about 119m thick within this well. The pore-pressure encountered in this Well was higher than normal (estimated to be 1.82 s.g.). The brine-saturated Garn Formation interval in this Well 6406/3-1 is overpressured (NPD). Therefore, we should expect a reduction in the velocity due to this overpressure effect. This is logical since overpressure soften the rock's properties, reduces differential stress and increases porosity (Simm et al., 2014). It should be noted that the velocity variations with the differential stress carried out in this study was solely based on the following parameters only: porosity, volume of clay and differential stress. The calculated average porosity within the brine-saturated Garn Formation Interval in this Well 6406/3-1 is 16%, the average volume of clay computed is 24% and the differential stress within the brine-saturated Garn Formation interval is 14.1 MPa. These parameters are within the range for the standard Eberhart-Phillips et al. (1989) model for porosity range of 2 to 30%, volume of clay of 0% to 50%. The average P-wave velocity within the brine saturated Garn Formation in this Well that was calculated using the Backus average is 3793 (m/s) while the S-wave velocity computed is 2618 (m/s). The crossplot between the velocities (P-wave and S-wave) and the differential stress is shown in Figure 3.2. The S-wave velocity fits very well into the curve made with the default parameters of the Eberhart-Phillips model, while the P-wave velocity tends to be a little lower that the predicted P-wave velocity by the Eberhart-Phillips model. The drop in the P-wave velocity maybe attributed to the overpressure within the brine saturated Garn Formation which might have increased the porosity. Other factors that were not considered in this research such as the effects of fractures of

volume of matrix within the Garn Formation might have been responsible too, but in the context of this work, the porosity is suspected to be controlling the drop in the P-wave in the brine saturated Garn Formation in this Well. Figure 3.3 confirms that porosity has a major control on the velocity in this Well. It shows that by increasing the porosity used for the Eberhart-Phillips model, the data point could fit into the model perfectly.

Well 6406/2-5 is an appraisal well drilled in the Kristin field within the Haltenbanken. Report at the NPD website shows that the brine saturated Garn Formation interval in this Well is overpressured. The results from the wire line logs analysis of this well shows the average porosity computed by the neutron log to be 10%, the average bulk density computed using simple arithmetic averaging over the brine-filled Garn interval is 2.49g/cc and the volume of clay computed is 20%. The velocities (P-Wave and S-wave) within the Garn Formation that was computed using the Backus averaging technique as discussed in section 3.6 shows the average P-wave velocity to be 4363m/s while the S-wave velocity is 2781m/s as shown in Table 3.2. The calculated differential stress within the brine-filled Garn Formation is 16 MPa. Ideally we should expect the velocity to drop due to the overpressure recorded within the Garn Formation interval, but it turns out that the velocity against the differential stress crossplot using the parameters from the brine saturated Garn Formation interval matches very well into the curve made with default parameters of the Eberhart-Phillips model. According to the model (Figure 3.2), the velocity is controlled by the differential stress within the brine filled Garn Formation. The velocity might have been also controlled by other factors such as the coordination number (the average number of contacts per individual grain) or effect of cement considering that the depth of the Garn Formation is very deep. These parameters (effect of cement) were not considered in this work, but they might have influenced the velocity within the Garn Formation.

Well 6506/11-3 is a wildcat well drilled in the Smørbukk field. The computed average porosity and bulk density within the Brine-filled Garn Formation interval is 15% and 2.40g/cc while the volume of clay is 8%. It should be noted that the neutron porosity and bulk density logs were used to compute these averages using a simple arithmetic Backus averaging technique. Computation of the average velocities (P-wave and S-wave) within the brine filled Garn Formation using the Backus averaging procedure as detailed in section 3.6, shows the P-wave velocity to be 4385m/s

and the S-wave velocity to 2691m/s. The cross-plot between the velocities (P-wave and S-wave) and the differential stress within the Garn Formation is shown in the Figure 3.2. The data point fits very well into the curves made by the Eberhart-Phillips model default parameters. This seems logical since the parameters (porosity, and clay content) for the brine saturated Garn Formation in this well falls within the default parameters for the Eberhart-Phillips model. Hence, we see a correct match between the data points and the fitting from the Eberhart-Phillips model. The model proves that the differential stress has a major control on the velocity within the brine saturated Garn Formation in this Well 6506/11-3 as shown in Figure 3.2 and 3.3 .

The Well 6406/6-1 is a wildcat well that was drilled in the Eta structure close to Smørbukk field within the Haltenbanken. The computed average bulk density and porosity within the Garn Formation using the Neutron porosity and Bulk density logs are 9% and 2.50g/cc while the clay content is 32%. The Backus averaging technique was applied to calculate the velocities (P-wave and S-wave) of the Garn Formation. The P-wave velocity is 4387m/s while the S-wave velocity is 2669m/s. The differential stress within the brine saturated Garn Formation which is the target Sandstone for this work is 19.1 MPa from my calculations. The crossplot between the differential stress and velocities (P-wave and S-wave) within the brine saturated Garn Formation for this Well shows a nice fit with the Eberhart-Phillips model as shown in Figure 3.2. This is logical since the parameters used are within the limits of the values acceptable by the Eberhart-Phillips' model. It also shows that differential stress has a major control to the velocity (P-wave and S-wave) within the brine saturated Garn Formation in this Well 6406/6-1.

Well 6506/11-1 is a wildcat well drilled in the Smørbukk field. The average porosity of the brine-filled Garn Formation is 11% while the Bulk-density was estimated to be 2.43g/cc, the average volume of clay within the brine filled Garn interval is 21%. The computed average P-wave velocity within the brine filled Garn formation of this well is 4253m/s while the S-wave is 2843m/s. The differential stress estimate within the Garn Formation is 25MPa. It is logical to say that the high differential stress within the Garn Formation had a limited control on velocity and that the porosity had a higher control in the Garn Formation within this Well according to the models in Figures 3.2 and 3.3. The crossplot between the velocities and the differential stress within the brine filled Garn Formation is shown in Figure 3.2. The S-wave velocity fits very well in the regressed line of the Eberhart-Phillips model, while the P-wave velocity fell a little below the model's regressed curve.

Well 6506/12-1 is the reference well for this work. It is drilled within the Smørbukk field. The brine saturated Garn Formation is about 219 metres thick measures from the mRKB. The average porosity and bulk density within the Garn Formation are 14% and 2.42g/cc respectively, while the average volume of clay is 8%. The differential stress was 36 MPa in this well. This shows that the Pore-pressure is relatively low within the brine saturated Garn Formation. The average velocities within the Garn Formation is 4538m/s for P-wave and 2792m/s for S-wave. The crossplots between the velocities and differential stress of the Garn Formation clearly matches the curve of the Eberhart-Phillips model as shown in Figure 3.2. The model proves that the differential stress has the major control on the velocity as regards to the parameters (porosity, clay content and differential stress) in the plot with reference to Figures 3.2 and 3.3.

In general, the velocities of the brine saturated Garn Formation from the selected Wells in the area of study for this work can be predicted by the Eberhart-Phillips model. The model shows that the porosity had a major control in the brine filled Garn Formation for Wells 6406/3-1 and 6506/11-1 while the differential stress controls the velocity in the brine saturated Garn Formation for the Wells 6406/2-5, 6506/11-3, 6406/6-1 and Well 6506/12-1 respectively. However, the effects of broken sand grains due to increase in stress (pressure), the mineralogical composition of the rock matrix, cementation, pore-shapes and anisotropy within the clay volume in the Garn Formation were not considered. These parameters could affect the velocity and could explain the mismatches between the model and some of the data points of the Garn-Formation from the selected according to Eberhart-Phillips et al. (1989) but these parameters considered in this model.

5.2 PART 2

The AVO response from the effects of lithology and overpressures are going to be analysed and differentiated using the results obtained from the single interface 1D AVO modelling in MATLAB and the layered 1D AVO modelling in Hampson Russell Geoview.

5.2.1 Single Interface 1D AVO modelling with MATLAB

This discussion is based on the results (Figures 4.6 to 4.11) of the single interface 1D AVO modelling between the Lyr on top of the brine saturated Garn Formation and the overburden Lyr-Spekke-Melke on top of the Garn Formation.

AVO is a function of the contrast in acoustic impedance and Poisson ratio (Rock-Physics-Associates, 2007). However, in the case of a brine-saturated sandstone, the Poisson ratio is negligible. Therefore, I will base my discussions only on the contrast in the acoustic impedance between the interfaces to analyse the potential effects of overpressure and lithology on the AVO responses at different differential stress conditions.

The reflectivity versus offset curve for the interface between the Lyr and brine saturated Garn at the in-situ differential stress condition (36MPa), shows a strong reflection coefficient or amplitude which decreases with increasing angles or offsets (Figure 4.6) typical of the class 1 AVO of the Rutherford and Williams (1989) classification. The gradient versus intercept crossplots also confirms this (Figure 4.7). The strong amplitude (high impedance) AVO response is obviously due to the difference in the acoustic impedance between the Lyr Formation layer and the brine saturated Garn Formation. The Lyr Formation consists of mainly marls interbedded with carbonates (Dalland et al., 1988), while the Garn Formation is a sandstone. The AVO response is controlled by the lithology differences at the interface. The amplitude of the reflection coefficient at the near offset or angle (0° to 30°) is 0.1357, while the amplitude is 0.0353 for the far offset or angle (30° to 40°) and 0.1146 for ultra-far offset or angle (40° to 45°). The amplitude decreases till the far angles (offsets) and starts increasing at angles (offsets) higher than 35° towards the ultra-far angles (offsets).

The 1D single interface AVO response of the overburden Lyr-Spekke-Melke and the brine saturated Garn Formation at the in-situ differential stress (36MPa) shows almost the same AVO response as that of the single layer interface between the Lyr Formation and the brine saturated Garn Formation (Figure 4.6). It displays a strong or high amplitude which decreases with increasing angle or offset typical of the Class 1 AVO response according to the Rutherford and Williams (1989). The gradient versus intercept cross-plot (Figure 4.7) also shows a negative gradient and positive intercept that is characterised by the class 1 AVO response. The amplitude at the near offset or angle (0° to 30°) is 0.1345, while the amplitude is 0.0292 for the far offset or angle (30° to 40°) and 0.0604 for ultra-far offset or angle (40° to 45°).

At 50MPa differential stress (assumed depletion condition), the single interface 1D AVO response for the interface between the Lyr Formation and the brine saturated Garn Formation shows a high amplitude that decreases with increasing angle or offset as shown in Figure 4.8 just like the case of the in-situ differential stress condition. Although the amplitude here is a little bit higher. At the near offset or angle (0° to 30°), the amplitude is 0.1386, while it is 0.0382 at far offset or angle (30° to 40°) and 0.1152 at ultra-far offset or angle. The gradient versus intercept AVO response (Figure 4.9) shows a negative gradient and positive intercept typical of the class 1 AVO response by Rutherford and Williams (1989) . The amplitude is as a result of the lithology effect.

The AVO response for the single interface 1D modelling for the overburden Lyr-Spekke-Melke and the brine saturated Garn Formation at 50 MPa differential stress is similar to that of the interface between the Lyr on top of the brine saturated Garn Formation (Figure 4.8). Although the amplitude is a little lower than that of the Lyr on top of the brine saturated Garn interface. The AVO response is of the class 1 response by Rutherford and Williams (1989) . The gradient versus intercept crossplots shows a negative gradient and a positive intercept typically that one the class 1 AVO (Figure 4.9). The amplitude of the reflection coefficient at the near offset or angle (0° to 30°) is 0.1373, at the far offset or angle (30° to 40°) it is 0.0318 and at ultra-far offset or angle, the amplitude is 0.0664.

At 20 MPa differential stress, the 1D single interface AVO response for the interface between the Lyr and the brine saturated Garn Formation shows a high amplitude which decreases with increasing offset or angle (Figure 4.10). The reflectivity curve shows a typical class 1 AVO response, according to Rutherford and Williams (1989) classifications. The gradient versus

intercept cross-plot (Figure 4.10) shows a negative gradient and a positive intercept typical for a class 1 AVO response of the Castagna et al. (1998) classification. The amplitude of the reflection coefficient at near angles (offset 0° to 30°) is 0.1223, at the far angles (offsets) (30° to 40°) it is 0.0301 and at ultra-far angles (offsets), the amplitude is 0.0782.

The AVO response of the interface between the overburden Lyr-Spekke-Melke and the brine filled Garn Formation at 20 MPa differential stress shows a strong amplitude which decreases with increasing offset (Figure 4.10). The amplitude is a little lower than that of the interface between Lyr and the brine filled Garn Formation. The AVO response is clearly a class 1 response, according to Rutherford and Williams (1989) as shown in Figure 4.10. The cross-plot between the gradient and the intercept also shows a typical class 1 AVO anomaly according to Castagna et al. (1998) . The amplitude for the near angles (offsets 0° to 30°) is 0.1210, 0.0248 for far angles (offset) and 0.0391 for ultra-far angles (offset).

The results of the single interface AVO modelling between the Lyr Formation and the brine saturated Garn Formation for the various differential stress conditions (36MPa, 50MPa and 20MPa) shows that reflectivity is lithology dependent, i.e. the difference in the acoustic impedances of the layers above and beneath the interface. The same is applicable for the interface between the overburden Lyr-Spekke-Melke and the brine saturated Garn Formation at the various differential stress conditions. The effect of lithology is predominant for the near and far angles (offsets) as can be seen in Figures 4.6, 4.8 and 4.10. The difference in the amplitude of reflection are not that much.

However, at the ultra-far angles (offsets) the effects of overpressure seem to be detected. For example, at 20MPa, the amplitude of the reflectivity is 0.0782 for the interface between the Lyr Formation and the Garn Formation, while the amplitude for the same interface at 36 MPa is 0.1146. This is about a 47% increase in the amplitude of reflection moving from 20 MPa differential stress condition to the 36 MPa differential stress condition. The same is applicable to the differential stress condition between 50 MPa and 20 MPa for the various interfaces (Lyr on top of the Garn and the overburden Lyr-Spekke-Melke on top of the brine saturated Garn Formation) at the ultra-far angles (offsets).

5.2.2 Layered AVO modelling in Hampson Russell Geoview.

The synthetic seismogram that was created using the Zoeppritz algorithm in Geoview for the interface between the overburden Lyr-Spekke-Melke and the brine saturated Garn Formation at in-situ differential stress condition (36MPa) is shown in Figure 4.13. We can see a strong, and flat amplitude that becomes noisy towards the ultra-far angles (offsets). It is obviously a peak and it denotes an increase in acoustic impedance. Figure 4.14 shows the reflectivity versus angles (offsets). The amplitude decreases marginally with increasing angles (offsets) for the near angles (offsets) 0° to 30°. The amplitude starts rising towards the far and ultra-far angles (offsets) (Figure 4.14). There is no phase change occurrence here, and the AVO response is of class 1 Rutherford and Williams (1989) classification. The gradient versus intercept cross-plot shows negative gradient with a positive intercept that typifies the class 1 AVO with reference to the Castagna et al. (1998) classifications (Figure 4.15). The amplitude at zero angle (offset) is 0.103204.

Figure 4.16 shows the synthetic seismogram for the interface between the Lyr Formation and the underlying brine saturated Garn Formation at 36MPa differential stress. It shows a high amplitude that corresponds to peak. It appears dimmed at far angles (offsets) a little and becomes strong again. The reflectivity decreases with increasing angles (offsets) up to 40° and starts to increase beyond this angle (offset) as shown in Figure 4.17. This is typical of the class 1 AVO classification by Rutherford and Williams (1989). The gradient versus intercept cross-plot (Figure 4.18) shows a negative gradient and positive intercept typical of the class 1 AVO classification by Castagna and Backus (1993). The amplitude at zero angle (offset) 0.163699.

The synthetic seismogram for interface between the overburden Lyr-Spekke-Melke and the underlying brine filled Garn Formation at 50 MPa differential stress is shown in Figure 4.19. It shows a strong amplitude. The amplitude of reflection decreases with angles (offsets) until 32.5° then it starts increasing. This is typical of the class 1 AVO (Rutherford and Williams, 1989) as shown in Figure 4.20. The gradient-intercept cross-plot shows a negative gradient and positive intercept of the class 1 AVO by Castagna et al. (1998) (Figure 4.21). The amplitude at zero angle (offset) is 0.125281.

Figure 4.22 shows the synthetic seismogram on the interface between the Lyr Formation and the underneath brine saturated Garn Formation using the Zoeppritz algorithm. It shows a high amplitude that becomes dim at the far angles (offset) and suddenly becomes very strong again. The sudden strong amplitude may be attributed to the effects of noise. This is clearly shown in the amplitude versus angles (offsets) in Figure 4.23 circled in the magenta colour. The amplitude decreases with increasing angles (offsets) until it dies out. It is clearly a class 1 AVO. The gradient versus intercept crossplot (Figure 4.24) shows a negative gradient and a positive intercept which is a characteristic of the class 1 AVO by Castagna et al. (1998). The amplitude at zero angle (offset) is 0.178294.

At 20MPa differential stress, the amplitude of the interface for the overburden Lyr-Spekke-Melke on top of the brine saturated Garn Formation appears strong (Figure 4.25) due to the difference in the acoustic properties of the different lithologies at the interface. The amplitude decreases with increasing angles (offsets) as can be seen in Figure 4.26. The reflection is a class 1 AVO according to classification by Rutherford and Williams (1989). The gradient versus intercept crossplot (Figure 4.27) shows a negative gradient and a positive intercept clearly that of class 1 AVO, according to Castagna et al. (1998).The amplitude at zero angle (offset) is 0.111172.

Figure 4.28 shows the synthetic seismogram for the interface between the Lyr Formation and the underneath brine saturated Garn Formation. It shows a strong amplitude that deems at ultra-far angles (offsets). The amplitude decreases with increasing angles (offsets). Phase changes occur at the far angles (offset). A break can be seen on the ultra-far angles (offset). This could be as a result of noise (Figure 4.29). The AVO response is obviously a class 1 AVO according to Rutherford and Williams (1989). The gradient versus intercept crossplot shows a negative gradient plotting against positive intercept values. This is a characteristic of the class 1 AVO response according to Castagna et al. (1998).

Generally the reflection amplitudes for the interface between the Lyr Formation and the brine saturated Garn Formation under the various differential stress conditions (20MPa, 36MPa, and 50MPa) are higher than that of the overburden Lyr-Spekke-Melke on top of the brine saturated Garn Formation (Table 4.6). This can be attributed to the difference in the lithologies. The Lyr Formation is essentially marls with interbedded carbonates, while the overburden Lyr-Spekke-

Melke can be described as a heterogeneous body of Formation. This might have influenced the amplitude.

The lithology effects still dominates when we compare the reflection amplitudes for the differential stress conditions at 20MPa to that of 50MPa. Using the interface between the Lyr Formation and the brine saturated Garn Formation as a reference here, the amplitude at 20MPa is 0.166584 and for 50MPa is 0.178294. This analysis shows a 7% decrease in amplitude if we move from 50MPa differential stress condition to 20MPa differential stress condition. It would be a 7% increase if we move from 20MPa to 50MPa which is not that significant enough to be attributed to the effects of overpressure.

A major anomaly can be seen between the reflection amplitudes for 20MPa and 36MPa differential stress condition. Ideally, we should have expected the amplitude to be higher for the 36MPa but it turns out that the amplitudes for 20MPa is higher than the amplitudes for 36MPa. This anomaly could be ascribed to effects of attenuation, anisotropy or limitations associated with AVO modelling which are not investigated in this work.

Essentially, the AVO modelling in Geoview for the various differential stress conditions shows that the effects of lithology dominates the reflection amplitudes. The effects of overpressure has been masked effectively by the lithology effect.

5.3 UNCERTAINTIES

The sources that could introduce errors in the results are as follows:

- The process of removing the Spekke-Melke Formations within the wireline logs in order have the Lyr Formation on top of the brine saturated Garn Formation in MATLAB.
- The effects of heterogeneity, anisotropy and attenuation in the overburden Lyr-Spekke-Melke was not considered in this work.
- The inherent limitations associated with the Zoeppritz equations and algorithm might have introduced some unknown errors in the result.

6.0. CONCLUSIONS

The conclusions that can be drawn from the analysis of the velocity variations within the brine saturated Garn Formation using the Eberhart-Phillips model are as follows:

- The standard Eberhart-Phillips model fits very well into data points when we plot the velocity of the brine saturated Garn Formation against the differential stress within the selected wells in this work.
- The Eberhart-Phillips model is able to predict the velocity variations within the brine saturated Garn Formation for the selected wells in the area of study considered in this work.
- The velocity within the brine-filled Garn Formation is predominantly controlled by the differential stress and the porosity of the Garn Formation.

From the analysis of the AVO modelling results as regards to this work, we can conclude the followings:

- The single interface 1D AVO modelling technique seems to be a little ineffective in detecting the effects of attenuation or anisotropy,
- The lithology effect predominates within the near angles (offsets), while the effect of overpressure is only detectable towards the ultra-angle (offset). However, in seismic acquisition the acceptable angle (offset) limit is 0° to 30°.
- In this work the effects of lithology on the AVO response masks the effects of overpressure for all the differential stress conditions at 20MPa, 36MPa and 50MPa. Therefore, it is not possible to detect overpressure as regards to the layered 1D AVO modelling in Hampson Russell Geoview as regards to this work.

6.1 RECOMMENDATIONS FOR FUTURE WORK

Interpretation of Geophysical data requires the integration of different data from several sources in other to minimize uncertainties and risks. In view of this, further research has to be done to investigate the effects of lithology and overpressure using the techniques applied in this study. A detailed study on the effects of attenuation, anisotropy, and the effects of diagenetic changes has to be considered for both the single interface and layered AVO modelling.

It would be nice to compare real data from brine saturated Garn Formations from different wells at different differential stress condition to ascertain how the reflectivity will respond to the effects of lithology and overpressure.

For the single interface 1D AVO modelling, overpressure seem to be detected at ultra-far angles. A comparison with real data should be done to verify this phenomenon. Although, the angles (offsets) valid in Geoscience is between 0° to 30°.

ACKNOWLEDGEMENTS

I thank my supervisor Associate Professor Kenneth Duffaut for being there always and for his guidance. I could not have asked for more.

I am also grateful to NPD Norway for providing the dataset I used in this work, and CGG for their consent to use the Geoview for my models.

I wish to express my profound gratitude to PTDF Nigeria who through a Scholarship Programme, fund my master's degree at NTNU.

I am eternally grateful to Almighty God for his grace in my life.

REFERENCE AND BIBLIOGRAPHY

Norwegian Petroleum Directorate [Online]. Available: http://www.npd.no [Accessed 17th June 2016].

AKI, K. & RICHARDS, P. 1980. Quantitative seisinology. *Theory and*.

AMINZADEH, F. & DASGUPTA, S. N. 2013. *Geophysics for Petroleum Engineers*, Newnes.

AVSETH, P., MUKERJI, T. & MAVKO, G. 2010a. *Quantitative seismic interpretation: Applying rock physics tools to reduce interpretation risk*, Cambridge University Press.

AVSETH, P., MUKERJI, T., MAVKO, G. & DVORKIN, J. 2010b. Rock-physics diagnostics of depositional texture, diagenetic alterations, and reservoir heterogeneity in high-porosity siliciclastic sediments and rocks—A review of selected models and suggested work flows. *Geophysics,* 75**,** 75A31-75A47.

BACKUS, G. E. 1962. Long-wave elastic anisotropy produced by horizontal layering. *Journal of Geophysical Research,* 67**,** 4427-4440.

BACON, M., SIMM, R. & REDSHAW, T. 2007. *3-D seismic interpretation*, Cambridge University Press.

BJORLYKKE, K. 2010. *Petroleum geoscience: From sedimentary environments to rock physics*, Springer Science & Business Media.

BLYSTAD, P. 1995. *Structural Elements of the Norwegian Continental Shelf: The Norweigan Sea Region*, Norwegian Petroleum Directorate.

BOLÅS, H. M. N. & HERMANRUD, C. 2003. Hydrocarbon leakage processes and trap retention capacities offshore Norway. *Petroleum Geoscience,* 9**,** 321-332.

BORGE, H. 2002. Modelling generation and dissipation of overpressure in sedimentary basins: an example from the Halten Terrace, offshore Norway. *Marine and Petroleum Geology,* 19**,** 377-388.

BOWERS, G. L. 1995. Pore pressure estimation from velocity data: Accounting for overpressure mechanisms besides undercompaction. *SPE Drilling & Completion,* 10**,** 89-95.

BRUCE, B. 2002. An introduction to this special section: Pore pressure. *The leading edge,* 21**,** 169-177.

BRUCE, B. & BOWERS, G. 2002. Pore pressure terminology. *The Leading Edge,* 21**,** 170-173.

CASTAGNA, J. & BACKUS, M. 1993. Offset-dependent reflectivity–Theory and practice of AVO analysis: SEG publication. Tulsa.

CASTAGNA, J. P., BATZLE, M. L. & EASTWOOD, R. L. 1985. Relationships between compressional-wave and shear-wave velocities in clastic silicate rocks. *Geophysics,* 50**,** 571-581.

CASTAGNA, J. P. & SWAN, H. W. 1997. Principles of AVO crossplotting. *The leading edge,* 16**,** 337-344.

CASTAGNA, J. P., SWAN, H. W. & FOSTER, D. J. 1998. Framework for AVO gradient and intercept interpretation. *Geophysics,* 63**,** 948-956.

CHOPRA, S. & CASTAGNA, J. 2014. AVO: SEG Investigations in Geophysics 16. *Society of Exploration Geophysicists, Tulsa, OK*.

DALLAND, A., WORSLEY, D. & OFSTAD, K. 1988. A lithostratigraphic scheme for the Mesozoic and Cenozoic succession offshore Norway north of 62 N. *NPD Bull,* 4**,** 67.

DUTTA, N. 2002. Geopressure prediction using seismic data: Current status and the road ahead. *Geophysics,* 67**,** 2012-2041.

DVORKIN, J., GUTIERREZ, M. A. & GRANA, D. 2014. *Seismic reflections of rock properties*, Cambridge University Press.

DVORKIN, J., MAVKO, G. & NUR, A. 1999. Overpressure detection from compressional-and shear-wave data. *Geophysical research letters,* 26**,** 3417-3420.

DVORKIN, J. P. 2008. Yet another V s equation. *Geophysics,* 73**,** E35-E39.

EBERHART-PHILLIPS, D., HAN, D.-H. & ZOBACK, M. D. 1989. Empirical relationships among seismic velocity, effective pressure, porosity, and clay content in sandstone. *Geophysics,* 54**,** 82-89.

EHRENBERG, S., GJERSTAD, H. & HADLER-JACOBSEN, F. 1992. Smorbukk Field: A Gas Condensate Fault Trap in the Haltenbanken Province, Offshore Mid-Norway: Chapter 21.

ELDHOLM, O. 1987. 1. EVOLUTION OF THE NORWEGIAN CONTINENTAL MARGIN: BACKGROUND AND OBJECTIVES1.

FALEIDE, J. I., BJØRLYKKE, K. & GABRIELSEN, R. H. 2015. Geology of the Norwegian continental shelf. *Petroleum Geoscience.* Springer.

FERTL, W. H. 1981. *Abnormal formation pressures*, Elsevier.

FJAR, E., HOLT, R. M., RAAEN, A., RISNES, R. & HORSRUD, P. 2008. *Petroleum related rock mechanics*, Elsevier.

FOSTER, D., SMITH, S., DEY-SARKAR, S. & SWAN, H. A closer look at hydrocarbon indicators. 63rd SEG meeting, Washington, DC, USA, Expanded Abstracts, 1993. 731-733.

FOSTER, D. J., KEYS, R. G. & LANE, F. D. 2010. Interpretation of AVO anomalies. *Geophysics,* 75**,** 75A3-75A13.

GREENBERG, M. & CASTAGNA, J. 1992. SHEAR-WAVE VELOCITY ESTIMATION IN POROUS ROCKS: THEORETICAL FORMULATION, PRELIMINARY VERIFICATION AND APPLICATIONS1. *Geophysical prospecting,* 40**,** 195-209.

HAMPSON-RUSSELL, C. 2013. *Geoview*. Canada patent application.

HAMPSON, D. 1991. AVO inversion, theory and practice. *The Leading Edge,* 10**,** 39-42.

HAN, D.-H., NUR, A. & MORGAN, D. 1986. Effects of porosity and clay content on wave velocities in sandstones. *Geophysics,* 51**,** 2093-2107.

HILTERMAN, F. J. Is AVO the seismic signature of rock properties? 1989 SEG Annual Meeting, 1989. Society of Exploration Geophysicists.

HOFMANN, R., XU, X., BATZLE, M., PRASAD, M., FURRE, A.-K. & PILLITTERI, A. 2005. Effective pressure or what is the effect of pressure? *The Leading Edge,* 24**,** 1256-1260.

HYNE, N. 2014. *Dictionary of petroleum exploration, drilling & production*, PennWell Corporation.

JOHNSTON, D. H. 2013. Practical applications of time-lapse seismic data. *Distinguished Instructor Short Course, SEG,* 16**,** 270.

LARSEN, R. M. & HEUM, O. 1988. Haltenbanken hydrocarbon province (offshore mid-Norway). *AAPG (Am. Assoc. Pet. Geol.) Bull.;(United States),* 72.

LI, Y., DOWNTON, J. & XU, Y. 2007. Practical aspects of AVO modeling. *The Leading Edge,* 26**,** 295-311.

MARTINIUS, A. W., RAVNÃ, R., HOWELL, J., STEEL, R. & WONHAM, J. 2014. *From Depositional Systems to Sedimentary Successions on the Norwegian Continental Margin (Special Publication 46 of the IAS)*, John Wiley & Sons.

MAVKO, G., MUKERJI, T. & DVORKIN, J. 2009. *The rock physics handbook: Tools for seismic analysis of porous media*, Cambridge university press.

NØTTVEDT, A. Dynamics of the Norwegian margin. 2000. Geological Society of London.

OSTRANDER, W. 1984. Plane-wave reflection coefficients for gas sands at nonnormal angles of incidence. *Geophysics,* 49**,** 1637-1648.

RICHARDS, P. G. & FRASIER, C. W. 1976. Scattering of elastic waves from depth-dependent inhomogeneities. *Geophysics,* 41**,** 441-458.

ROCK-PHYSICS-ASSOCIATES 2007. Professional Level Rock Physics for seismic amplitude interpretation. 365.

RUTHERFORD, S. R. & WILLIAMS, R. H. 1989. Amplitude-versus-offset variations in gas sands. *Geophysics,* 54**,** 680-688.

SCHÖN, J. 2011. *Physical properties of rocks: A workbook*, Elsevier.

SHUEY, R. 1985. A simplification of the Zoeppritz equations. *Geophysics,* 50**,** 609-614.

SIMM, R., BACON, M. & BACON, M. 2014. *Seismic Amplitude: An Interpreter's Handbook*, Cambridge University Press.

SMITH, G. & GIDLOW, P. 1987. Weighted stacking for rock property estimation and detection of gas. *Geophysical Prospecting,* 35**,** 993-1014.

TINGAY, M. R., HILLIS, R. R., SWARBRICK, R. E., MORLEY, C. K. & DAMIT, A. R. 2009. Origin of overpressure and pore-pressure prediction in the Baram province, Brunei. *AAPG Bulletin,* 93**,** 51-74.

VEGA, S., MUKERJI, T., MAVKO, G. & PRASAD, M. 2003. Stanford Rock Physics Laboratory.

WANG, Z. 2001. Fundamentals of seismic rock physics. *Geophysics,* 66**,** 398-412.

WIGGINS, R., KENNY, G. & MCCLURE, C. 1983. A method for determining and displaying the shear-velocity reflectivities of a geologic formation. *European Patent Application,* 113944.

ZOEPPRITZ, K. & VIIIB, E. 1919. On the reflection and propagation of seismic waves. *Gottinger Nachrichten,* 1**,** 66-84.

APPENDICES

APPENDIX A

Theoretical Bounds:

Examples of theoretical bounds in rock physics are the Reuss and the Voigt bounds. Theoretical bounds in rock physics describes the physical limits of the elastic, poroelastic properties of a mixture of minerals and fluids. For example, the Ruess average determines the effective limits of the lower bound of porosity-velocity behaviour of sandstones, while the Voigt average determines the upper bound as shown in plate 1 (Simm et al., 2014). Bounds represents the rock as an elastic composite, and there are devoid of idealizations and approximations (Avseth et al., 2010b).

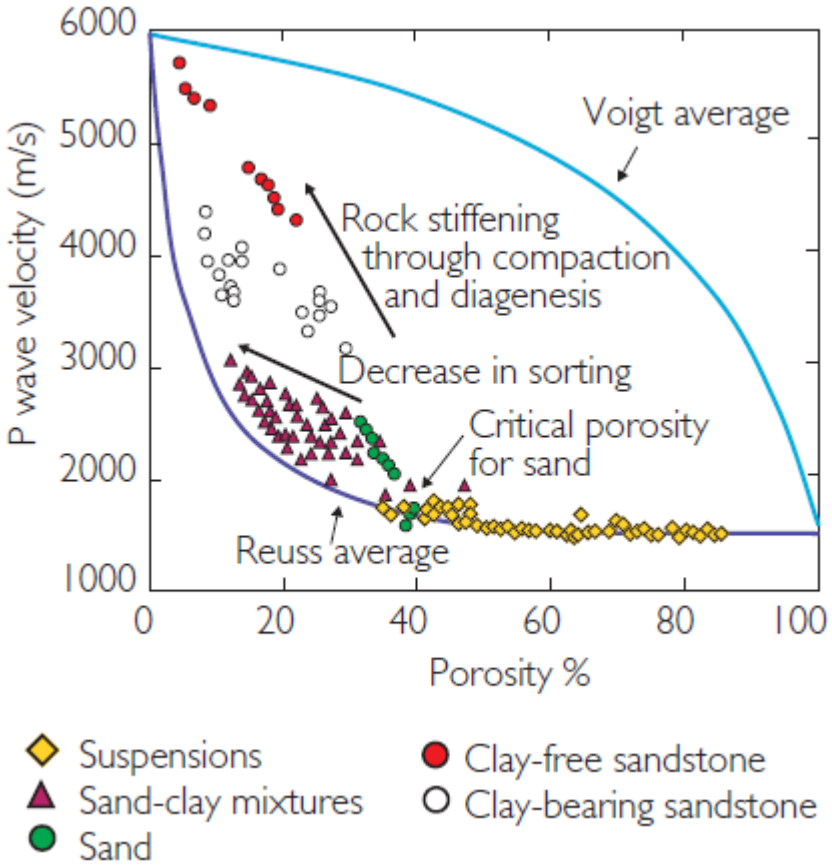

Plate 1: Shows the P-wave velocity versus Porosity for a variety of water saturated sediments, Indicating the Ruess and the Voigt average. Adapted from Simm et al. (2014).

Considering a mixture of quartz and water, as follows.

The Voigt modulus of the mixture is given as;

$$K_{voigt} = K_{quartz}Vol_{quartz} + K_{water}Vol_{water} \quad (1)$$

where

K_{quartz} is the Bulk modulus of the Quartz minerals,

K_{water} is the Bulk modulus of water,

Vol_{quartz} is the volume fraction of Quartz minerals,

Vol_{water} is the volume fraction of water.

The Reuss modulus is expressed as;

$$\frac{1}{K_{Reuss}} = \frac{Vol_{quartz}}{K_{quarz}} + \frac{Vol_{water}}{K_{water}} \quad (2)$$

Another type of commonly used rock physics theoretical bound is the Hashin-Shrikman bound. It is more complicated than the Ruess and Voigt bounds. See Avseth et al. (2010b), Mavko et al. (2009) for details.

Although bounds does not predict the variation of velocities of brine saturated sandstones, they are very useful mixing laws that could give accurate interpolation of sorting and cementing trends. Theoretical Bounds are valuable in the descriptions of suspensions and fluid mixtures for input into the Gassmann equation (Avseth et al., 2010b).

Gassmann Equation

The Gassmann's equation tells how the properties of rocks are influenced by changing the fluid in-fill for example replacing water with Hydrocarbon. The bulk modulus of a fluid saturated rock is calculated using the Bulk moduli of the rock frame (the skeleton rock sample), solid frame (the rock forming mineral) and the pore-fluid (water, gas, or oil) (Wang, 2001).

Some assumptions are applied to the use of the Gassmann's equation includes;

- The rock is homogenous and isotropic,
- All pore spaces are interconnected or communication,
- The fluids that fills the pore spaces are frictionless,
- The fluids and the pores does not interact,
- The rock system under consideration is undrained.
- The steps involved in carrying out fluid substitution using the Gassmann's equation involves;

Start with measured velocities and density ($V_{p1,}V_{s1}$ and ρ,)

Calculate the both the Shear and Bulk modulus measured with fluid 1:

$$K_1 = \rho_1 \left[(V_{P1})^2 - \frac{4}{3}(V_{S1})^2 \right] \quad (3)$$

$$\mu_1 = \rho_1 (V_{S1})^2 \quad (4)$$

Compute the Frame Modulus using:

$$\frac{K_1}{K_s - K_1} = \frac{K_{fr}}{K_s - K_{fr}} + \frac{K_f}{\phi(K_s - K_f)} \quad (5)$$

Where:

K_{fr}= Frame moduli,

K_s = Solid moduli (This is usually known e.g 37GPa for Quartz Grains)

K_f= Fluid moduli, (Usually known e.g. 2.5GPa for Brine)

ϕ= Porosity. (Measured from the Density or Neutron logs)

Compute the Bulk density of the rock using the second fluid:

$$\rho_2 = (1 - \phi)\rho_s + (\phi\rho_f) \quad (6)$$

Where:

ρ_s= Density of the matrix (This is usually given as 2,65g/cc for Quartz minerals obtained from cores),

ρ_f= Density of the fluid (This is usually given as 1.03g/cc for Brine).

Compute the Bulk modulus of the Saturated Sandstone using the Frame Bulk modulus from step 3, Porosity using:

$$K_{sat} = K_{fr} + \frac{K_f}{\varphi} \frac{\alpha^2}{1 + \frac{K_f}{\varphi K_s}(\alpha - \varphi)} \quad (7)$$

Where:

$$\alpha = 1 - \frac{K_f}{K_s}, \quad (8)$$

Compute the new Shear and Compressional Velocity using K_{sat} from step 5, ρ_2 from step 4;

Since Shear wave is not influenced by fluid, then

$$\mu_1 = \mu_2, \quad (9)$$

$$V_p = \sqrt{\frac{K_{sat} + \frac{4}{3}(\mu_2)^2}{\rho_2}} \quad (10)$$

(Vega et al., 2003)

Wyllie's (time average) equation:

It shows the relationship between velocity and porosity for a well for a fluid filled, consolidated sediment. The Wyllie's equation states that the sonic interval transit time is derives from the addition of the transit time through the pore fluid and that through the solid matrix (Simm et al., 2014).

This is mathematically expressed as:

$$t_{total} = \varphi t_{fluid} + (1 - \varphi) t_{solid} \quad (11)$$

Where:

φ= Porosity (fraction),

t_{fluid}= Interval transit time through the fluid,

t_{solid}= Interval transit time through the rock's matrix.

Han's Relations:

Han's relations shows the empirical relationship between porosity, compressional wave velocity and clay content. The experiment is carried out in the laboratory using well consolidated sandstones. According to Simm et al. (2014), the essence of the clay content is to soften the rock and reduce the compressional wave velocity.

From the experiment carried out under a high pressure of 40 MPa,

$$Vp = 5.59 - 6.93\varphi - 2.18C \quad (12)$$

$$Vs = 3.52 - 4.91\varphi - 1.89C \quad (13)$$

Where: Vp is in km/s, C is clay content, φ is the porosity.

Appendix B

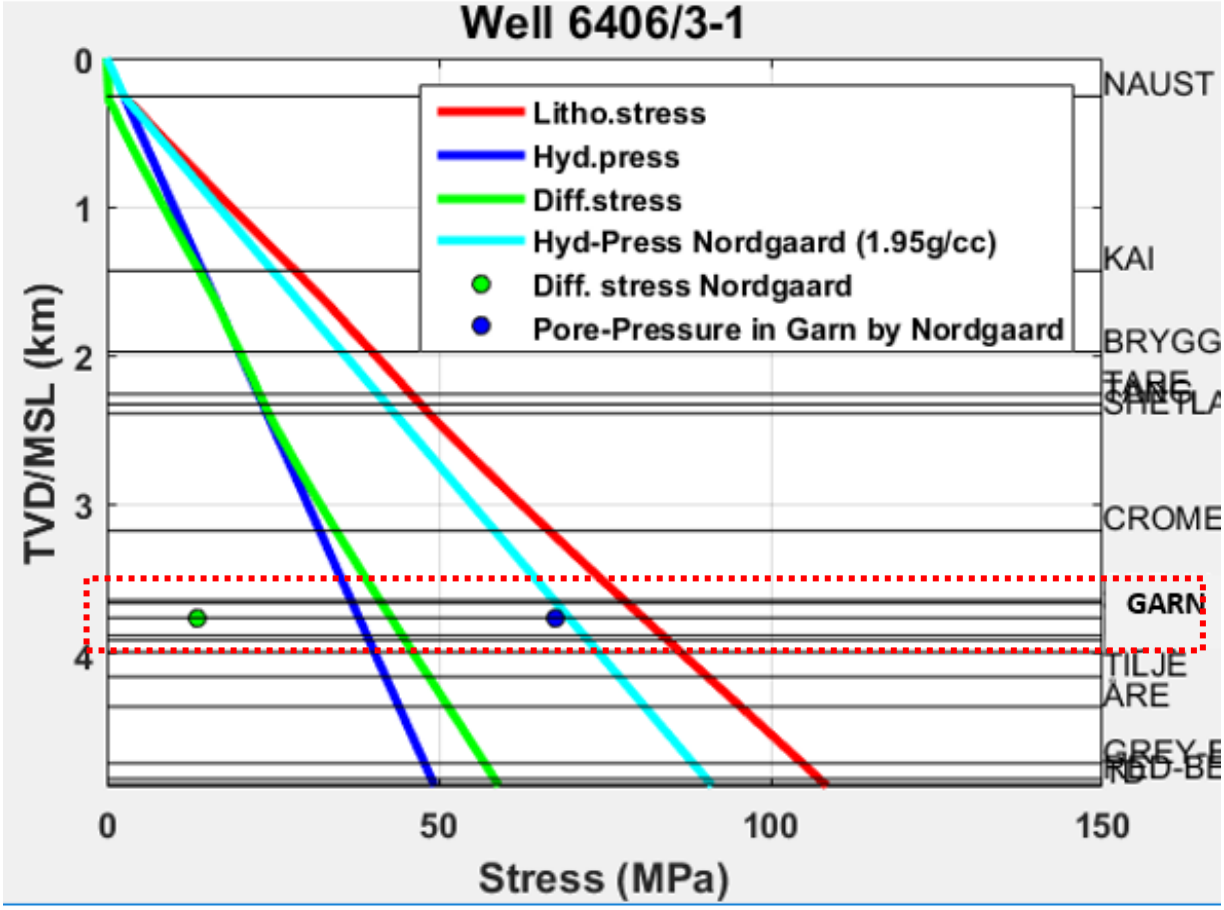

Plate 2: Plot showing the fluid pressure as a funtion of depth for well 6406/3-1 computed with Matlab. The data used in the computation was based on the Bolås and Hermanrud (2003) article.

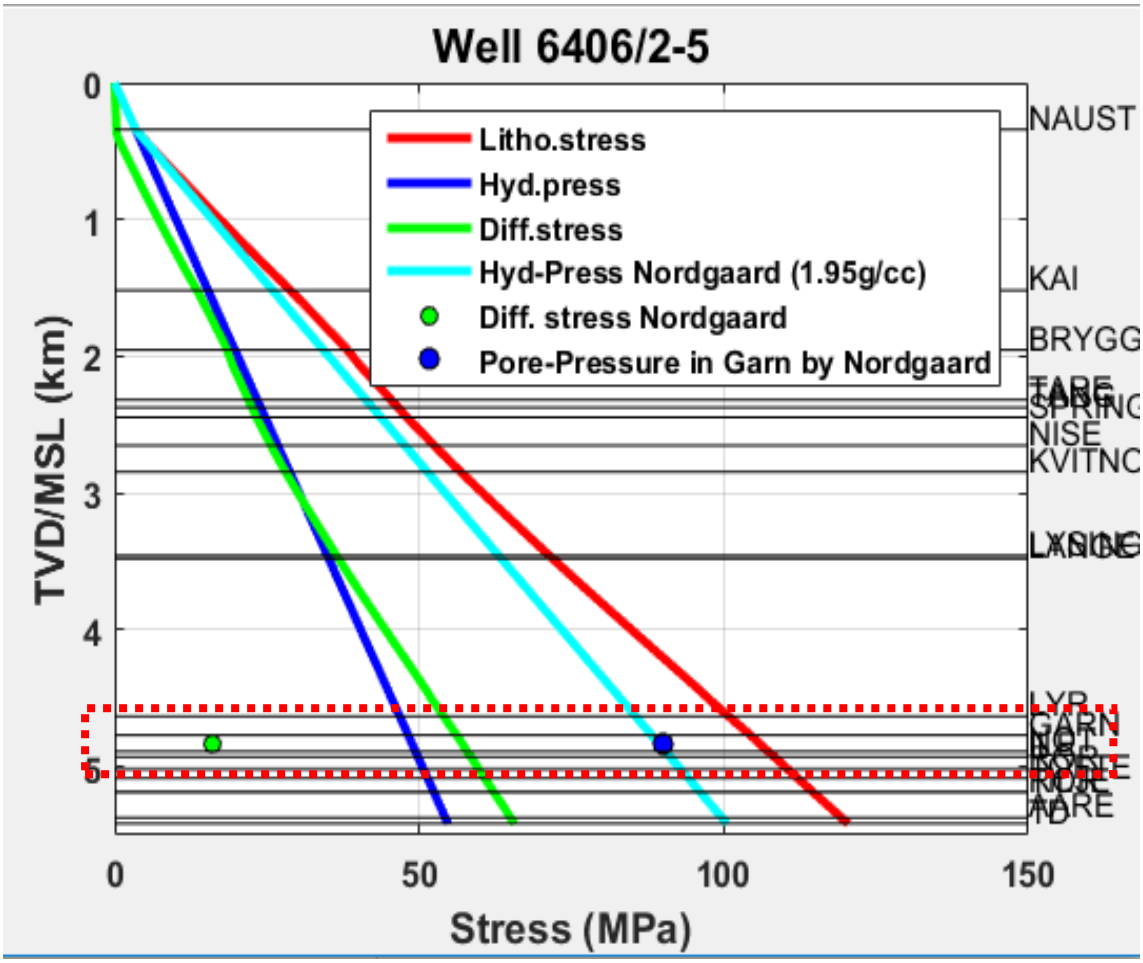

Plate 3: Plot showing the fluid pressure as a function of depth for well 6406/2-1 computed with Matlab. The data used in the computation was based on Bolås and Hermanrud (2003) article.

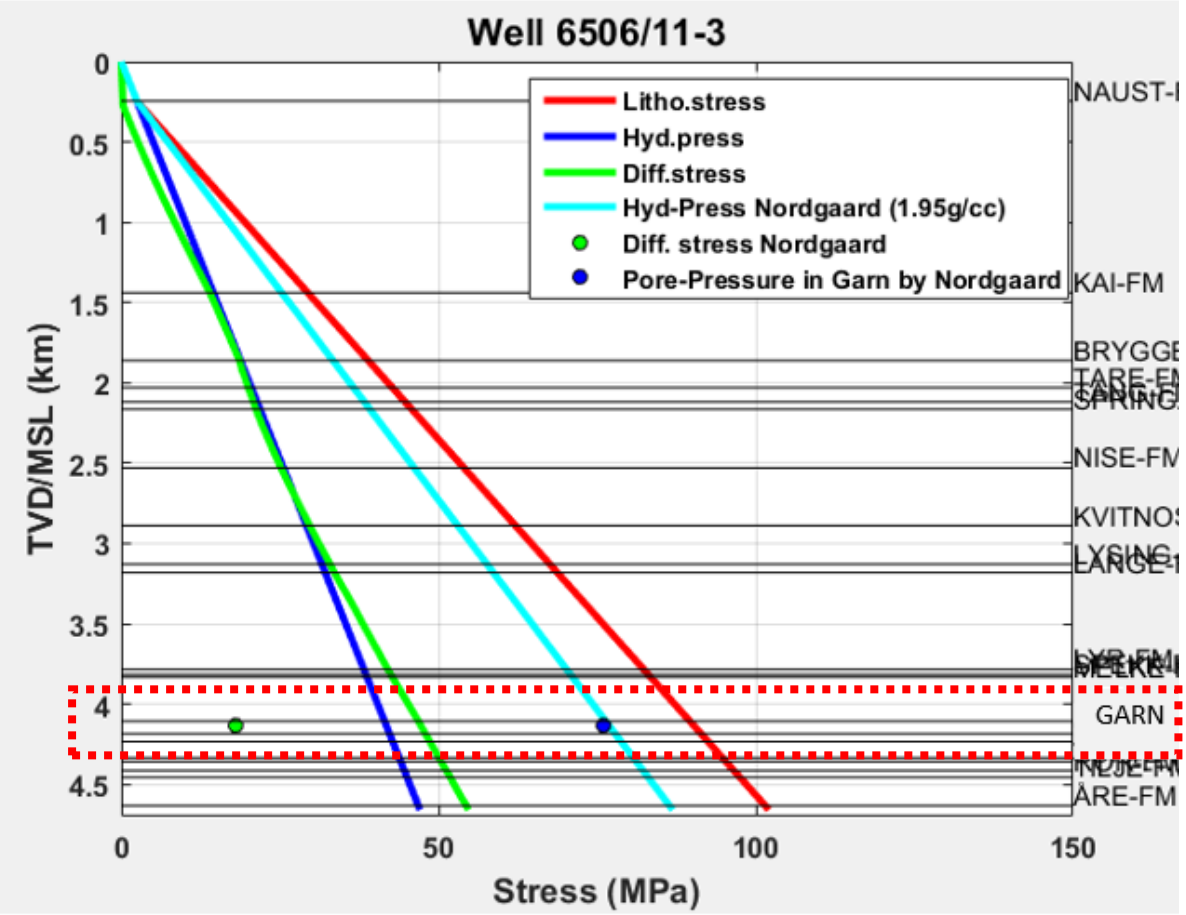

Plate 4: Plot showing the fluid pressure as a funtion of depth for well 6506/11-3 computed with Matlab. The data used in the computation was based on Bolås and Hermanrud (2003)

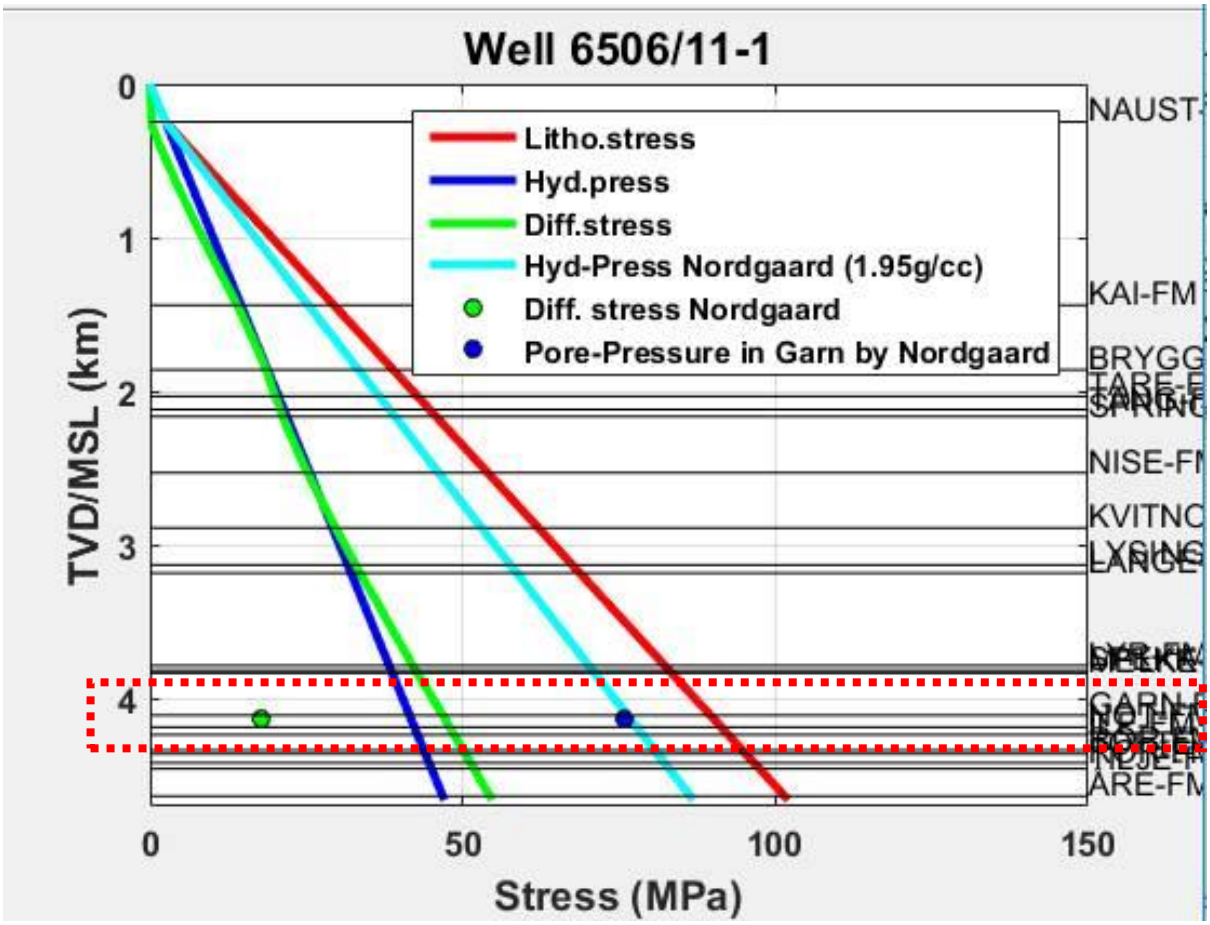

Plate 5: Plot showing the fluid pressure as a funtion of depth for well 6506/11-1 computed with Matlab. The data used in the computation was based on Bolås and Hermanrud (2003) article.

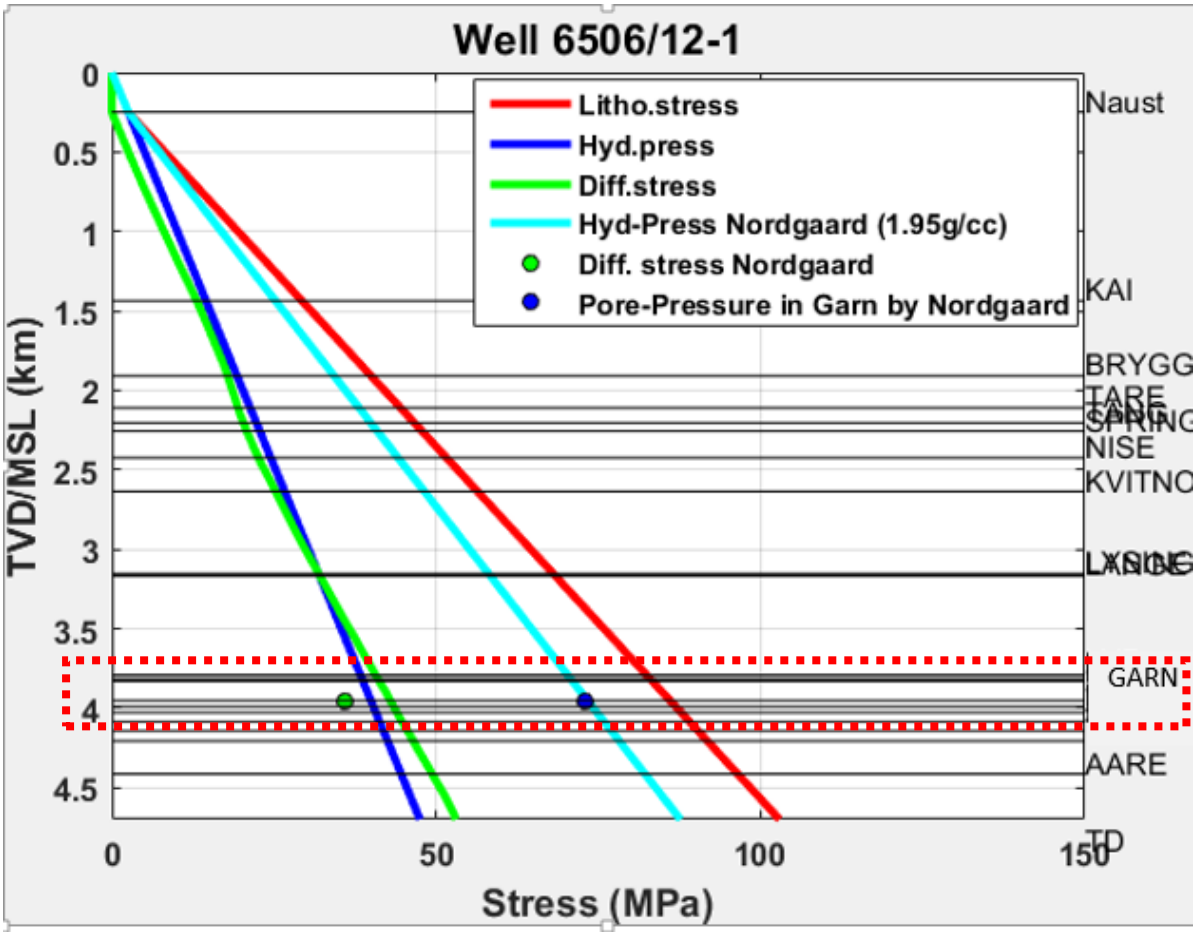

Plate 6: Plot showing the fluid pressure as a funtion of depth for well 6506/12-1 computed with Matlab. The data used in the computation was based on the Bolås and Hermanrud (2003) article.

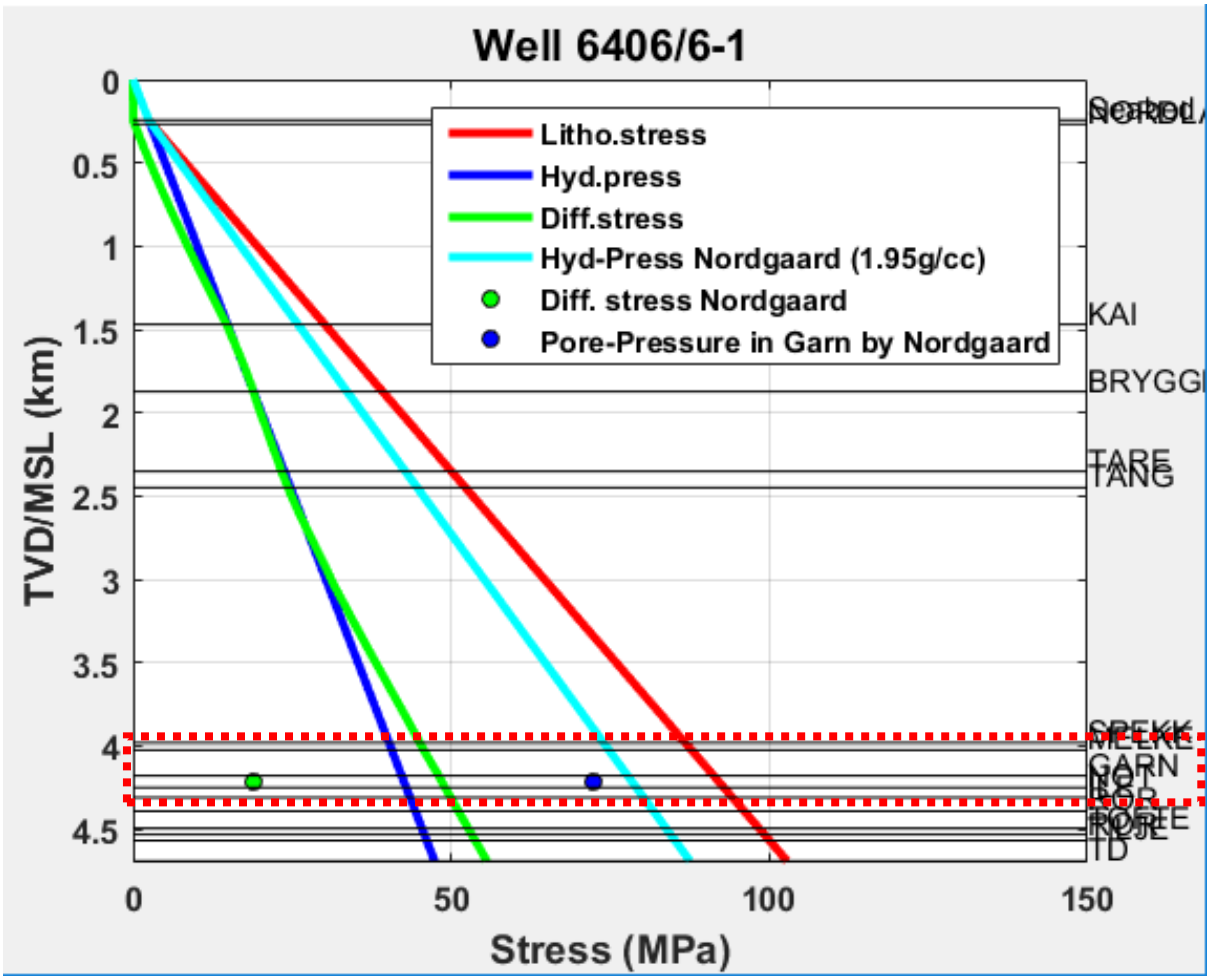

Plate 7: Plot showing the fluid pressure as a funtion of depth for well 6406/6-1 computed with Matlab. The data used in the computation was based on the Bolås and Hermanrud (2003) article.

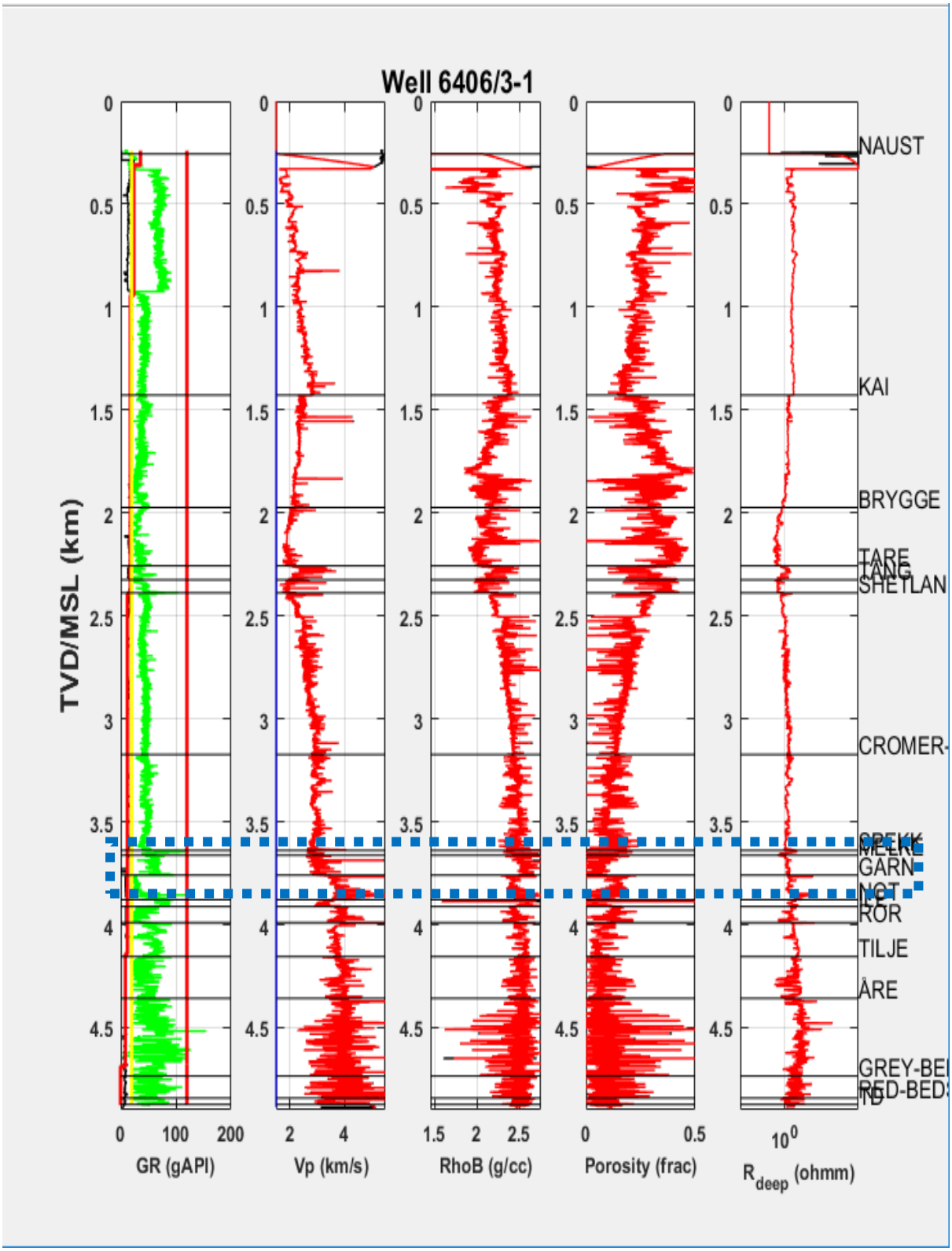

Plate 8: Well log signatures from the well 6406/3-1 generated from Matlab. Track 1: GR log, Track 2: P-Wave Velocity log, Track 3: Density log, Track 4: Porosity log, Track 5: Resistivity log

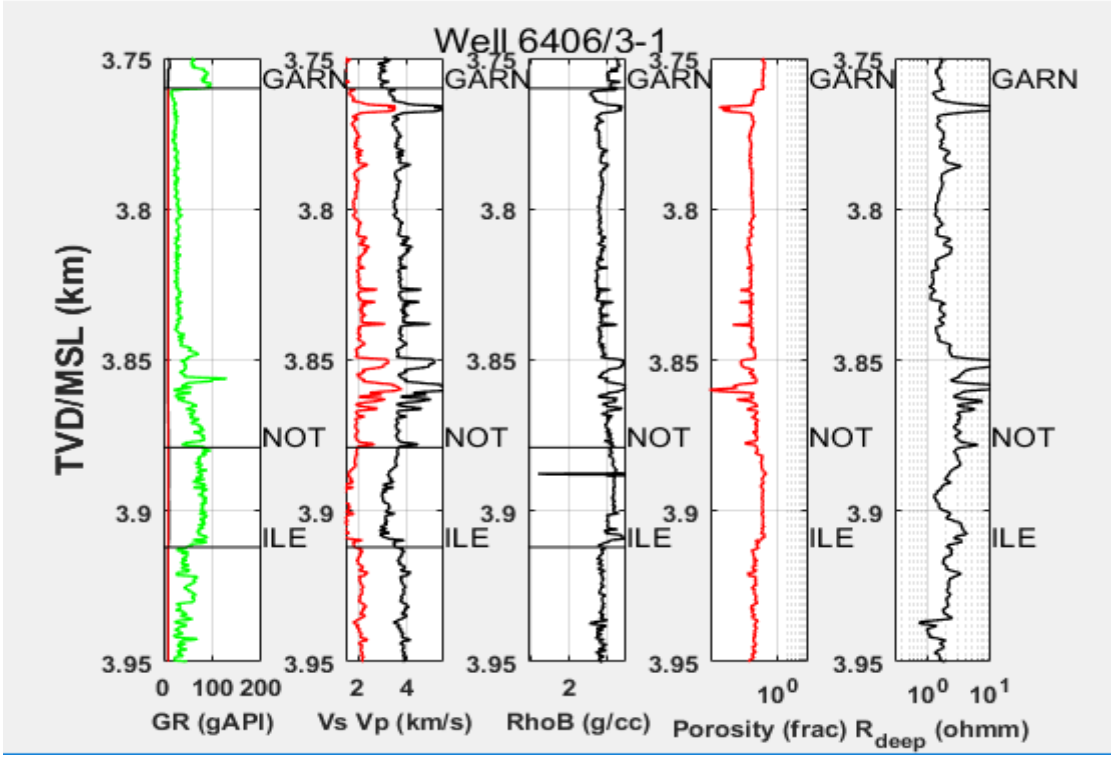

Plate 9: Well log signatures from well 6406/3-1 generated from Matlab. Track 1: GR log, Track 2: P-Wave Velocity log, Track 3: Density log, Track 4: Porosity log, Track 5: Resistivity log (Zoomed-in at the Garn Formation Interval).

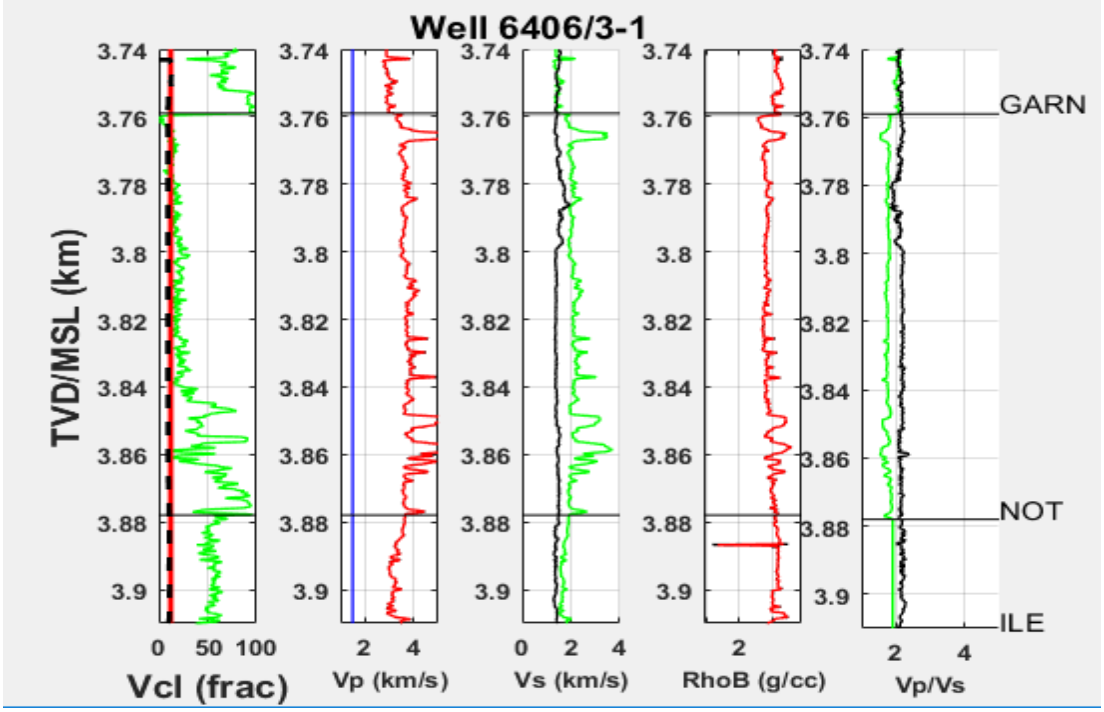

Plate 10:Well log signatures from well 6406/3-1 generated from Matlab. Track 1: VCl log, Track 2: P-Wave Velocity log, Track 3: S-Wave Predicted log (green=Greenberg-Castagna, black=mudrock, Track 4: Density log, Track 5: Vp/Vs log (Zoomed-in at the Garn Formation Interval).

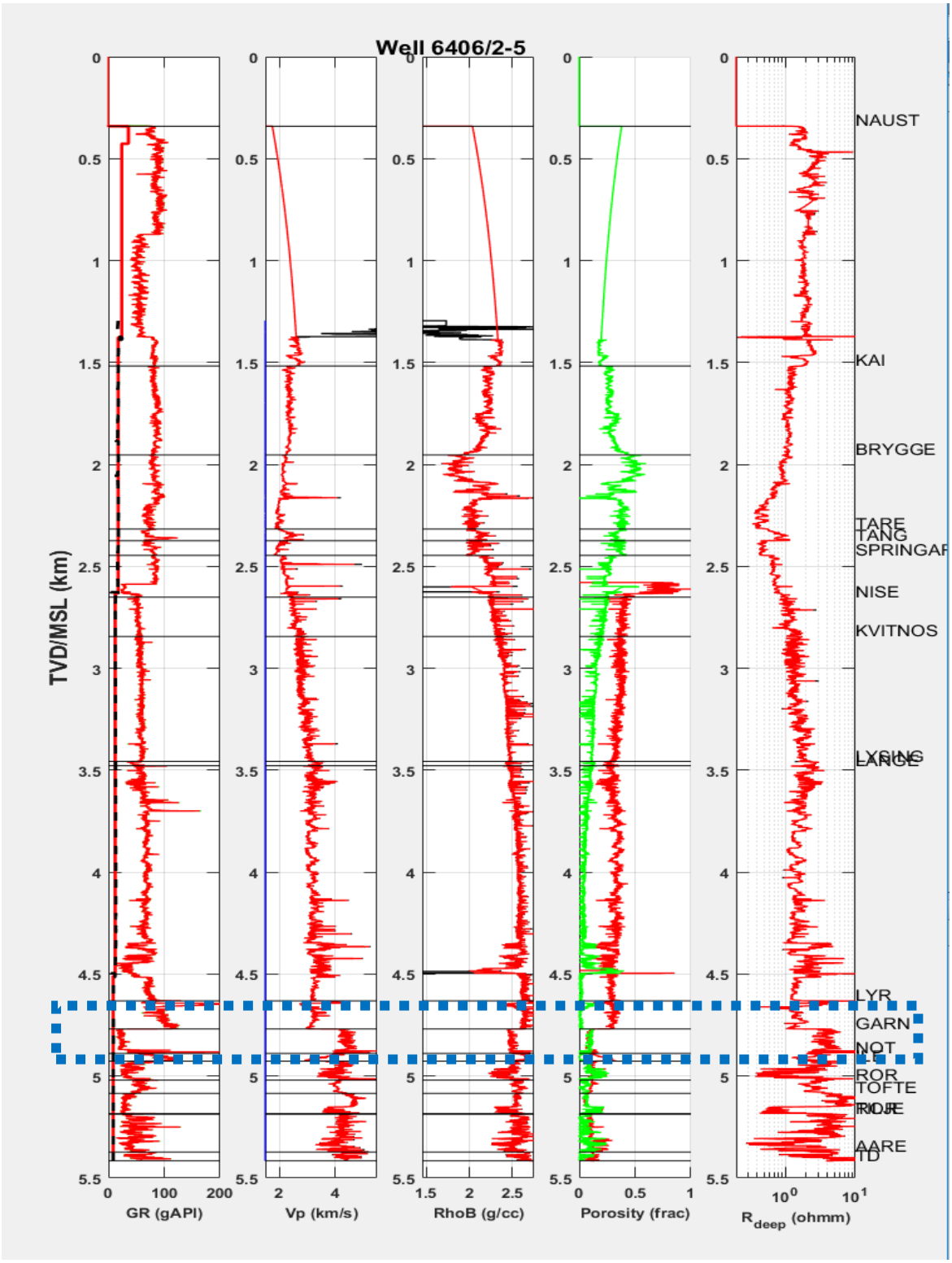

Plate 11: Well log signatures from well 6406/2-5 generated from Matlab. Track 1: GR log, Track 2: P-Wave Velocity log, Track 3: Density log, Track 4: Porosity log, Track 5: Resistivity log.

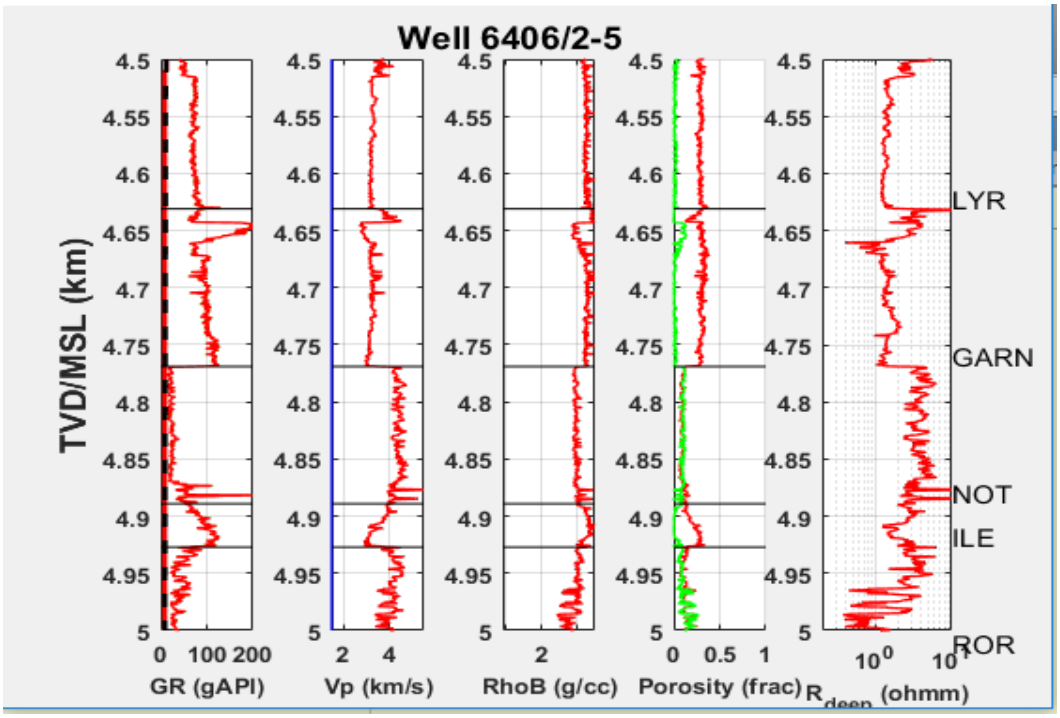

Plate 12: Well log signatures from well 6406/2-5 generated from Matlab. Track 1: GR log, Track 2: P-Wave Velocity log, Track 3: Density log, Track 4: Porosity log, Track 5: Resistivity log (Zoomed-in at the Garn Formation Interval).

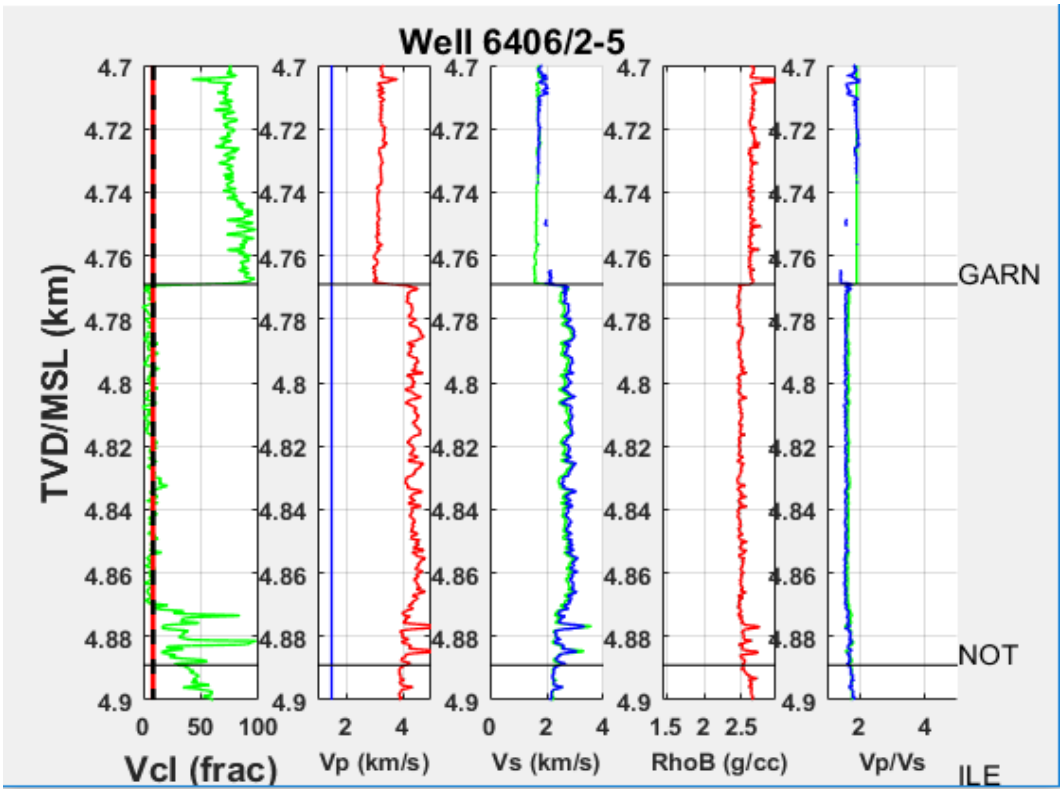

Plate 13: Well log signatures from well 6406/2-5 generated from Matlab. Track 1: VCl log, Track 2: P-Wave Velocity log, Track 3: S-Wave Predicted log (green=Greenberg-Castagna, black=mudrock, Track 4: Density log, Track 5: Vp/Vs log (Zoomed-in at the Garn Formation Interval).

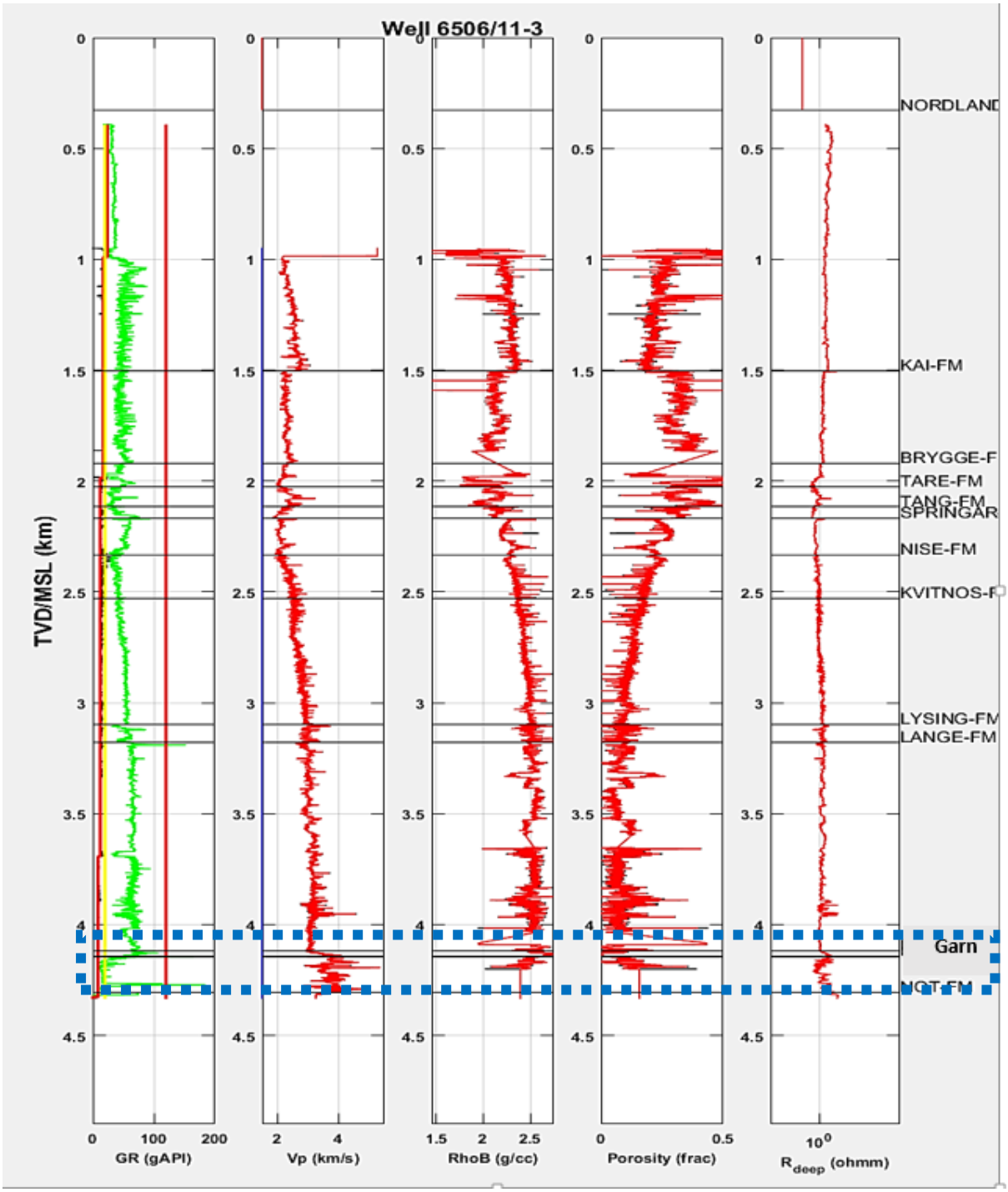

Plate 14: Well log signatures from well 6506/11-3 generated from Matlab. Track 1: GR log, Track 2: P-Wave Velocity log, Track 3: Density log, Track 4: Porosity log, Track 5: Resistivity log.

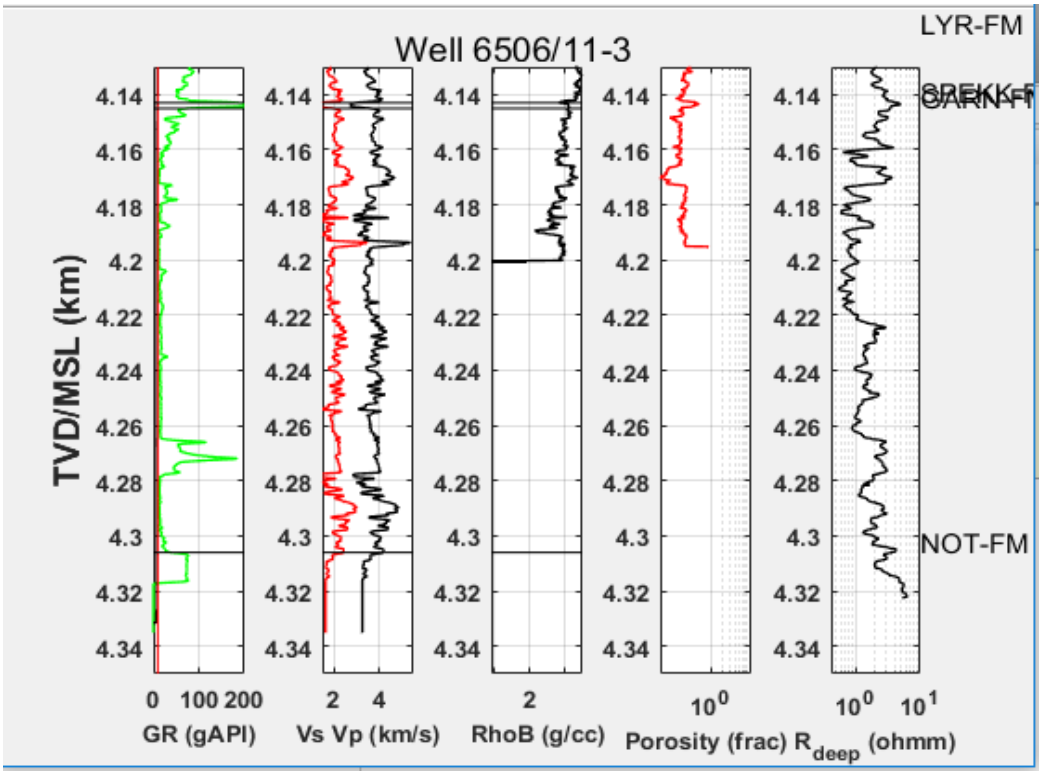

Plate 15: Well log signatures from well 6506/11-3 generated from Matlab. Track 1: GR log, Track 2: P-Wave Velocity log, Track 3: Density log, Track 4: Porosity log, Track 5: Resistivity log (Zoomed-in at the Garn Formation Interval).

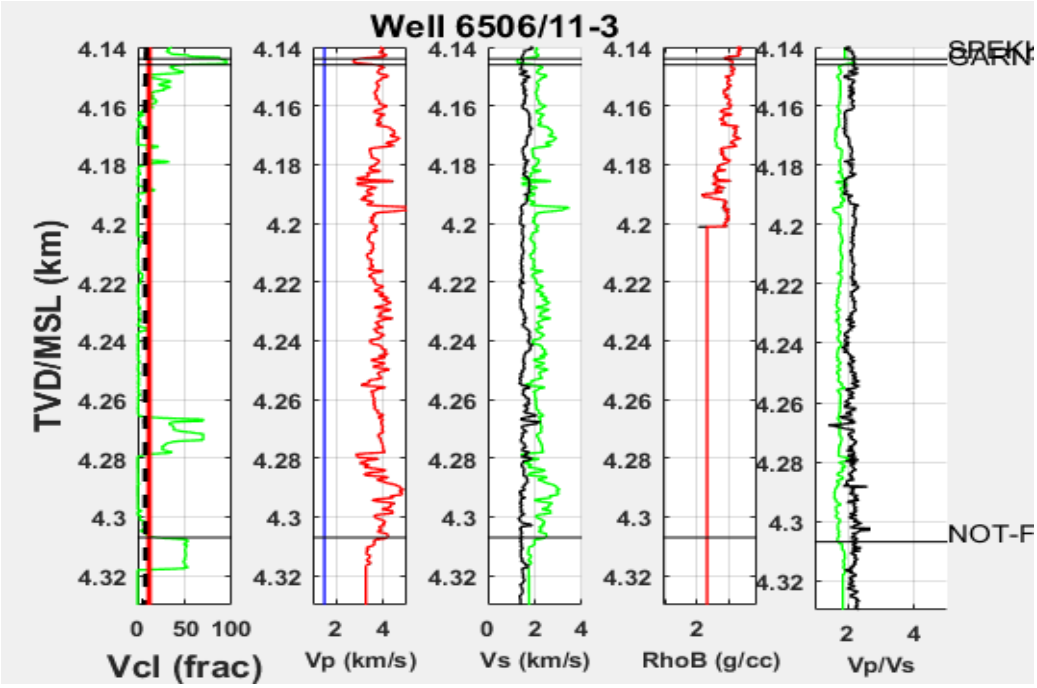

Plate 16:Well log signatures from well 6506/11-3 generated from Matlab. Track 1: VCl log, Track 2: P-Wave Velocity log, Track 3: S-Wave Predicted log (green=Greenberg-Castagna, black=mudrockTrack4: Density log, Track 5: Vp/Vs log (Zoomed-in at the Garn Formation Interval).

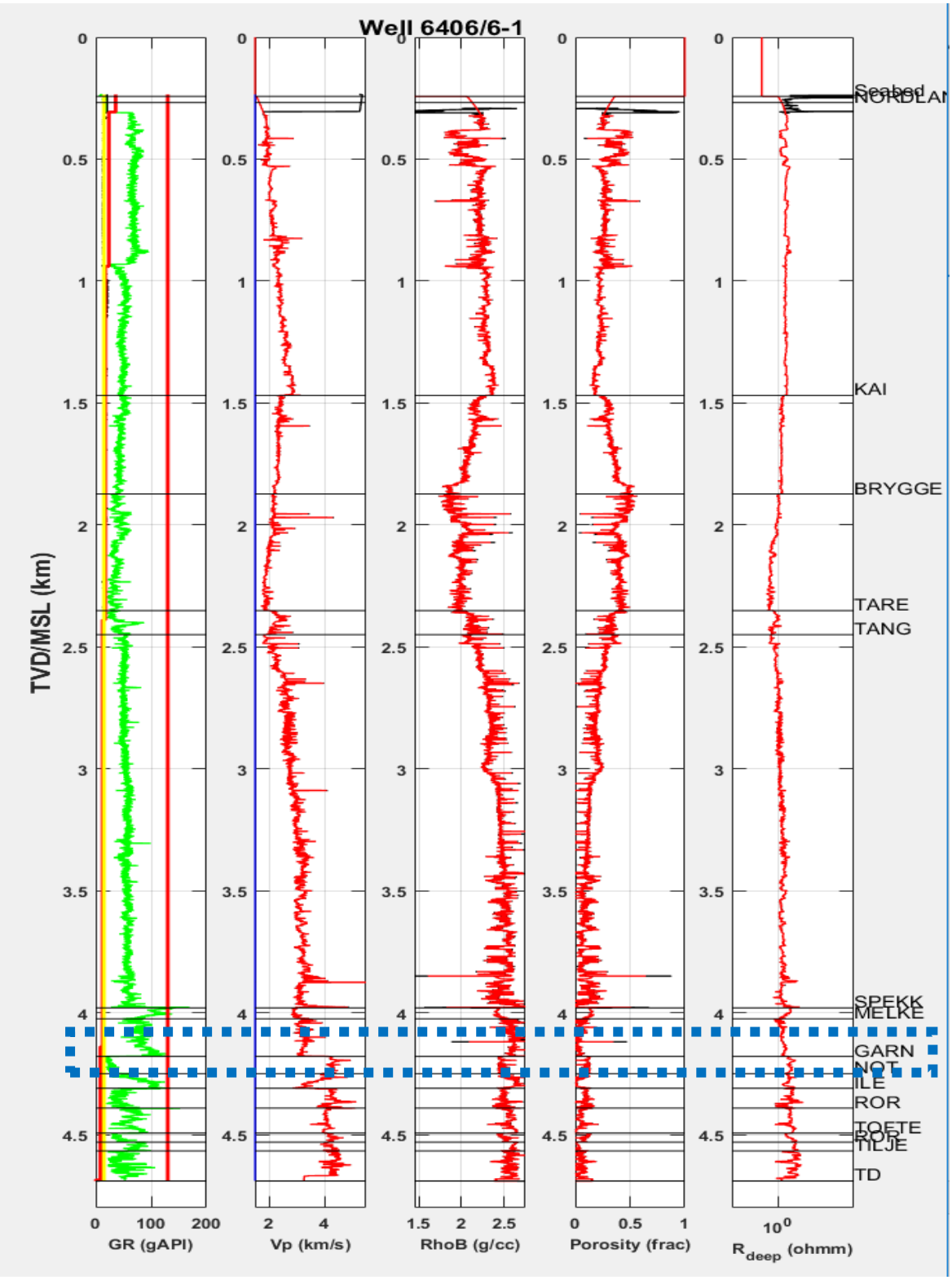

Plate 17: Well log signatures from the well 6406/6-1 generated from Matlab. Track 1: GR log, Track 2: P-Wave Velocity log, Track 3: Density log, Track 4: Porosity log, Track 5: Resistivity log.

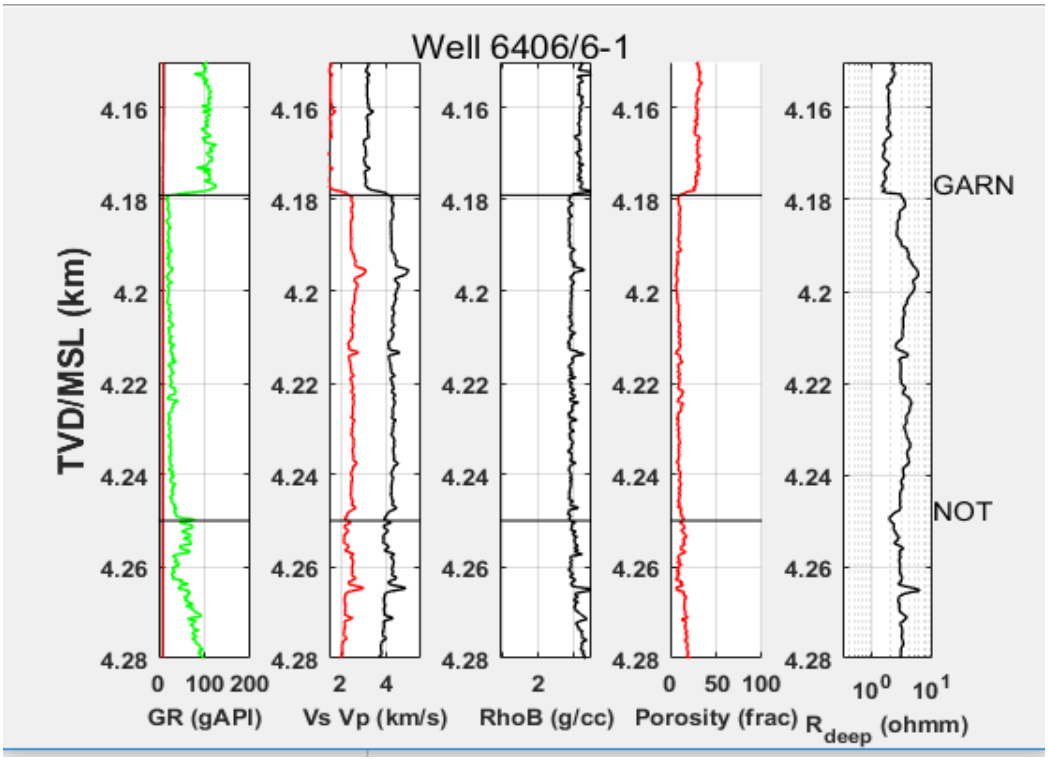

Plate 18: Well log signatures from the well 6406/6-1 generated from Matlab. Track 1: GR log, Track 2: P-Wave Velocity log, Track 3: Density log, Track 4: Porosity log, Track 5: Resistivity log (Zoomed-in at the Garn Formation Interval).

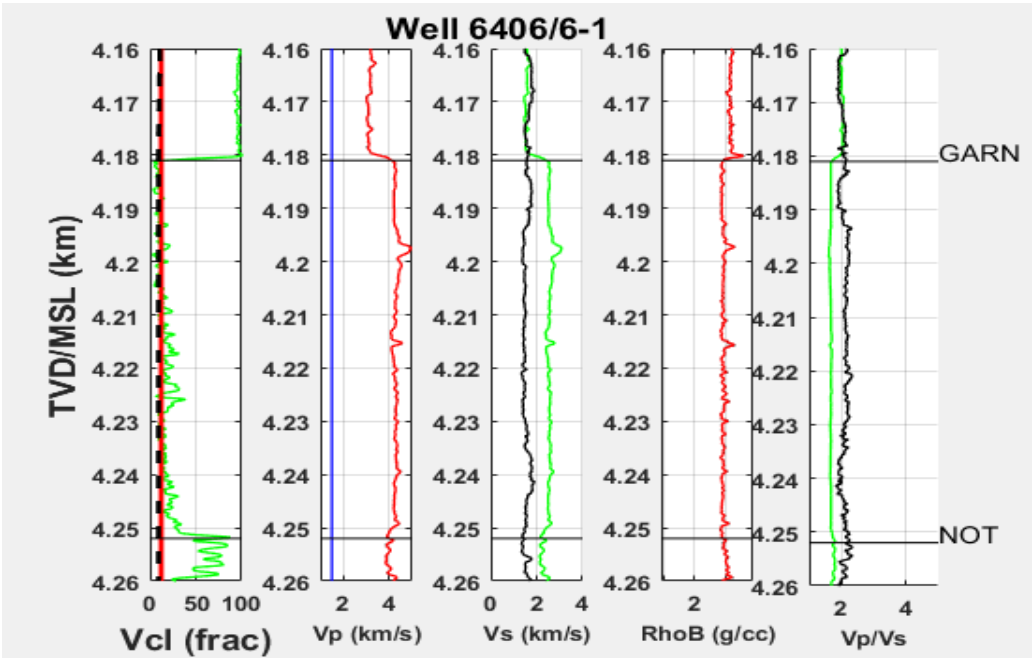

Plate 19: Well log signatures from well 6506/12-1 generated from Matlab. Track 1: VCl log, Track 2: P-Wave Velocity log, Track 3: S-Wave Predicted log (green=Greenberg-Castagna, black=mudrock, Track 4: Density log, Track 5: Vp/Vs log (Zoomed-in at the Garn Formation Interval).

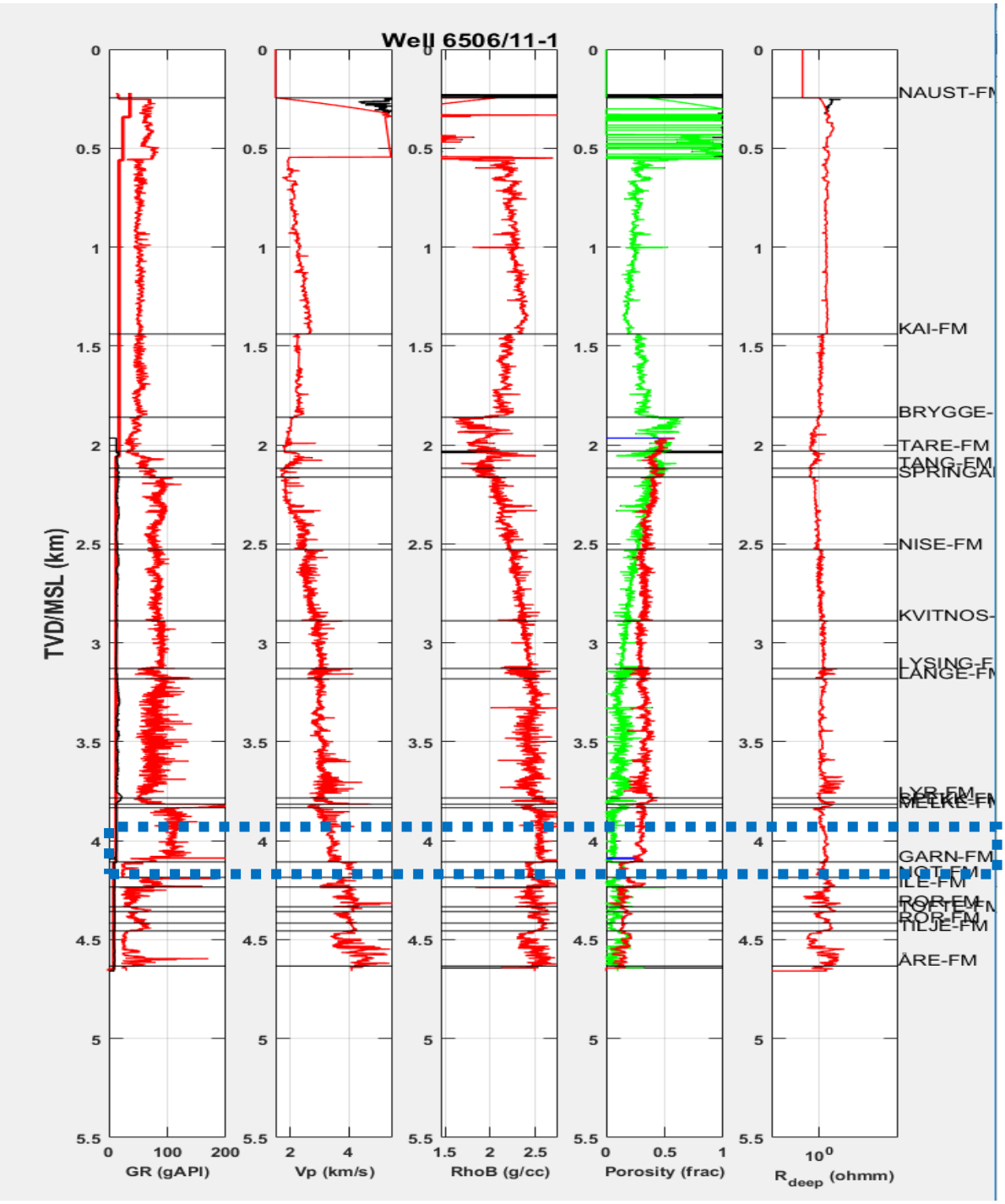

Plate 20: Well log signatures from well 6506/11-1 generated from Matlab. Track 1: GR log, Track 2: P-Wave Velocity log, Track 3: Density log, Track 4: Porosity log, Track 5: Resistivity log.

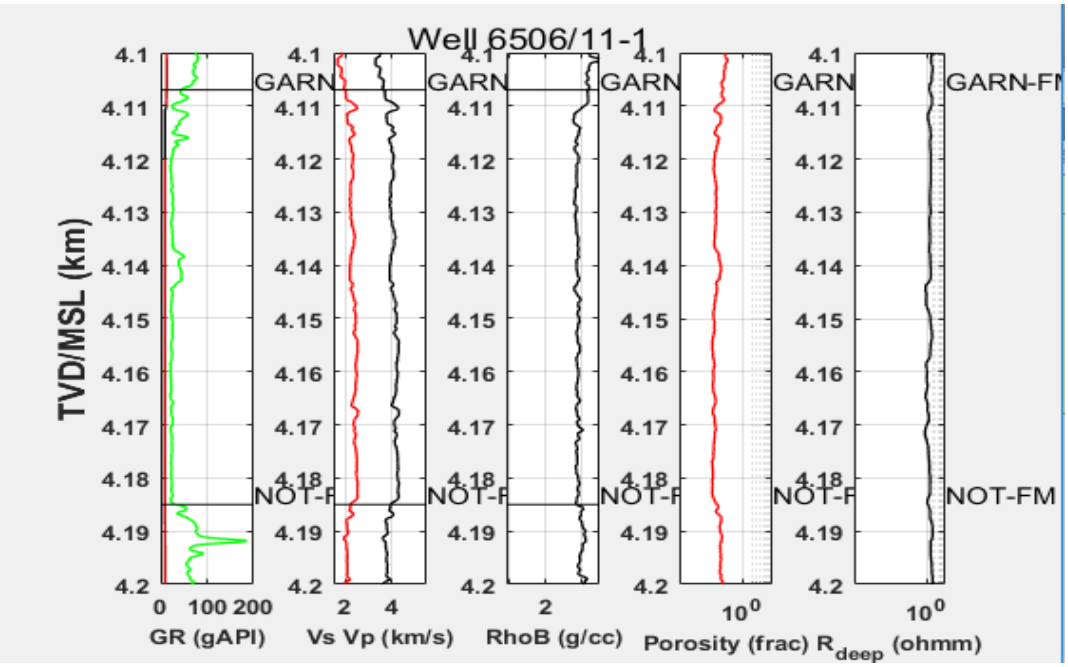

Plate 21: Well log signatures from well 6506/11-1 generated from Matlab. Track 1: GR log, Track 2: P-Wave Velocity log, Track 3: Density log, Track 4: Porosity log, Track 5: Resistivity log (Zoomed-in at the Garn Formation Interval).

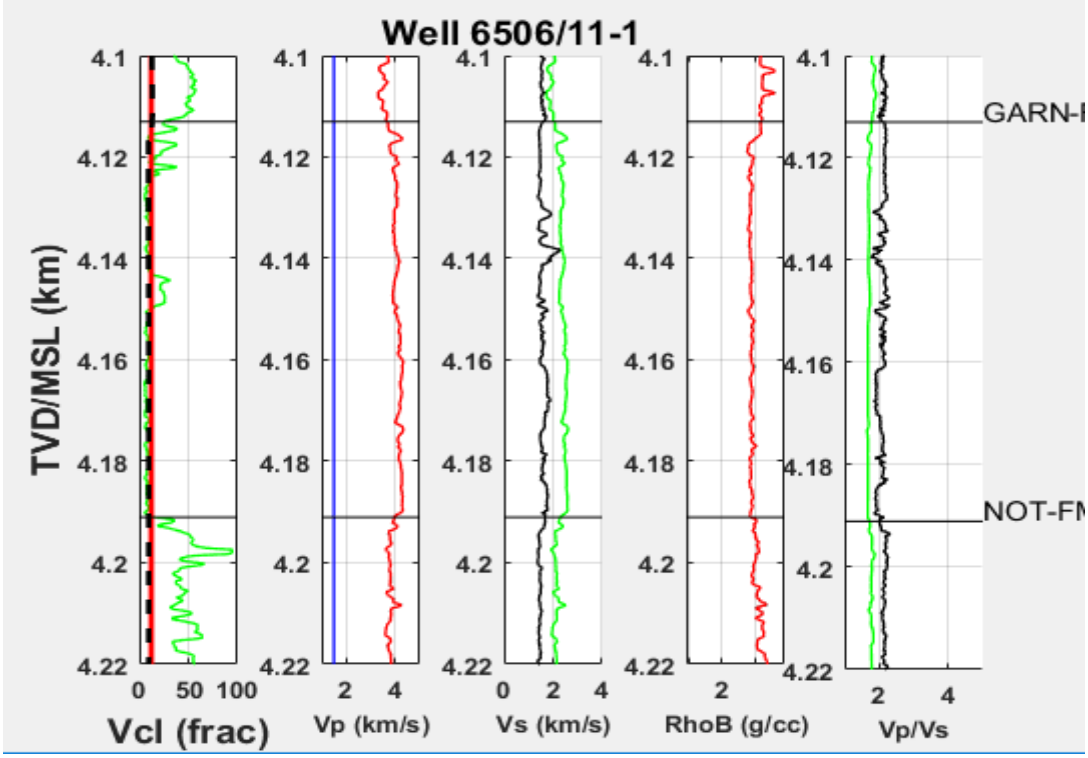

Plate 22: Well log signatures from well 6506/11-1 generated from Matlab. Track 1: VCl log, Track 2: P-Wave Velocity log, Track 3: S-Wave Predicted log (green=Greenberg-Castagna, black=mudrock, Track 4: Density log, Track 5: Vp/Vs log (Zoomed-in at the Garn Formation Interval).

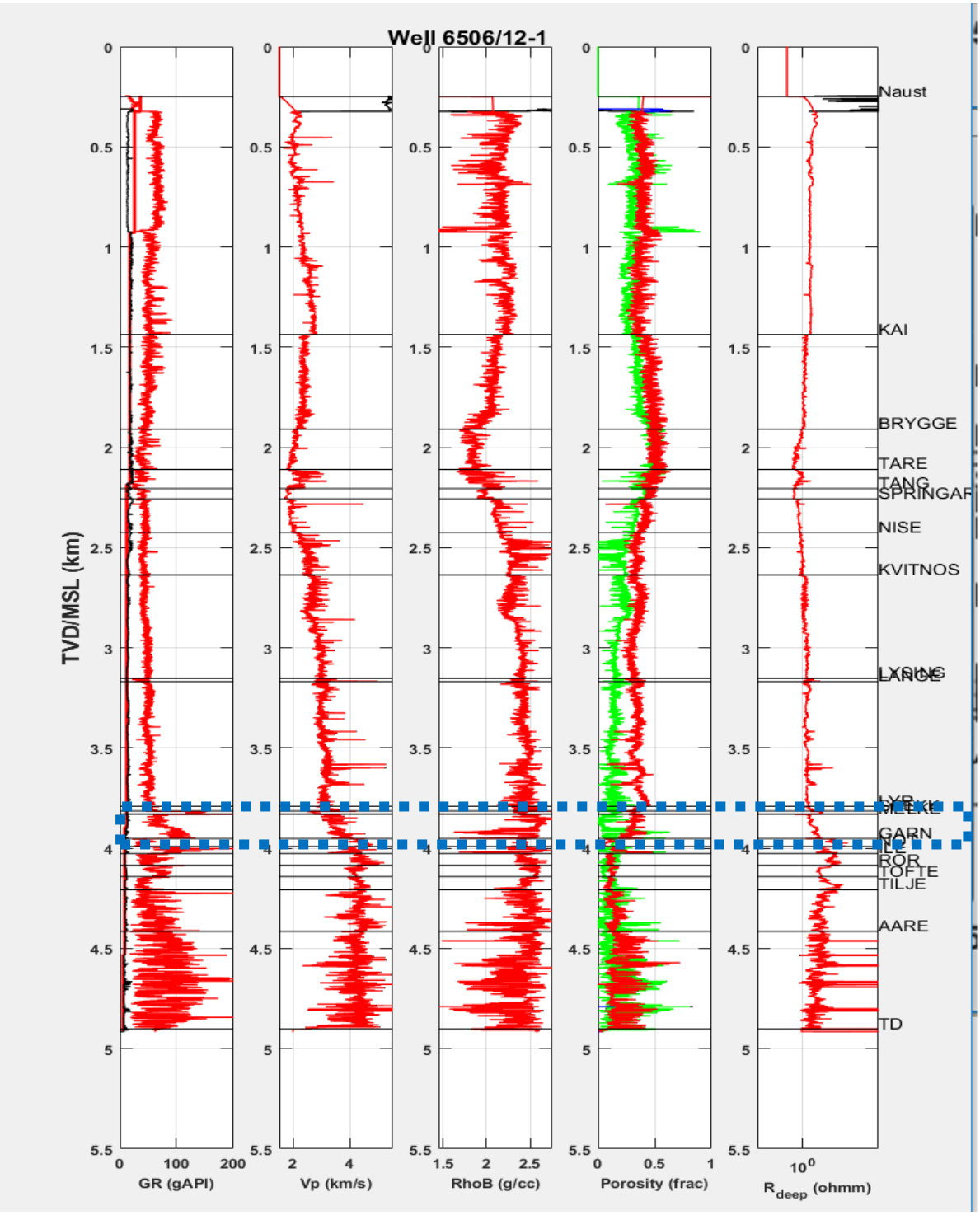

Plate 23: Well log signatures from the well 6506/12-1 generated from Matlab. Track 1: GR log, Track 2: P-Wave Velocity log, Track 3: Density log, Track 4: Porosity log, Track 5: Resistivity log.

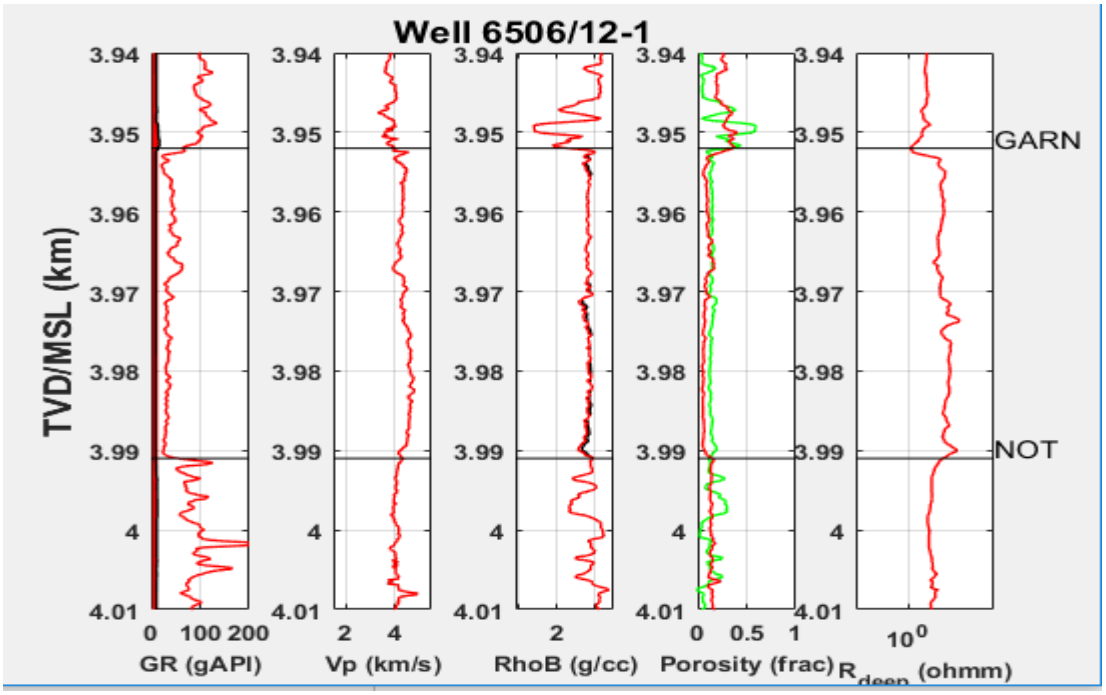

Plate 24: Well log signatures from the normal pressured well 6506/12-1 generated from Matlab. Track 1: GR log, Track 2: P-Wave Velocity log, Track 3: Density log, Track 4: Porosity log, Track 5: Resistivity log (Zoomed-in at the Garn Formation Interval).

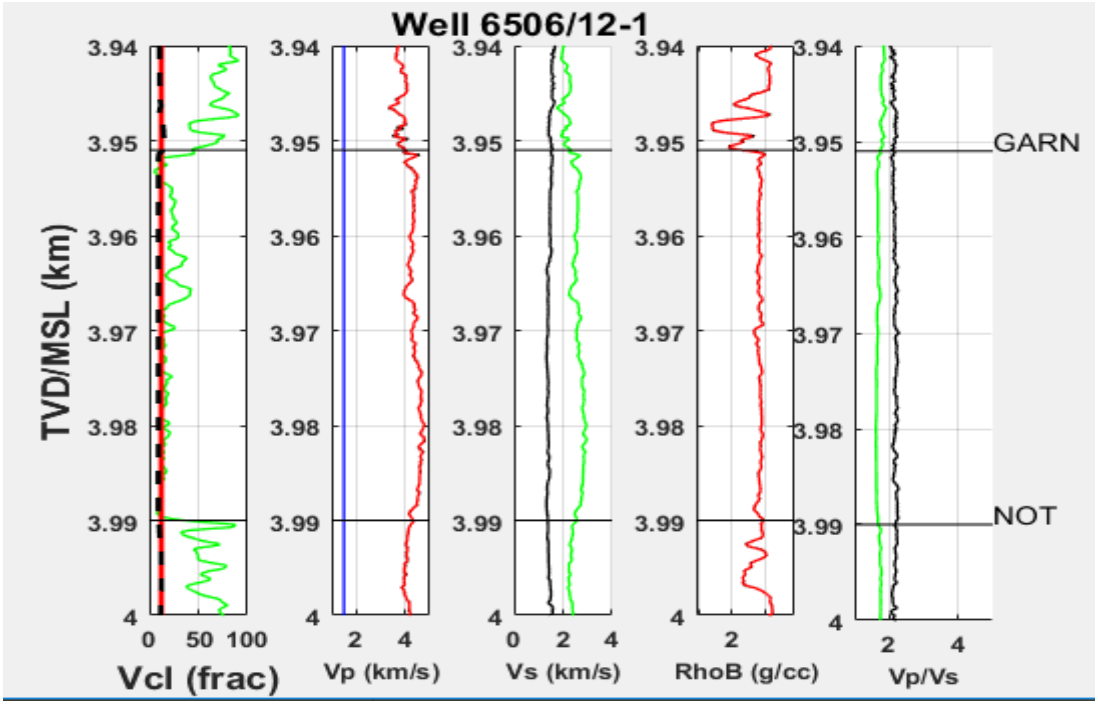

Plate 25: Well log signatures from well 6506/12-1 generated from Matlab. Track 1: VCl log, Track 2: P-Wave Velocity log, Track 3: S-Wave Predicted log (green=Greenberg-Castagna, black=mudrock, Track 4: Density log, Track 5: Vp/Vs log (Zoomed-in at the Garn Formation Interval).